REGULATION OF EXOCYTOSIS BY

SYNTAXIN 4-MUNC18C COMPLEXES

Jenna Lee Jewell

Submitted to the faculty of the University Graduate School
in partial fulfillment of the requirements
for the degree
Doctor of Philosophy
in the Department of Biochemistry & Molecular Biology
Indiana University

July 2010

Accepted by the Faculty of Indiana University, in partial fulfillment of the requirements for the degree of Doctor of Philosophy.

_____

Debbie C. Thurmond, Ph.D. -Chair

Doctoral Committee

_____

Patricia J. Gallagher, Ph.D.

May 12 2010

_____

Peter J. Roach, Ph.D.

_____

Zhong-Yin Zhang, Ph.D.

DEDICATION

This work is dedicated to my mother, Sherry L. Rowe. Without her support and guidance I would not be where I am today. I would also like to dedicate this work to my husband, Vincent S. Tagliabracci, for inspiring me to be a better scientist and for always pushing me to be the best that I can be.

ACKNOWLEDGEMENTS

I would like to thank my advisor Dr. Debbie Thurmond who is not only a great mentor but a good friend. Without her direction, encouragement, and teachings none of this would be possible. I would like to acknowledge the current and former members of the Thurmond lab who have in one way or another assisted me: Dr. Eunjin Oh, Wei Luo, Rapheal Tonade, Alice Ke, Dr. Zhanxiang Wang, Mike Kalwat, Erica Daniel, Dr. Dean Wiseman, and Latha Ramalingam. In particular I would like to thank Dr. Eunjin Oh for the invaluable training she has given me. I would like to thank Mike Kalwat for all of his help with experiments and editing grants/manuscripts. I would also like to thank Mike Kalwat and Latha Ramalingam for not only being wonderful colleagues to work with but amazing friends. Our conversations throughout the day I will miss greatly.

Next, I would like to thank my committee members Dr. Patricia Gallagher, Dr. Peter Roach, and Dr. Zhong-Yin Zhang. I would like to thank Dr. William Bosron, Dr. Jeffrey Elmendorf, and Dr. Anna Depaoli-Roach. All of these individuals have assisted me in the development of this work through suggestions and constructive criticism. I would also like to thank Cathy Meyer, Lixuan Tackett, Dr. Samy Meroueh, Sara Bennett, and Yichun Chen for assisting me with experiments in this thesis.

And finally I would like to thank my family: Mom, Vinnie, Libby and Chanel, Grandma Elaine, Suz and Vince.

ABSTRACT

Jenna Lee Jewell

REGULATION OF EXOCYTOSIS BY SYNTAXIN 4-MUNC18C COMPLEXES

Type 2 diabetes involves defects in glucose-stimulated insulin secretion (GSIS) from the pancreatic beta cells in combination with defects in peripheral (muscle and adipose) tissue glucose uptake. Both GSIS and glucose uptake are regulated by Syntaxin 4 (Syn4)-Munc18c complexes. Importantly, reports link obesity and Type 2 diabetes in humans with changes in protein levels of Munc18c and Syn4; yet the molecular mechanisms underlying this requirement remain unclear. The central hypothesis proposed is that Syn4-Munc18c complexes are modulated by post-translational modifications and novel interactions. Toward this, we found that Syn4-Munc18c complexes are regulated by tyrosine phosphorylation of Munc18c at Y219 in beta cells. Munc18c tyrosine phosphorylation disrupts Syn4-Munc18c complexes, which leads to an increase in Munc18c associating with the double C2 domain protein Doc2β. Disruption of Syn4-Munc18c upon tyrosine phosphorylation results in an increase in Syn4-SNARE complex formation and GSIS from beta cells. Similarly, tyrosine phosphorylation of Munc18c at Y219 and also Y521, disrupts its association with Syn4 in insulin-stimulated 3T3L1 adipocytes and skeletal muscle. *In vitro* kinase assays further suggested that the insulin receptor tyrosine kinase targeted Y521 of Munc18c. Further investigations using 3T3L1 adipocytes and skeletal muscle extracts indicate that Munc18c interacts with the insulin receptor tyrosine kinase in an insulin-dependent manner, resulting in phosphorylation of Munc18c, coordinate with the timing of its dissociation from Syn4. Finally, we found that stimulus-induced changes occurred also with Syn4, most notably in the islet beta cells. Syn4-mediated insulin release requires F-actin remodeling to mobilize insulin granules to the plasma membrane. Our studies reveal that Syn4 directly associates with F-actin in MIN6 beta cells, and that the disruption of this complex correlates with increases in glucose-stimulated insulin secretion. Future studies will focus upon the potential link between Syn4, F-actin remodeling with Munc18c,

to further gain understanding of the requirements for Syn4-Munc18c complexes in insulin secretion. In sum, given the parallels of Munc18c tyrosine phosphorylation in regulating Syn4-Munc18c interaction and exocytosis in beta cells and peripheral tissues, manipulations of this complex may have therapeutic potential as a strategy to treat Type 2 diabetes.

Debbie C. Thurmond, Ph.D. -Chair

TABLE OF CONTENTS

LIST OF TABLES xiii

LIST OF FIGURES xiv

LIST OF ABBREVIATIONS xvii

CHAPTER 1: INTRODUCTION 1

1.1 COORDINATION OF WHOLE BODY GLUCOSE HOMEOSTATSIS 2

1.2 SNARE-MEDIATED EXOCYTOSIS 3

1.3 INSULIN GRANULE EXOCYTOSIS 4

1.4 GLUT4 VESICLE TRANSLOCATION 8

1.5 DIFFERENTIAL SNARE ISOFORM FUNCTION IN EXOCYTOSIS EVENTS OF GLUCOSE HOMEOSTASIS 13

1.5.1 The Syntaxin Family 13

1.5.2 SNAP25, SNAP23, SNAP29 14

1.5.3 The VAMP Family 14

1.6 THE SEC1/MUNC18 (SM) PROTEIN FAMILY 15

1.7 MUNC18C AND SNARE PROTEIN MOUSE MODELS: ALTERATIONS OF GLUCOSE HOMEOSTASIS 16

1.7.1 Syntaxin Mouse Models 16

1.7.2 Munc18 Mouse Models 19

1.7.3 VAMP and SNAP Mouse Models 20

1.8 MUNC18-SYNTAXIN COMPLEXES: MOLECULAR MECHANISMS 21

1.8.1 Protein-protein Interaction Studies-*In Vitro* 21

1.8.2 Protein-protein Interaction Studies in Cells and Tissues Impact of Post-translational Modifications 24

1.8.3 Impact of Additional Binding Partners on SM-Syntaxin Interactions 25

Doc2β 25

Munc13-1 27

WNK1 27

80K-H 29
Rab3A 29
Synip 29
Tomosyn and Cab45b 30
1.9 NOVEL ROLES FOR MUNC18C AND SYNTAXIN PROTEINS IN GRANULE MOBILIZATION AND PROTEIN REFILLING 31
1.10 HYPOTHESIS 32
CHAPTER 2: THE TYROSINE PHOSPHORYLATION OF MUNC18C INDUCES A SWITCH IN BINDING SPECIFICITY FROM SYNTAXIN 4 TO DOC2β 33
2.1 INTRODUCTION 34
2.2 MATERIALS AND METHODS 35
2.2.1 Materials 35
2.2.2 Plasmids 35
2.2.3 Cell Culture, Transient Transfections and Secretion Assays 36
2.2.4 Tandem Affinity Purification (TAP) 37
2.2.5 Subcellular Fractionation 37
2.2.6 Co-immunoprecipitation and Immunoblotting 38
2.2.7 Recombinant Proteins and Interaction Assays 39
2.2.8 Surface Plasmon Resonance 39
2.2.9 Computer Modeling 40
2.2.10 Statisitical Analysis 40
2.3 RESULTS 41
2.3.1 Munc18c-Syntaxin 4 Binary Complexes Predominate in Detergent Lysates 41
2.3.2 Doc2β Preferentially Associates with Tyrosine Phosphorylated Munc18c 45
2.3.3 The Hc-linker Region of Syntaxin 4 (Amino Acids 118-194) Confers Binding to Munc18c 47

2.3.4 The Hc-Linker Region (118-194) of Syntaxin 4 Competitively Inhibits Munc18c-Syntaxin 4 Associaiton 50
2.3.5 Functional Impact of Hc-Linker Region (Amino Acids 118-194) Expression Upon Insulin Exocytosis 53
2.3.6 The 118-194 Region Does Not Associate with Phosphorylated Munc18c 58
2.3.7 Modeling the Munc18c-Syntaxin 4 Complex Interaction Sites 58
2.4 DISCUSSION 64
CHAPTER 3: IDENTIFICATION OF AN INSULIN-STIMULATED MUNC18C TYROSINE KINASE IN ADIPOCYTES AND SKELETAL MUSCLE 69
3.1 INTRODUCTION 70
3.2 MATERIAL AND METHODS 71
3.2.1 Materials 71
3.2.2 Plasmids 71
3.2.3 Cell Culture and Transient Transfection 72
3.2.4 Co-immunoprecipitation and Immunoblotting 72
3.2.5 *In Vitro* Kinase Assays 72
3.2.6 Computer Modeling 75
3.2.7 Myc-GLUT4-EGFP Translocation Analysis 75
3.2.8 Confocal Microscopy 75
3.2.9 Statistical Analysis 75
3.3 RESULTS 76
3.3.1 Insulin Stimulates Munc18c-IR Association Concurrent with Munc18c Tyrosine Phosphorylation in Adipocytes and Skeletal Muscle 76
3.3.2 Pervanadate Mimics the Effects of Insulin 78
3.3.3 Inhibition of IR Activity Decreases its Association with and Tyrosine Phosphorylation of Munc18c 81

3.3.4 Munc18c Becomes Tyrosine Phosphorylated Upstream of PI3K 84
3.3.5 The IR Phosphorylates Munc18c at Tyrosine 521 84
3.3.6 Munc18c Becomes Phosphorylated at Tyrosine 219 in Adipocytes 87
3.3.7 Depletion of Munc18c Decreases GLUT4 Translocation to Plasma Membrane 87
3.4 DISCUSSION 94
CHAPTER 4: FILAMENTOUS ACTIN REGULATES INSULIN EXOCYTOSIS THROUGH DIRECT INTERACTION WITH SYNTAXIN 4 97
4.1 INTRODUCTION 98
4.2 MATERIALS AND METHODS 99
4.2.1 Materials 99
4.2.2 Plasmids 99
4.2.3 Cell Culture, Transient Transfection and Secretion Assays 100
4.2.4 Immunofluorescence and Confocal Microscopy 101
4.2.5 Electron Microscopy 101
4.2.6 Subcellular Fractionation 102
4.2.7 Co-immunoprecipitation and Immunoblotting 102
4.2.8 Recombinant Protein and Interaction Assays 103
4.2.9 Statisitcal Analysis 104
4.3 RESULTS 105
4.3.1 F-actin Function is Conserved Between Human and Rodent Islet Beta Cells 105
4.3.2 Glucose-induced Dissociation of F-actin from Syntaxin 4 111
4.3.3 F-actin Directly Associates with Only the Syntaxin 4 Isoform 111

4.3.4 Selective Separation of Syntaxin 4 from F-actin Enhances Granule Mobilization and Exocytosis 118
4.3.5 Disruption of F-actin Binding to Syntaxin 4 Enhances Granule Mobilization and Syntaxin 4 Accessibility 122
4.4 DISCUSSION 123
CHAPTER 5: CONCLUDING REMARKS 133
APPENDIX A: PERMISSION TO REPRODUCE PREVIOUSLY PUBLISHED MATERIAL 139
APPENDIX B: ADDITONAL EXPERIMENTS 141
REFERENCES 143
CURRICULUM VITAE

LIST OF TABLES

Table 1-1	Expression of v- and t-SNARE Isoforms in Adipose, Skeletal Muscle and Pancreatic β-cells	6
Table 1-2	Comparison of Exocytosis Events of Insulin Granules, GLUT4 Vesicles and Synaptic Vesicles	7
Table 1-3	Genetically-engineered Mouse Models of SNARE Protein Ablation/Over-expression for Studies of Glucose Homeostasis *In Vivo*	11
Table 1-4	SM-Syntaxin Binding Specificities	18

LIST OF FIGURES

Figure 1-1	SNARE Core Complex Formation	5
Figure 1-2	Glucose-stimulated Insulin Secretion from the Islet Beta Cell	9
Figure 1-3	Glucose Uptake Via Insulin-stimulated GLUT4 Translocation and Fusion in Muscle and Adipose Tissues	12
Figure 1-4	Proposed Models of Munc18c-Syntaxin 4 Interaction	26
Figure 1-5	Modeling of Munc18c-Syntaxin 4 Interaction	28
Figure 2-1	Munc18c Associates with the SNARE Complex *In Vitro* Depending On Which Protein is Tagged with GST	43
Figure 2-2	Munc18c Does Not Co-immunoprecipitate with VAMP2 in Detergent Solubilized MIN6 Cell Lysates	44
Figure 2-3	An Inverse Correlation Between Syntaxin 4 and Doc2β Association withTyrosine Phosphorylated Munc18c	46
Figure 2-4	The Region Containing the HC and Linker Domains (118-194) of Syntaxin 4 Binds Directly to Munc18c *In Vitro*	48
Figure 2-5	Sequence Alignment of Hc-Linker Regions Amongst Mammalian Plasma Membrane-localized Syntaxin Isoforms	51
Figure 2-6	The Hc-linker Region of Syntaxin 4 Effectively Competes with Full Length Soluble Syntaxin 4 for Binding of Munc18c *In Vitro*	52
Figure 2-7	Residues 118-194 of Syntaxin 4 Bind to Munc18c in CHO-K1 and MIN6 Beta Cells	54
Figure 2-8	The Hc-linker Region (118-194) of Syntaxin 4 Interacts with Endogenous Munc18c and is Important for Insulin Exocytosis	55
Figure 2-9	Syntaxin 4 (118-194) Does Not Bind to Phosphorylated Munc18c	60
Figure 2-10	Sensorgram Depicting the Kinetic Analysis of Munc18c Binding to Syntaxin 4	61

Figure 2-11	Ribbon Representation of the Munc18c-Syntaxin 4 Complex	62
Figure 3-1	Insulin Stimulation Increases Munc18c Tyrosine Phosphorylation	77
Figure 3-2	Munc18c -IR Association Increases Upon Insulin Stimulation	79
Figure 3-3	IR-Munc18c Complexes are Mutually Exclusive of Syntaixin 4-Munc18c Complexes	80
Figure 3-4	Munc18c Tyrosine Phosphorylation and Munc18c-IR Binding was Reduced Following Treatment with the IR Inhibitor HNMPA-$(AM)_3$	82
Figure 3-5	Munc18c Becomes Tyrosine Phosphorylated Upstream of PI3K in the Insulin Signaling Pathway	85
Figure 3-6	The IR Phosphorylates Munc18c on Tyrosine 521 *In Vitro*	86
Figure 3-7	Munc18c Tyrosine 219 Becomes Phosphorylated in 3T3L1 Adipocytes	88
Figure 3-8	The Knockdown of Munc18c Decreases Plasma Membrane GLUT4	89
Figure 3-9	The Effect of Munc18c Tyrosines 219 and 521 in Insulin-Stimulated GLUT4 Translocation	92
Figure 3-10	Modeling of Munc18c Y219 and Y521 Residues	96
Figure 4-1	Latrunculin Potentiates Insulin Secretion in Human Islets-Conservation of Function with Rodent Islets and Cultured Beta Cells	105
Figure 4-2	Latrunculin Causes Increased Granule Accumulation at the Plasma Membrane in the Absence of Glucose	109
Figure 4-3	Glucose-induced Dissociation of F-actin from Syntaxin 1A and Syntaxin 4	112
Figure 4-4	Syntaxin 4 but not Syntaxin 1A Binds Directly to F-actin *In Vitro*	115

Figure 4-5 The Region Containing the Ha-Hb Domains of Syntaxin 4 is Necessary and Sufficient to Confer Direct Binding to F-actin 116
Figure 4-6 Expression of Syntaxin 4 Residues 39-112 in MIN6 cells Results in Dissociation of the Endogenous F-actin-Syn4 Association and Increased Glucose-stimulated Secretion 120
Figure 4-7 Like Latrunculin Treatment, Expression of EGFP-(39-112) Mobilizes Granules into the PM Compartment from the Storage Granule Pool Under Basal Conditions 124
Figure 4-8 EGFP-Syntaxin4 (39-112) Expression Increases Syntaxin 4 Accessibility but not VAMP2 Docking/Fusion at Syntaxin 4 Sites 125
Figure 4-9 Model Depicting Potential Mechanism of Regulation of Insulin Exocytosis by F-actin-Syntaxin 4 Complexes Under Basal and Glucose Stimulated Conditions 128

ABBREVIATIONS

ADP	Adenosine Diphosphate
ATP	Adenosine Triphosphate
BSA	Bovine Serum Albumin
CBP	Calmodulin Binding Peptide
CHO-K1	Chinese Hamster Ovary Cell Line
CDK	Cyclin Depednent Kinase
CPX	Complexins
Cyt	Cytosol
DAPK	Death Associated Protein Kinase
DMEM	Dulbecco's Modified Eagle's Medium
DMSO	Dimethyl Sulfoxide
DTT	Dithiothreitol
ECL	Enhanced Chemiluminescence
EDC	N-ethyl-N'-dimethylaminopropyl Carbodimide
EGFP	Enhanced Green Fluorescent Protein
EM	Electron Microscopy
ER	Endoplasmic Reticulum
FBS	Fetal Bovine Serum
FL	Full Length
FT	Flow-through
GLUT	Sodium Independent Glucose Transporter
GSIS	Glucose-Stimulated Insulin Secretion
GST	Glutathione S-transferase Fusion Protein
HUVECs	Human Umbilical Vein Endothelial Cells
IB	Immunoblott
IP	Immunoprecipitation
IR	Insulin Receptor
IRS	Insulin Receptor Substrate
MIN6	Mouse Insulinoma Cell Line
MKRBB	Modified Kreb's Ringer Bicarbonate Buffer

N/A	Not Applicable
ND	Not Determine
NHS	N-hydroxysuccinimide
NMR	Nuclear Magnetic Resonance
NP40	Non-ionic Detergent P-40
PBS	Phosphate Buffer Saline
PCR	Polymerase Chain Reaction
PDGF	Platelet Derived Growth Factor
PDGFR	Platelet Derived Growth Factor Receptor
PDK-1	Phosphoinositide-dependent kinase-1 (PDK-1)
PH	Pleckstrin Homology
PIP2	Phosphatidylinositol (4,5) bisphosphate
PIP3	Phosphatidylinositol (3,4,5) triphosphate
PI3K	Phosphatidylinositide Kinase
PKB	Protein Kinase B
PKC	Protein Kinase C
PM	Plasma Membrane
PMSF	Phenylmethylsulfonylfluoride
PP2B	Phospahtase Protein 2B
PTB	Phosphotyrosine Binding Domain
PVDF	Polyvinylidene difluoride
pV	Pervanadate
RIA	Radioimmunoassay
RRP	Readily Releasable Pool
Rus	Resonance Units
SBP	Streptavidin Binding Peptide
SDS-PAGE	Sodium Dodecylsulfate Polyacrylamide Gel Electrophresis
Ser	Serine
SG	Storage Granule
SH2	Src Homology 2 Domains
SNAP	Synaptosome Associated Protein

SNARE	Soluble N-ethylmaleimide Sensitive Factor Attachment Protein Receptor
Synip	Syntaxin-interacting Protein
Syn 4	Syntaxin 4 Protein
TAP	Tandem Affinity Purification
TG	Transgenic
TGN	Trans Golgi Network
Thr	Threonine
TIRFM	Total Internal Reflection Fluorescence Microscopy
Tyr	Tyrosine
t-SNARE	Target SNARE
VAMP	Vesicle Associated Membrane Protein
VDCC	Voltage-Dependent Calcium Channels
v-SNARE	Vesicle SNARE
WT	Wild Type
Y	Tyrosine

CHAPTER 1: INTRODUCTION

Some of the text in this Chapter is reproduced from:

Jewell JL, Oh E, and Thurmond DC. 2010. Exocytosis mechanisms underlying insulin release and glucose uptake: conserved roles for Munc18c and syntaxin 4. Am J Physiol Regul Integr Comp Physiol., 298:R517-31.

Author Contributions: Tables and some text were generated by Oh E. Jewell JL produced the majority of text and Figures present in this chapter.

Diabetes is a condition characterized by high blood sugar (glucose) levels that result from defects in insulin secretion, action, or both. There are three major forms of diabetes: Type 1, Type 2, and gestational diabetes. According to the American Diabetes Association as of 2007, 23.6 million people in the United State have diabetes. However, out of the 23.6 million it is estimated that 5.7 million people still remain undiagnosed. In 2006, diabetes was reported as the seventh leading cause of death in the United States. Diabetes is also the leading source of adult blindness, nerve damage, kidney disease, and lower-limb amputation (3). Type 2 diabetes represents 90-95% of all cases, and is caused by a combination of genetic and non-genetic factors which results in insulin secretion defects in the pancreas and insulin resistance in the muscle and adipose tissue (3). Some of the non-genetic factors that influence Type 2 diabetes include increasing age, obesity, and physical inactivity (3). Type 1 diabetes, also referred to juvenile diabetes, represents 5-10% of all cases that results from autoimmune destruction of the insulin-secreting beta cells, leading to hyperglycemia. Gestational diabetes represents approximately 3-5% of cases, and occurs in pregnancies when hormones from the placenta counteract insulin action in the mother. Mothers with gestational diabetes have a 63% increase in their risk of developing Type 2 diabetes later in life, therefore interventions could be extremely useful for this population (4). Thus, by understanding the mechanisms involved in regulating the coordination of whole body glucose homeostasis we may begin to develop therapeutic strategies to prevent or treat patients who suffer from diabetes.

1.1 COORDINATION OF WHOLE BODY GLUCOSE HOMEOSTASIS

Circulating blood glucose levels are tightly regulated in mammals and are maintained at about 5 mM (~80-100 mg/dL). Following intake of high-carbohydrate food, blood glucose levels rise to approximately 8 mM (~120-140 mg/dL), which under normal homeostatic circumstances induces the pancreas to secrete insulin from the beta cells within the Islets of Langerhans. This release of insulin subsequently signals to the liver to reduce glucose output while

simultaneously inducing clearance of excess glucose from the blood by the skeletal muscle and adipose tissue. Normally, this process restores the blood glucose levels to 5 mM within 2 hours after the meal. However during pathological progression from normal to clinically-defined Type 2 Diabetes, there are clear and progressive aberrations in both insulin secretion as well as glucose uptake/clearance mechanisms. Given that a significant number of proteins required for insulin secretion and glucose clearance are identical, alterations in their abundance and/or function would materially impact both mechanisms and increase susceptibility to aberrant glucose homeostasis.

1.2 SNARE-MEDIATED EXOCYTOSIS

The SNARE (soluble N-ethylmaleimide sensitive factor attachment protein receptor) core complex is composed of three proteins in a heterotrimeric 1:1:1 ratio: *1)* Syntaxin, a 35 kDa protein containing an N-terminal regulatory domain, a C-terminal SNARE domain, and a C-terminal transmembrane domain anchoring it to the plasma membrane (PM); *2)* SNAP23 or SNAP25, two complementary isoforms that lack transmembrane domain anchors but localize to the PM due to palmitoylated cysteine residues; and *3)* VAMP2 (also known as synaptobrevin), an 18 kDa protein containing a C-terminal transmembrane domain anchoring it to the vesicle membrane. As depicted in Figure 1-1, the vesicle (v-) SNARE VAMP2 pairs with the two target PM (t-) SNAREs Syntaxin and SNAP23/25 forming the SNARE core complex. Together, the three SNARE proteins produce a stable bundle of the four α-helices, with one α-helix from VAMP, one from Syntaxin, and the remaining two from SNAP23/25 [reviewed in (5)]. This complex is remarkably SDS-resistant once formed. To date, 6 v-SNARE isoforms and 11 t-SNARE isoforms have been identified in cell types relevant to insulin secretion and insulin action (Table 1-1). Interestingly, the underlying vesicle/granule exocytosis events of insulin secretion and glucose uptake share numerous commonalities with those of neuronal synaptic vesicle exocytosis (Table 1-2). Glucose-stimulated insulin secretion (GSIS) from the pancreatic beta cell and glucose uptake in the muscle and adipose are both

mediated by the same SNARE protein isoforms: Syntaxin 4, SNAP23 and VAMP2 [reviewed in (6,7)]. Additionally, beta cells use t-SNARE isoforms Syntaxin 1 and SNAP25 to mediate the first-phase of insulin secretion (8). However, key differences exist which distinguish the specialization of events in each cell type (summarized in Table 1-2).

1.3 INSULIN GRANULE EXOCYTOSIS

Elevated post-prandial glucose levels trigger a signaling cascade in the pancreatic islet beta cells to elicit insulin release (Figure 1-2), depicted as an ~8-step process [reviewed in (35,36)]. First, glucose entry into beta cells is facilitated via the plasma membrane-localized glucose transporter, GLUT2. GLUT2 has a relatively low affinity (K_M ~30 mM) for glucose, is constitutively present within the plasma membrane, and does not require SNARE proteins for translocation and membrane localization. Following GLUT2-facilitated uptake, glucose is phosphorylated by glucokinase to generate glucose-6-phosphate, which is subsequently metabolized via mitochondrial oxidative phosphorylation to effect an increase in intracellular ATP:ADP ratio (step 2). Elevated beta cell ATP levels induce closure of ATP-dependent potassium channels (step 3), resulting in cell depolarization (step 4) and an influx of calcium ions (Ca^{2+}) through voltage-dependent calcium channels (step 5) to yield a net increase in the intracellular Ca^{2+} concentration ($[Ca^{2+}]_i$; step 6). The increase in $[Ca^{2+}]_i$ signals SNARE complex formation (step 7) to facilitate insulin release from the granules (step 8), although the precise mechanism(s) by which Ca^{2+} triggers granule fusion remains somewhat unresolved.

Insulin secretion occurs in pulsatile fashion synchronized with Ca^{2+} influxes during two major phases, and is termed ‘biphasic’. First-phase insulin secretion occurs within 5-10 minutes following beta cell stimulation. Second-phase is less robust than first-phase, but can be sustained for several hours if elevated blood-glucose levels persist (37-40). These two phases of secretion are thought to utilize separate pools of insulin-containing granules. First-phase secretion appears to arise from plasma membrane pre-docked granules, termed

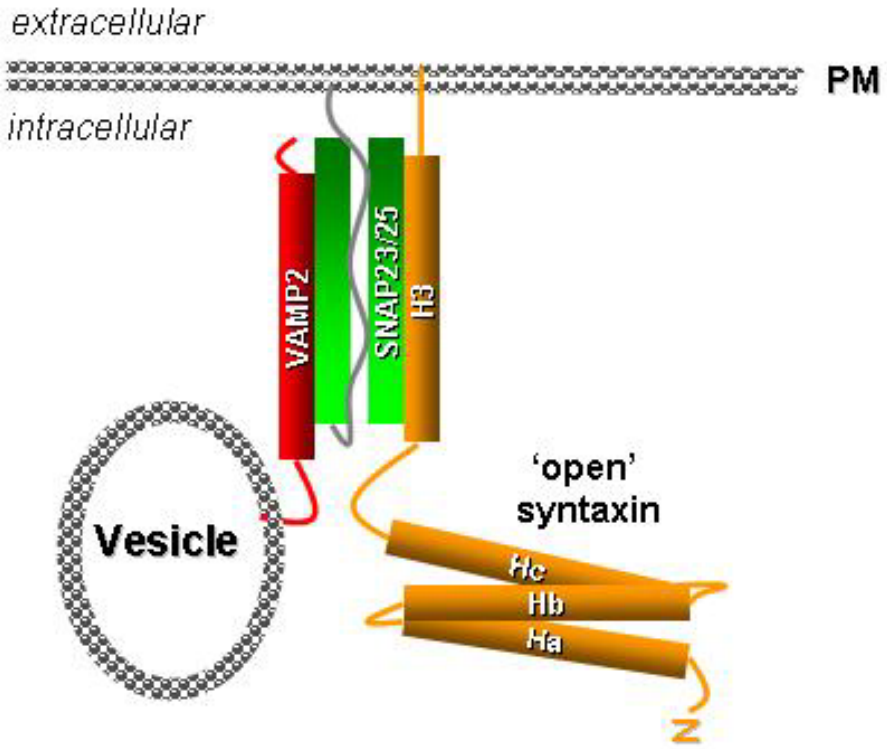

Figure 1-1 SNARE Core Complex Formation. Upon stimulation, Syntaxin (orange) adopts an 'open' conformation exposing its H3 domain (also called the SNARE domain) to associate with SNARE domains from VAMP2 (red) and SNAP23/25 (green) to form the four α-helical bundle characteristic of the SNARE core complex.

Table 1-1 Expression of v- and t-SNARE Isoforms in Adipose, Skeletal Muscle and Pancreatic β-cells

	Tissue (Localization)	Function	References
v-SNARE			
VAMP2/Synaptobrevin	Pancreatic β-cells, adipocyte, muscle (vesicles)	Exocytosis of insulin granules (β-cells), GLUT4 vesicles at the PM	(9-12)
VAMP3/Cellubrevin	Pancreatic β-cells, adipocyte, muscle (vesicles)	Exocytosis of insulin granules (β-cells), GLUT4 vesicles at the PM	(11-14)
VAMP4	Adipocyte, muscle (TGN)	ND	(12,15)
VAMP5/myobrevin	Adipocyte, muscle (PM)	Myogenesis	(12,16)
VAMP7/TI-VAMP	Adipocyte (PM, endosome)	Osmotic shock-induced GLUT4 translocation	(12)
VAMP8/Endobrevin	Pancreatic β-cells, adipocyte (endosome)	GLUT4 endocytosis, insulin secretion (β-cells)	(12,17)
t-SNARE			
Syntaxin 1A	Pancreatic β-cells (PM)	First phase insulin secretion in pancreatic β-cells	(18-20)
Syntaxin 2/Epimorphin	Pancreatic β-cells, adipocyte (PM)	ND	(21-23)
Syntaxin 3	Pancreatic β-cells, adipocyte (PM)	ND	(14,23,24)
Syntaxin 4	Pancreatic β-cells, adipocyte, muscle (PM)	Both phases of insulin secretion (β-cells), GLUT4 translocation	(9,21,25,26)
Syntaxin 5	Adipocyte (TGN)	GLUT4 endocytosis in adipocyte	(24)
Syntaxin 6	Adipocyte, muscle (TGN)	Putative involvement in GLUT4 endocytosis (adipocytes)	(27-29)
Syntaxin 7	Pancreatic β-cells, adipocyte (endosome)	ND	(27,30)
Syntaxin 8	Adipocyte (endosome)	ND	(27)
Syntaxin 10	Muscle	ND	(31)
Syntaxin 12	Adipocyte	ND	(27)
Syntaxin 16	Adipocyte (TGN)	GLUT4 intracellular trafficking	(28)
SNAP23	Pancreatic β-cells, adipocyte, muscle (PM)	Exocytosis of insulin granules (β-cells), GLUT4 vesicles at the PM	(32,33)
SNAP25	Pancreatic β-cells (PM)	Exocytosis of insulin granules (β-cells)	(34)

ND, not determined; N/A, not applicable; PM, plasma membrane; TGN, trans golgi network; ER, endoplasmic reticulum

Table 1-2 Comparison of Exocytosis Events of Insulin Granules, GLUT4 Vesicles and Synaptic Vesicles

Insulin Secretion	GLUT4 Vesicle Translocation	Neurotransmitter Release
Large secretory granules (>100 nm radius)	Large secretory granules (>100 nm radius)	Small synaptic vesicles (<25 nm radius)
Recycling via Golgi complex	Recycling via Golgi complex	Local recycling
Two secretion phases: 1st fast (spans 6-10 min); 2nd, slow and sustained (10 min-hrs)	Slow (5-15 min) and sustained	Fast, short-lasting secretion (0.1-6 ms)
Small number of predocked granules	Few predocked vesicles	Large number of predocked vesicles
Exocytosis targeted to large plasma membrane section	Exocytosis targeted to large plasma membrane section	Exocytosis restricted to synaptic active zone
Complex secretory mixes (e.g., multiple peptides, catecholamines, nucleotides)	Cargo proteins to integrate into the plasma membrane	Release of one or two low-molecular-weight compounds
SNARE isoforms: Syntaxins 1 and 4, SNAP23 and SNAP25, VAMP2	SNARE isoforms: Syntaxin 4, SNAP23, VAMP2	SNARE isoforms: Syntaxin 1, SNAP25, VAMP2
SM isoforms: Munc18-1, Munc18c	SM isoform: Munc18c	SM isoform: Munc18-1
Latrunculin potentiates secretion	Latrunculin inhibits GLUT4 translocation	Latrunculin potentiates secretion

the ‘readily releasable pool’ (RRP), while second-phase secretion is believed to involve release from a granule pool deeper within the cell, the ‘storage-granule pool,’ which presumably replenishes the RRP (41,42). In addition, KCl and other non-nutrient secretagogues can induce a first-phase type release, while only fuel-type secretagogues, such as glucose, an produce a sustained second-phase insulin release (43). First and second-phase release events also differ in their requisite SNARE protein isoforms. First-phase insulin release utilizes Syntaxin 1A, Syntaxin 4, SNAP25 or SNAP23, and the v-SNARE VAMP2, whereas second-phase secretion is managed by Syntaxin 4, SNAP25 or SNAP23, and VAMP2, but specifically not Syntaxin 1A (Table 1-3).

1.4 GLUT4 VESICLE TRANSLOCATION

Approximately 80% of homeostatic glucose clearance is handled by skeletal muscle, with the remainder by adipose and other insulin responsive tissues. Skeletal muscle glucose clearance involves transduction of the extracellular insulin signal into intracellular signaling events to induce translocation of intracellular GLUT4 vesicles to the surface of muscle cell t-tubule and sarcolemmal membranes. In this process, SNARE-regulated GLUT4 vesicle fusion is the most distal event [reviewed in (44-46)]. Under basal conditions, GLUT4 protein is localized to intracellular vesicles within cells, and unlike GLUT2, GLUT4 has a higher affinity for glucose (K_M ~4 mM). Insulin signaling to evoke GLUT4-mediated glucose clearance entails at least 11 steps, as modeled in Figure 1-3. The process ensues with insulin binding to extracellular α-subunits of the insulin receptor (IR) present on the surface of muscle cells and adipocytes (step 1), inducing tyrosine autophosphorylation within the IR protein and increased kinase activity of the IR β-subunits (step 2). Tyrosine autophosphorylation of the IR fosters recruitment of IR substrates, including the canonical Insulin Receptor Substrate (IRS), typically through a phosphotyrosine binding (PTB) domain. Once bound, substrates are themselves tyrosine-phosphorylated (step 3). Phosphorylated receptor substrates then serve as additional recruitment targets for specific proteins containing Src Homology 2

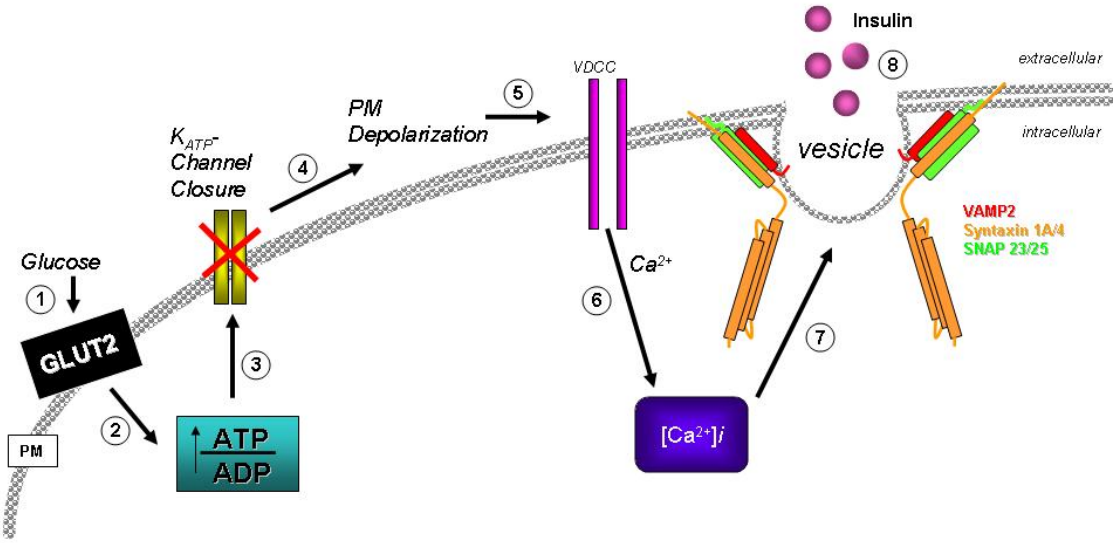

Figure 1-2 Glucose-Stimulated Insulin Secretion from the Islet Beta Cell. An 8-step model: (1) Glucose enters the cell through the constitutively active PM localized GLUT2 transporter and gets metabolized, which in turn (2) increases the ATP:ADP ratio resulting in (3) the closure of the ATP dependent potassium channels (K_{ATP}). The closure of the K_{ATP} channels leads to (4) plasma membrane (PM) depolarization, (5) opening of the voltage-dependent calcium channels (VDCC), causing calcium influx into the cell (6). As a result, intracellular calcium [Ca^{2+}]*i* levels rise, and through a largely uncharacterized series of events, the SNARE proteins mediate (7) vesicle fusion to facilitate (8) insulin release.

(SH2) domains, including phosphatidylinositide kinase (PI3-Kinase). Once recruited, PI3-Kinase is activated to catalyze the phosphorylation of phosphatidylinositol (4, 5) bisphosphate (PIP2) at the 3' position, yielding phosphatidylinositol (3, 4, 5) trisphosphate (PIP3) (step 4). 3-Phosphoinositide-dependent kinase-1 (PDK-1) is able to recognize the 3' position of PIP3 with its PH (Pleckstrin homology) domain and is recruited to the plasma membrane where it is activated (step 5). At the plasma membrane, PDK-1 phosphorylates and activates AKT/PKB (also known as protein kinase B, step 6) along with atypical PKC isoforms zeta and lambda (aPKC). As well-defined as these initial signaling steps are, the identities of downstream substrates/targets of these serine/threonine kinases which result in GLUT4 vesicle translocation remain unclear, although some recent progress has been made: Akt signals downstream (step 7) to AS160 (a Rab GTPase-activating protein) (63), and AS160 signals downstream to multiple Rab targets (step 8) (64). Rab proteins have been described in GLUT4-containing vesicles (step 9), and are presumed to facilitate their trafficking to/docking at the plasma membrane. However, a gap exists in our understanding beyond this step to link to the SNARE complex at the plasma membrane: t-SNARE isoforms Syntaxin 4 and SNAP23 with the v-SNARE VAMP2 are known to be required for GLUT4 vesicles to fuse with the plasma membrane (step 10) to facilitate glucose uptake into the skeletal muscle cell (step 11).

Independent of insulin, exercise and muscle contraction have also been shown to increase glucose uptake into skeletal muscle, although far less is known regarding the requirements and mechanisms of SNARE proteins in this process. It is clear that exercise increases the translocation of GLUT4 and VAMP2 to the plasma membrane of human and rat skeletal muscle (65). VAMP3 was also initially implicated in contraction-stimulated GLUT4 translocation, but subsequent studies of skeletal muscle from VAMP3 (-/-) mice failed to support this role (58). With the plethora of knockout mouse models of SNARE proteins now available, it is anticipated that the requirements and roles for these proteins in exercise-stimulated glucose uptake will be forthcoming.

Table 1-3 Genetically-engineered Mouse Models of SNARE Protein Ablation/Over-expression for Studies of Glucose Homeostasis *In Vivo*

Genotype	Aberration	Phenotype	References
Syntaxin			
Syntaxin 1A (-/-)	No Syntaxin 1A expression	Fewer docked granules during only first phase of insulin secretion	(19)
Syntaxin 1B (-/-, open)	Syntaxin 1B LE expression only, no endogenous	ND	(47)
Syntaxin 1A (-/-), Syntaxin 1B (-/-, LE)	No Syntaxin 1A or 1B, LE mutant expression	ND	(47)
Syntaxin 1A Tg	Beta cell specific Syntaxin 1A over-expression, decreased Munc18-1 expression	Fasting hyperglycemia, impaired glucose tolerance and insulin exocytosis	(48)
Syntaxin 4 (-/+)	Reduced Syntaxin 4 and Munc18c expression, null lethal	Insulin resistant; reduced GLUT4 translocation; defective insulin secretion	(26,49)
Syntaxin 4 Tg	Increased Syn4 and Munc18c expression in pancreas, skeletal muscle and adipose tissues only	Insulin sensitive; enhanced GLUT4 translocation and insulin secretion	(25,26)
Munc18			
Munc18-1 (-/-, -/+)	Reduced expression of Munc18-1, null lethal	ND	(50,51)
Munc18-1 Tg	Over-expression of Munc18-1 in neuron	ND	(52)
Munc18c Tg	Over-expression of Munc18c	Insulin resistant; impaired insulin secretion	(53)
Munc18c (-/-)	No Munc18c expression	Enhanced GLUT4 uptake in MEF-derived adipocytes	(54)
Munc18c (-/+)	Reduced Munc18c expression, null lethal by E7.5	Insulin resistant; impaired insulin secretion; reduced GLUT4 translocation in skeletal muscle	(55,56)
VAMP			
VAMP2 (-/-)	No VAMP2 expression, lethal	ND	(57)
VAMP3 (-/-)	No VAMP3 expression	Normal insulin and glucose tolerance, and normal glucose uptake	(58)
VAMP8 (-/-)	No VAMP8 expression	ND	(59,60)
SNAP25 (-/-, -/+)	Reduced SNAP25 expression, null lethal at birth	ND	(61)
SNAP23 (-/+)	Reduced SNAP23 expression	ND	(62)

ND, not determined; Tg, transgenic; (-/-), homozygous; (-/+) heterozygous

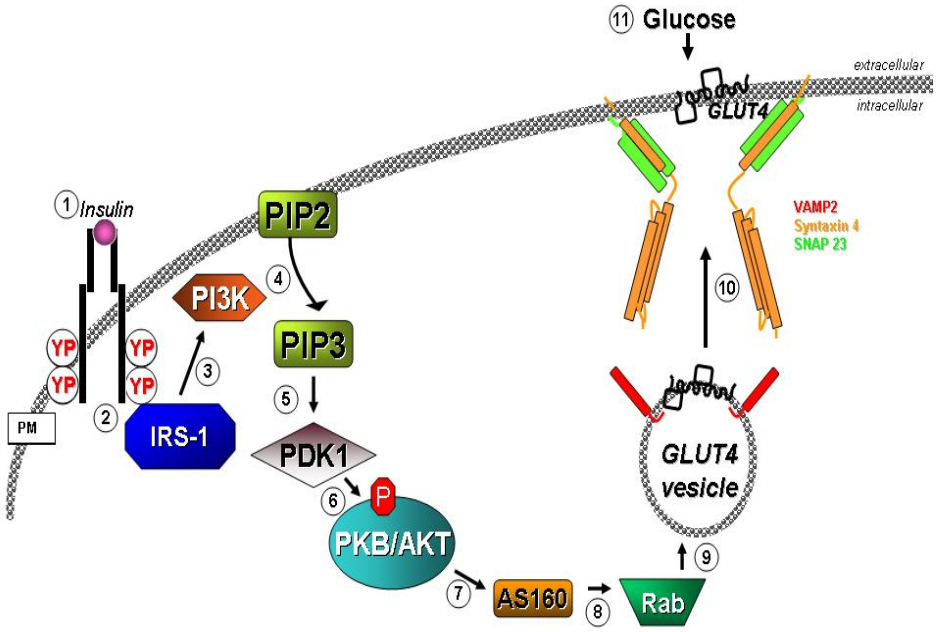

Figure 1-3 Glucose Uptake Via Insulin-Stimulated GLUT4 Translocation and Fusion in Muscle and Adipose Tissues. An 11-step model: (1) extracellular insulin binds to the β-subunit of the insulin receptor (IR), triggering autophosphorylation and activation of the β-subunit kinase activity. (2) This induces recruitment of IRS-1, and (3) IRS-1 recruits PI3-K. (4) PI3-K phosphorylates PIP2 to yield PIP3. (5) PIP3 recruits PDK1 to the PM, where it (6) phosphorylates and activates AKT. (7) AKT phosphorylates AS160, and (8) AS160 targets multiple Rabs present on GLUT4 containing vesicles (9), although the precise mechanisms beyond this remain unclear. (10) Vesicle fusion occurs via the SNARE proteins resulting in GLUT4 integration into the PM to facilitate (11) glucose uptake.

1.5 DIFFERENTIAL SNARE ISOFORM FUNCTION IN EXOCYTOSIS EVENTS OF GLUCOSE HOMEOSTASIS

Insulin secreting islet beta cells and insulin-responsive muscle and adipose cells contain multiple isoforms of each of the SNARE proteins required for the distal exocytosis events occurring at the plasma membrane (Table 1-1).

1.5.1 The Syntaxin Family

The pancreatic beta cell expresses plasma membrane-localized Syntaxin isoforms 1A, 2, 3 and 4, though additional non-plasma membrane Syntaxin isoforms are also expressed, although their function in exocytosis remains untested (Table 1-1). To date, only isoforms 1A and 4 are clearly known to be required for insulin exocytosis (19,26), primarily from data obtained using knockout mouse models. Syntaxin 1A (-/-) knockout mice show selectively impaired insulin release during the first phase, while islets from Syntaxin 4 heterozygous (-/+) knockout mice display defects in both first and second phases of GSIS. Furthermore, islets isolated from transgenic mice over-expressing Syntaxin 4 in the islet secrete approximately 30% more insulin in both phases, implying a positive role for Syntaxin 4 in both first- and second-phase insulin secretion (26). Oddly, Syntaxin 1 over-expressing transgenic mice show insulin resistance with impaired insulin secretion (48). Although the molecular basis for this phenotype is unclear, it has been hypothesized that stoichiometry of particular SNARE proteins in cells is crucial to optimal function in exocytosis.

In contrast to pancreatic beta cells and neuronal cells, neither muscle nor adipose tissues-two of the primary insulin-responsive tissues-express Syntaxin 1, but instead appear to rely upon Syntaxin 4 (21,23,66). Syntaxin 4 (-/+) mice exhibit a blunted insulin-stimulated GLUT4 translocation and decreased glucose uptake into skeletal muscle (49). Consistent with this, transgenic mice over-expressing Syntaxin 4 in skeletal muscle tissue show a two-fold increase in GLUT4 translocation into the sarcolemmal and t-tubule membranes of hindlimb muscle (25). Syntaxin 4 is thus the only syntaxin isoform currently known to be implicated in insulin-stimulated GLUT4 vesicle translocation. Recently, GLUT4

was found to be expressed in the hypothalamus, suggesting that Syntaxin 4 has a role in the brain as well (67). Syntaxin isoforms 2, 3, 5, 6, 7, 8 and 12 are reportedly expressed in adipocytes but not as critical participants in insulin-stimulated GLUT4 vesicle exocytosis (Table 1-1).

1.5.2 SNAP25, SNAP23 and SNAP29

SNAP25, the principal neuronal isoform, is present in the beta cell but absent from muscle and adipose cells (11,34). SNAP23 is also expressed in beta cells, and is capable of compensating for an absence of SNAP25 (68). However, skeletal muscle and adipose express and utilize only SNAP23 (69-71). SNAP29 is also widely expressed (72), though it differs from SNAP23 and SNAP25 in that it binds to intracellularly-localized syntaxin isoforms in addition to the plasma membrane-bound syntaxins (73). SNAP29 has not yet been reported to function in insulin exocytosis or GLUT4 vesicle exocytosis.

1.5.3 The VAMP Family

There are seven currently identified VAMP isoforms, all of which are attached by a C-terminal transmembrane domain to vesicle/granule membranes, including insulin granules, synaptic vesicles, GLUT4-containing vesicles, or ER-Golgi compartments (74). Islet beta cells express VAMP2/synaptobrevin, VAMP3/cellubrevin and VAMP8, with VAMP2 as the predominate isoform required for GSIS (10,17,75). Remarkably, 3T3L1 adipocytes express all VAMP isoforms except for VAMP1 (12), but only VAMP2, VAMP3, and VAMP7 have been directly linked to GLUT4 vesicle exocytosis (58,76). In skeletal muscle, VAMP2, 3, 5 and 7 co-immunoprecipitate with GLUT4 vesicles, and all but VAMP3 translocate to the plasma membrane with GLUT4 in response to contraction (77). In L6 myoblasts, VAMP7/TI-VAMP is expressed and required for both insulin stimulated and osmotic shock triggered-GLUT4 vesicle translocation (78).

1.6 THE SEC1/MUNC18 (SM) PROTEIN FAMILY

In the early 1990's, the yeast Sec1p protein was implicated as a regulator of SNARE assembly and exocytosis, through its ability to directly interact with Syntaxin. Homologues were subsequently identified in *C. elegans* (unc18), *D. melanogaster* (Rop), and mammals [reviewed in (79)]. Collectively, proteins of this type are referred to as 'SM' proteins, for Sec1/Munc18. The mammalian members of this family, Munc18 proteins, are ~66-68 kDa soluble proteins with no apparent transmembrane domain, yet are frequently found at the plasma membrane through direct interaction with their cognate Syntaxins (80,81). Plasma membrane-associated SM proteins present in mammalian cells include Munc18a, Munc18b and Munc18c (also referred to as -1, -2 and -3, respectively); non-plasma membrane-associated mammalian SM proteins are mVps45 and mSly1. Endogenous Munc18a (referred to as Munc18-1 hereafter) and Munc18b bind to the Syntaxin isoforms 1-3, whereas Munc18c binds with high-affinity solely to Syntaxin 4 (Table 1-4).

The regions/residues within the SM proteins that are responsible for syntaxin partnering specificity are still undetermined, remarkable given the degree of similarity that exists amongst Munc18 isoforms (Munc18b and Munc18c show 62% and 51% amino acid identity, respectively, to Munc18-1). Munc18 proteins bind with high affinity to Syntaxin at the plasma membrane (82). However, the Munc18 proteins are soluble and equally abundant in the cytosolic compartment as they are at the membrane, though cytosolic Munc18 proteins are not associated with syntaxins (1,81,83). Munc18 proteins are presumed to localize to the plasma membrane by association with membrane-localized proteins, such that increased expression of Syntaxin 4 selectively attracts Munc18c to the plasma membrane (81). The purpose or function of soluble Munc18 within the cytosolic cellular compartment is currently unknown. Islet beta cells express all three isoforms, while adipocytes and skeletal muscle express only Munc18b and Munc18c (14,84). Depletion studies using RNAi or genetic ablation of either Munc18-1 or Munc18c typically show loss of exocytic

function, indicative of their conserved functional importance in SNARE-mediated exocytosis events (50,55,56).

1.7 MUNC18 AND SNARE PROTEIN MOUSE MODELS: ALTERATIONS OF GLUCOSE HOMEOSTASIS

Reduced protein and/or mRNA levels of Syntaxin 1A, Syntaxin 4 and/or Munc18c have been reported in islets and skeletal muscle of diabetic and obese human patients (85,86). Similarly, rodent models of obesity and diabetes, including the GK rat, Zucker rat, ob/ob and streptozotocin-induced diabetes mouse models exhibit significantly lower levels of these same SNARE isoforms (87-90). In corroborating fashion, numerous knockout and transgenic mouse models selectively targeted for SNARE and Munc18 proteins have defects in glucose homeostasis (Table 1-3). As nearly all of the classic whole-body SNARE and Munc18 protein homozygous knockout mice die either in embryogenesis or at birth, the majority of the current understanding arises from studies utilizing haploinsufficient mouse models. Overall, data generally support the concept that Type 2 Diabetes is a polygenic disease, likely emanating from multiple haploinsufficiencies. Since these are *in vivo* models of altered glucose homeostasis, effects upon whole body homeostasis as well as the tissue-specific effects underlying the whole body phenotypes are discussed together below.

1.7.1 Syntaxin mouse models: Mouse models of Syntaxin 1A protein over-expression (beta cell specific transgenic), Syntaxin 4 protein over-expression (pancreas, skeletal muscle and adipose specific transgenic), Syntaxin 1A and/or Syntaxin 1B deficient and Syntaxin 4 haploinsufficient have been generated, and many characterized for glucose homeostatic control (Table 1.3).

Syntaxin 1: Consistent with clonal cell studies and Syntaxin 1A ablation/interference, islets isolated from classic whole-body Syntaxin 1A knockout mice display impaired first-phase insulin release associated with a decrease in pre-docked granules as determined by total internal reflection fluorescence microscopy (TIRFM) and electron microscopy (EM), and show

normal expression levels of Munc18-1 and Munc18b (19,103). Surprisingly, mice with beta-cell specific over-expression of Syntaxin 1A display fasting hyperglycemia, hypoinsulinemia, and impaired glucose tolerance (48). One possible explanation for this disparate phenotype may be reduced Munc18-1 levels in the Syntaxin 1A over-expressing islets, but the cause of the decreased Munc18-1 is unclear.

Syntaxin 4: Syntaxin 4 homozygous (-/-) null mice die early in embryogenesis, apparently due to a requirement for Syntaxin 4 in the fusion of the GLUT8-containing vesicle with the plasma membrane in the mouse blastocyst (104). However, Syntaxin 4 heterozygous (-/+) knockout mice are viable and exhibit insulin resistance and impaired insulin secretion (49). This insulin resistance is largely due to significantly reduced skeletal muscle glucose uptake and GLUT4 translocation, while the insulin secretion deficit is attributed to decreased first- and second-phase insulin release (26). Notably, in addition to the expected 50% decrease in Syntaxin 4 protein in the Syntaxin 4 (-/+) mouse tissues, Munc18c protein levels were decreased in parallel, while no other protein levels were altered (49). In consistent fashion, Syntaxin 4 over-expressing transgenic mice show a parallel upregulation of endogenous Munc18c protein abundance in the three tissues over-expressing the Syntaxin 4 transgene: adipose, skeletal muscle and pancreas (25). Syntaxin 4 transgenic mice show increased insulin sensitivity, which is likely linked to their increased GLUT4 translocation and enriched GLUT4 deposition in the sarcolemmal and t-tubule membranes of skeletal muscle (25). Islets isolated from Syntaxin 4 transgenic mice also exhibit 30% greater GSIS during both phases (26). These data corroborate studies which correlate reduced Syntaxin 4 and Munc18c protein levels with aberrant insulin action in human and mouse skeletal muscle (85,88). Collectively, these findings raise the possibility that strategies which increase Syntaxin 4 protein levels may coordinately protect against the development of insulin secretion and insulin resistance defects.

Unlike skeletal muscle and islet cells, primary adipocytes do not exhibit significant changes to glucose uptake, either in the Syntaxin 4 over-expressing

Table 1-4 SM-Syntaxin Binding Specificities

	SM Proteins	Syntaxin Partner	Function	Reference
M. musculus	Munc18a/-1	Syntaxin 1, 2, 3	Synaptic vesicle exocytosis	(80)
	Munc18b/-2	Syntaxin 1, 2, 3	Apical membrane trafficking	(91,92)
	Munc18c/-3	Syntaxin 4	GLUT4 vesicle exocytosis, insulin granule secretion	(1,81,93-95)
	mSly1	Syntaxin 5, 18	ER to golgi transport	(96,97)
	mVPS45	Syntaxin 16/Tlg2p	TGN transport	(98,99)
H. Sapiens	Munc18a/-2	Syntaxin 3	Primary neutrophil granule fusion	(100)
	Munc18c/-3	Syntaxin 4	Insulin action in human skeletal muscle	(85,100)
	ND	Syntaxin 1A	Neuronal disorder (migraine predisposition)	(101)
	ND	Syntaxin 7,8	Heterotypic fusion of late endosome	(102)

ND, not determined

transgenic mice or the Syntaxin 4 (-/+) knockout mice (25,49). Although this seemingly contrasts with the earlier 3T3-L1 adipocyte studies implicating Syntaxin 4 in glucose uptake, it is important to note that those early studies utilized a dominant-negative mutant form of Syntaxin 4 to interfere with endogenous VAMP2 trafficking and ablate insulin-stimulated GLUT4 translocation (9), an approach which does not necessarily reflect a requirement for Syntaxin 4. As such, whether or not there is an absolute requirement for Syntaxin 4 in GLUT4 vesicle translocation in adipocytes, or-assuming Syntaxin 4 is required-a minimum "threshold" Syntaxin 4 required, remain questions open for investigation.

1.7.2 Munc18 Mouse Models:

SM proteins in yeast, flies, and worms have been universally characterized as positive and essential regulators of exocytosis events. Moreover, the impairment phenotypes of Munc18-1 (-/+) knockout (50,52) and Munc18c (-/+) knockout (55,56) mouse models indeed support a positive role for these SM proteins in exocytosis events *in vivo* (Munc18-1 and Munc18c homozygous knockouts are lethal). In terms of glucose homeostasis, the Munc18c heterozygous knockout mouse model exhibits glucose intolerance due to peripheral insulin resistance coupled with deficient GSIS (55,56). Insulin-stimulated GLUT4 vesicle translocation in the Munc18c (-/+) hindlimb skeletal muscle was abolished, indicating that Munc18c deficit is likely responsible for the peripheral insulin resistance (55). In terms of GSIS impairment, RNAi-mediated depletion of Munc18c from isolated islets or clonal beta cells in culture recapitulate the defective GSIS seen in the Munc18c (-/+) knockout islets (56). In contrast to previously discussed studies of SM proteins as positive factors in exocytosis, a line of MEF-derived adipocytes from a second Munc18c (-/-) mouse model showed increased GLUT4 presence in plasma membrane subcellular fractions (54). However, since this model consists of derived rather than primary cells or tissues, direct comparisons cannot be made. With regards to the role of Munc18-1 in glucose homeostasis, the Munc18-1 (-/+) mice have yet to be

assessed for defects. However, intriguing data gained by RNAi-mediated depletion of Munc18-1 from clonal beta cells suggest they would likely have defects in GSIS that would contribute to glucose intolerance (105).

A transgenic mouse model of Munc18c protein over-expression in adipose, skeletal muscle and pancreas, akin to the Syntaxin 4 over-expression transgenic mouse model (Table 1-3), exhibits peripheral insulin resistance resulting from impaired insulin-stimulated glucose uptake and GLUT4 vesicle exocytosis, and decreased GSIS (53). This *in vivo* phenotype fully recapitulated data from Munc18c protein over-expression in 3T3-L1 adipocytes, skeletal muscle and islet beta cells (81,93,95,106). Notably, Munc18c transgenic mice and Munc18c (-/+) knockout mice have normal Syntaxin 4 protein abundance, suggesting that Syntaxin 4 expression directs Munc18c expression, but not vice versa (53,55).

The negative effect of SM protein over-expression has been demonstrated in Drosophila (107). The interpretation of these data is that the overly abundant SM proteins bind to and sequester cognate endogenous Syntaxins, preventing interaction with the v-SNARE proteins, and in so doing, impair exocytosis. However, Munc18-1 over-expression in neuronal cells in culture enhances exocytosis (108), and over-expression of Munc18-1 in clonal beta cells has no effect upon insulin secretion [(105); Oh and Thurmond, unpublished results]. With regards to whether SM proteins have a positive or negative role, these disparate results may arise from differential protein abundance and stoichiometry, since over-expression studies rarely control for protein expression level on a per cell basis. Alternatively, the differences may be related to the different types of exocytosis reactions in which Munc18-1 and Munc18c reportedly participate, with Munc18-1 functioning in rapid vesicle release (synaptic neurotransmission and first-phase insulin release) and Munc18c serving in sustained second phase insulin release and GLUT4 vesicle exocytosis events (Table 1-2).

1.7.3 VAMP and SNAP Mouse Models*:*

Of the two v-SNARE isoforms found in insulin-secreting and insulin-responsive cell types, only VAMP3 (-/-) knockout mice have been characterized

for glucose homeostasis. Though VAMP3 was initially implicated in GLUT4 vesicle translocation in 3T3-L1 adipocytes (9,13,109) using dominant-negative and toxin cleavage approaches, VAMP3 null mice show normal insulin and glucose tolerance (58). Insulin-stimulated glucose uptake into adipocytes is normal in these mice, suggesting that VAMP3 is dispensable for GLUT4 translocation, perhaps due to compensation from VAMP2. VAMP2 (-/+) knockout mice thrive while the null mice die immediately after birth (57). Furthermore, calcium-triggered synaptic vesicle exocytosis in neurons of VAMP2 haploinsufficient mice is significantly impaired, and given the numerous overlaps between this neuronal process and that of first-phase insulin release from the beta cell, it is anticipated that VAMP2 would be required for glucose homeostasis *in vivo*, provided it remains the only other v-SNARE protein in these tissue types. VAMP8 (-/-) knockout mice survive and have apparent defects in pancreatic acinar cell zymogen granule content and platelet secretion (59,60), although they have yet to be characterized for glucose homeostasis.

Although SNAP25 homozygous (-/-) knockout mice fail to thrive beyond birth, studies conducted using embryonic and fetal tissue have a demonstrated lack of evoked synaptic vesicle exocytosis (61). While SNAP25 and SNAP23 heterozygous (-/+) knockout mice do thrive, no characterizations of potential effects upon whole body glucose homeostasis or insulin release from isolated islets are reported to date.

1.8 MUNC18-SYNTAXIN COMPLEXES: MOLECULAR MECHANISMS

1.8.1 Protein-protein Interaction Studies-*In Vitro*:

The functional *in vivo* models and cell-based studies of SM and Syntaxin proteins indicate that SM-Syntaxin coupling is the key to understanding exocytosis events, and is pertinent to many diseases. By 1999, the first structures of Munc18-1 bound to Syntaxin 1A were obtained, solved using crystallographic and NMR approaches (110-112), where Munc18-1 was seen to hold Syntaxin in a ‘closed’ conformation in a 1:1 stoichiometric complex, and interpreted as a conformation precluding Syntaxin participation in SNARE core

complex assembly (modeled in Figure 1-4A). Studies of SNARE proteins in cell and tissue lysates support this model, along with *in vitro* ultracentrifugation studies showing the exclusion of Munc18-1/nSec1 protein from the SNARE core complex (113). More recently, the Munc18c isoform has been co-crystallized with the N-terminal 19 residue peptide of Syntaxin 4, indicating the importance of this particular site for protein-protein interaction (114). While it was initially argued that this interaction fostered a new conformation (modeled in Figure 1-4B), subsequent studies in adipocytes have cast doubt on its relative importance in relevant exocytosis events (115).

A third binding mode has recently been proposed, whereby the SM protein associates with the four alpha-helical bundle comprised by the SNARE core complex (modeled as Figure 1-4C). Support for this new binding mode comes from *in vitro* reconstitution assays using recombinant Munc18-1, Syntaxin 1A, SNAP-25 and VAMP2 proteins (116). This model relies upon the hypothesis that Munc18-1 functions principally as a positive and necessary factor to promote exocytosis, consistent with the mouse model data. The latest mechanistic hypothesis incorporates the SNARE binding protein Complexin (117,118). Complexins (CPXs), also named synaphins, were originally described in neuronal cells to play an essential role in Ca^{2+}-dependent neurotransmitter release (119-121). *In vitro*, complexins bind to assembled heterotrimeric SNARE complexes (122). However the question of whether they promote or inhibit SNARE-regulated exocytosis is unresolved due to conflicting *in vivo* data (123). Complexins do not appear to bind individual SNARE proteins, but a recent study shows that CPX1 can bind to Syntaxin/SNAP25 binary complexes (124). Furthermore, it has been reported that Munc18-1 and CPX1 can bind simultaneously to the SNARE complex (125). Complexin expression in beta cells was noted prior to the emergence of the current mechanistic model (126), and as such its linkage to the insulin exocytosis mechanism has not yet been determined.

Detection of Munc18-SNARE complex association, as depicted in Figures 1-4B and C, requires low-stringency assay conditions, where little to no detergent

is included (<0.1% Triton X-100). In contrast, older titration studies performed under higher stringency conditions demonstrated the ability of Munc18-1 to displace SNAP25 and VAMP2 from Syntaxin 1 (80,127,128). Similarly, Munc18c reduces the binding of SNAP23 to Syntaxin 4 in a concentration-dependent manner when evaluated in 1% Triton X-100 solubilized cell lysates (69), yet under low-stringency detergent conditions Munc18c binding to Syntaxin 4-bound SNARE core complexes was detected (129). While the benefit of low-stringency buffers has enabled detection of the otherwise elusive transient docking complex, co-immunoprecipitation data obtained from cell or tissue lysates currently supports only Model A (Figure 1-4A). Interestingly, a novel immunofluorescent approach conducted in cells supports the concept of an intermediate transition complex of Syntaxin 1 bound simultaneously to Munc18-1 and SNAP25, and that the addition of VAMP2 subsequently displaced Munc18-1 (130). Biochemical validation of the formation of this and the macromolecular complexes in Models B and C by endogenous proteins in these cell types awaits further investigation. Ultrastructural analyses of Munc18-1 in complex with Syntaxin 1A (110), and Munc18c complexed with the N-terminal peptide of Syntaxin 4 (but not the entire soluble region of Syntaxin 4 protein) (114), have yielded considerable insight into the potential function(s) of these complexes. Syntaxin 4 contains four cytosolic alpha helices: from the N-terminus the domains are Ha, Hb, Hc, and H3, followed by a transmembrane domain, as determined by its homology to Syntaxin 1. The C-terminal H3 domain is the canonical SNARE protein motif which participates in the SNARE core complex (111), and based upon homology, the bundled coils of Syntaxin 4 are predicted to fit into the cleft of an arch/crescent-shaped Munc18c (Figure 1-5A). The Hc and H3 domains are connected by a flexible linker region believed to catalyze syntaxin's transition from a 'closed' to an 'open' conformation, with the open form being active for engagement in the SNARE core complex. The N-terminal peptide of Syntaxin 4 fits into a small pocket near the top of the overall Munc18c "crescent" shape (114), although the sufficiency of this region to confer binding of Syntaxin 4 to Munc18c has been refuted. The minimal binding region of Syntaxin 4 needed to

confer to Munc18c remains unknown. Moreover, mutations in Munc18c which significantly impair binding to Syntaxin 4 are situated at the apex of the crescent (1,2,115), distanced from the arched cleft, and in close proximity to the binding sites for Doc2β and the Syntaxin 4 N-terminal peptide (Figure 1-5B). The significance of Doc2β is discussed in a subsequent section.

1.8.2 Protein-protein Interaction Studies in Cells and Tissues-Impact of Post-Translational Modifications:

Munc18-Syntaxin complexes are regulated through post-translational modifications, including serine/threonine phosphorylation, tyrosine phosphorylation, O-linked glycosylation, and nitrosylation of either or both proteins. Serine phosphorylation of Munc18-1 by protein kinase C and/or threonine phosphorylation by Cdk5 (cyclin-dependent kinase 5) disrupts Munc18-Syntaxin interaction and promotes secretory granule exocytosis (131-135). Munc18c has been shown recently to be phosphorylated by protein kinase C, causing dissociation from Syntaxin 4 and increasing SNARE complex assembly in pancreatic acinar cells (136). Syntaxin 1A can also be phosphorylated at serine by the death-associated protein kinase (DAPK), which significantly decreases its interaction with Munc18-1 (137). The catalytic subunit of the serine/threonine phosphatase protein 2B (PP2B) has been shown to directly interact with Munc18c in human umbilical vein endothelial cells (HUVECs) (138).

While serine/threonine phosphorylation of Munc18 or Syntaxin isoforms in insulin-secreting or insulin-responsive cell types has yet to be demonstrated, both proteins can undergo tyrosine phosphorylation in a stimulus-dependent manner. In clonal MIN6 beta cells, Munc18c becomes tyrosine phosphorylated at residue Tyr219, and as a result dissociates from Syntaxin 4 (95,139). In 3T3-L1 adipocytes, Munc18c residue Tyr521 was modified in response to either insulin or PDGF stimulations (140,141). Interestingly, Tyr521 resides in a disordered region, though prediction mapping places it in close proximity to Tyr219 (Figure 1-5B), suggesting that this vicinity of Munc18c may be an important site for stimulus-induced conformational changes. In addition, Syntaxin

4 becomes phosphorylated at residues Tyr115 and Tyr251 in insulin-stimulated 3T3-L1 adipocytes (140). Remarkably, Syntaxin 4 does not appear to undergo tyrosine phosphorylation in clonal beta cells (95). Syntaxin 1A was recently shown to become S-nitosylated at Cys145 decreasing its binding to Munc18-1 *in vitro (142).* Furthermore, Munc18c can be modified by O-linked glycosylation in 3T3-L1 adipocytes under insulin-resistant conditions caused by glucosamine, concurrent with impaired insulin-stimulated GLUT4 translocation (143) and deficient Munc18c localization to the plasma membrane (144).

1.8.3 Impact of Additional Binding Partners on SM-Syntaxin Interactions:

While *in vitro* studies are invaluable for detailing kinetic and binding site information, cellular studies have elucidated a major role for post-translational modifications in how the SM-syntaxin complexes associate and dissociate. Moreover, SM-syntaxin complex accessory proteins which are relevant to insulin secretion and insulin action have been identified, as discussed below.

Doc2β: As a soluble 45 kDa double C2 domain-containing protein Doc2β, is expressed in adipocytes and islet beta cells, and exerts positive effects upon GLUT4 vesicle and insulin granule exocytosis events, respectively (139,145-147). In islet beta cells, Doc2β protein over-expression increases GSIS by ~40%, and the siRNA-mediated depletion of Doc2β attenuates insulin release (146,147), with similar effects observed in 3T3-L1 adipocytes (145). Doc2β can mediate similar outcomes in synaptic vesicle exocytosis through association of its first C2 binding domain (C2A) with Munc18-1 (148). In islet beta cells, the second C2 domaiṇ (C2B) mediates its association with residues 173-255 of Munc18c, including the regulatory Y219 phosphorylation site (146). Whether or not this is somehow linked to Doc2β association remains untested. Doc2β effectively competes with Syntaxin 4 for Munc18c binding, and its endogenous association with Munc18c is required for GSIS. In contrast, it has been suggested that Doc2β instead exerts its effects through interaction with Syntaxin 4 in a calcium-dependent manner (147). Although calcium was present in both beta cell studies,

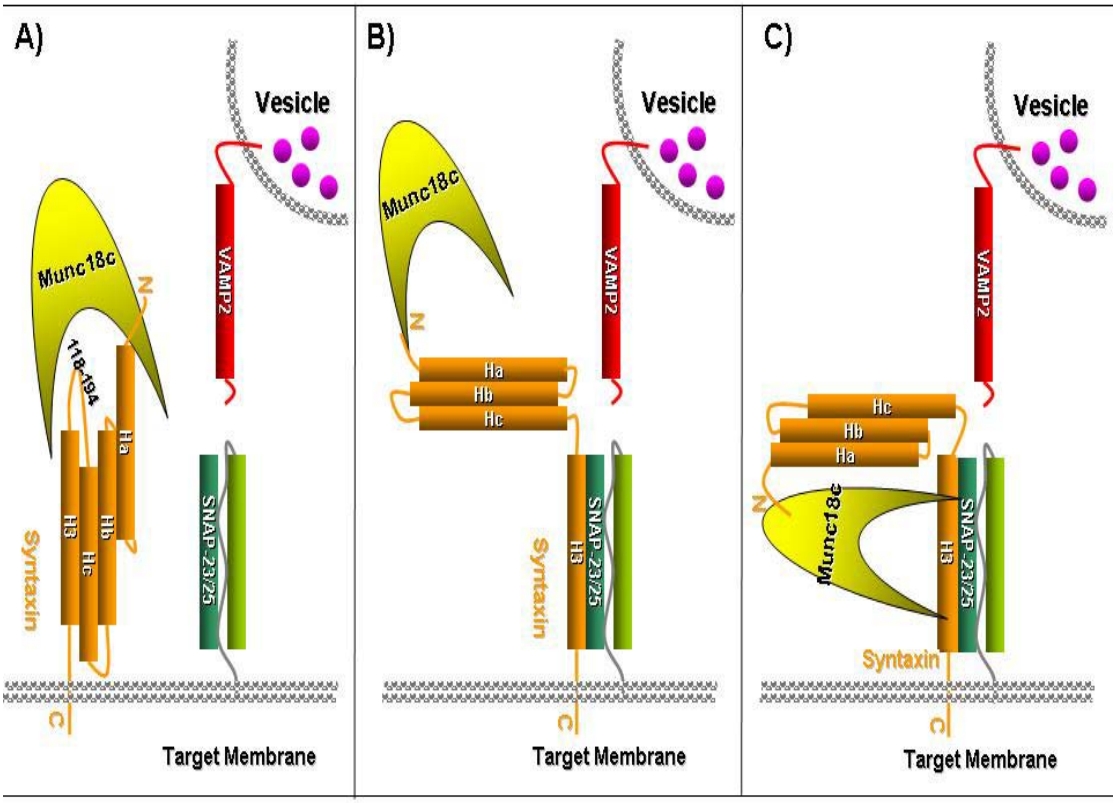

Figure 1-4 Proposed models of Munc18c-Syntaxin 4 Interaction. (A) Unstimulated state model of Munc18 holding Syntaxin in a 'closed' conformation which in turn inhibits Syntaxin from being able to participate in the SNARE tertiary complex, thus inhibiting exocytosis. (B) A new model in the field derived from *in vitro* data; in stimulated state Munc18 remains bound to 'open' Syntaxin at the N-terminus allowing Syntaxin to participate in the SNARE core complex. (C) Munc18 interacts with the SNARE core complexes through the four α-helical bundle.

methodological differences such as use of low stringency binding conditions, use of calcium-chelators, and use of a transmembrane-containing insoluble syntaxin protein may have permitted detection of Syntaxin 4 association with Doc2β (145,146). Alternatively, a very recent report shows that Doc2β interacts directly with the SNARE complex (149). Thus, while there is full agreement that Doc2β plays a positive role in Syntaxin 4-mediated exocytosis, details of the underlying mechanism must await further examination.

Munc13-1: Munc13-1 is a soluble 200 kDa protein expressed in pancreatic islet beta cells (86,150), but not in adipocytes or skeletal muscle. Munc13-1 is composed of one C1 and two C2 domains which mediate phorbol ester and diacylglycerol binding and phospholipid-dependent Ca^{2+} binding, respectively. Munc13-1 can pair directly with Munc18-1, Doc2β or Syntaxin 1A (148,151). Munc13-1 over-expression amplifies insulin secretion and is proposed to function in granule priming (150). Reduced expression of Munc13-1 is observed in islets isolated from diabetic humans or Zucker fa/fa rats (86,150), consistent with glucose intolerance and the deficient insulin release characteristics of Munc13-1 (-/+) knockout mice (152), and is therefore believed to have a required role in insulin exocytosis.

WNK1: A unique member of the serine/threonine kinase family, WNK1 (**W**ith **N**o **K** (lysine)) has been linked to the inherited hypertension syndrome Pseudohypoaldosteronism II (153,154). WNK1 is a soluble 230 kDa kinase expressed in 3T3-L1 adipocytes and islet beta cells (155,156), and is a Munc18c binding protein (157). WNK1 and Munc18c associate via direct interaction of the N-terminal 172 residues of Munc18c (distinct from residues bound by Doc2β and the kinase domain of WNK1, and competitive inhibition of this complex impairs Syntaxin 4-mediated insulin granule exocytosis (157). Also, WNK1-Munc18c complexes are found localized to the plasma membrane, though complexes are also found in the cytosol, a unique feature amongst Munc18c binding proteins to date. There are two other unique features of this complex: *1)* despite the

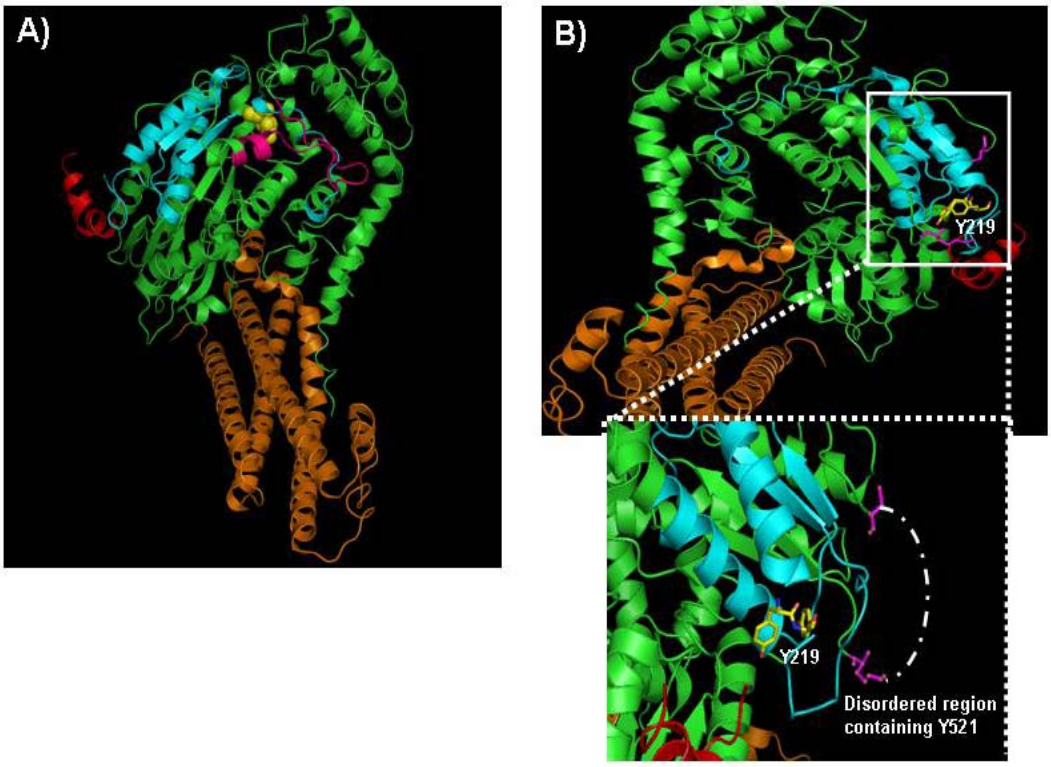

Figure 1-5 Modeling of Munc18c-Syntaxin 4 interaction. *(A)* Depicting full length Munc18c (green) interacting with Syntaxin 4 (orange). The peptide termed 18c/pep3 (residues 460-483) is illustrated in pink and arginine 240 shown in yellow; both have been shown to play important roles in Munc18c-Syntaxin 4 interaction (1,2). *(B)* Upper panel-Munc18c Tyr219 sits in the Doc2β binding region on Munc18c (blue) juxtaposed to the binding cleft for the N-terminus of Syntaxin 4 (red). Lower panel-enlarged view of the boxed region, illustrating the close proximity between Tyr219 and Tyr521, though Tyr521 is not present in the crystal structure due to its location within a disorder region (drawn into the model with white dashed line).

requirement for the kinase domain of WNK1, its intrinsic kinase activity is apparently dispensable for interaction (i.e. Munc18c does not serve as a WNK1 substrate); *2)* siRNA-mediated WNK1 depletion does not affect insulin secretion from clonal beta cells nor glucose uptake into adipocytes (155), complicating specific designation of its role in exocytosis events pertinent to glucose homeostasis.

80K-H: The 80K-H protein (80 kDa) was originally identified as a PKCζ binding partner and is widely expressed, especially at the plasma membrane of insulin-sensitive 3T3L1 adipocytes and L6 myotubes (158). 80K-H has been implicated in vesicle trafficking events via a close relationship to the protein VASAP-60 (159), and in GLUT4 vesicle transport through its ability to interact with both Munc18c and PKCζ in an insulin-dependent manner (158,160). The requirement of 80K-H in glucose uptake *in vivo* and/or primary cells and its putative role as a signaling link between PKCζ and Munc18c awaits further investigation.

Rab3A: Rab proteins are a large family of small GTPases responsible for the regulation of many membrane trafficking events and are thought to participate in insulin exocytosis as well as GLUT4 vesicle exocytosis through interaction with Munc18-Syntaxin complexes. However, despite efforts over the past decade, only Rab3A, a Munc18-1 binding protein, has been identified to date (161), with no Munc18c binding candidate to modulate insulin action as of yet. Rab3 null mice exhibit glucose intolerance coupled to ablated first-phase insulin release but without insulin resistance (162), consistent with its role as solely a Munc18-1 and not a Munc18c binding factor.

Synip: Synip (syntaxin-interacting protein) is a 62 kDa protein that was initially discovered as a novel Syntaxin 4-binding protein and has been implicated in the control of glucose transport and GLUT4 vesicle translocation in 3T3-L1 adipocytes (163). It binds only to the Syntaxin 4 isoform in an insulin-sensitive manner. This mechanism appears to function through Synip phosphorylation at

Ser99 in response to activation of Akt2, and subsequent dissociation from Syntaxin 4 to promote GLUT4 vesicle exocytosis (164,165), although this is a disputed finding (166). Synip expression in βHC-9 clonal beta cells has also been reported and a role for it implicated in Syntaxin 4-mediated insulin exocytosis using an over-expression paradigm (167). Synip knockout mice or RNAi-mediated knockdown data will be required to determine if Synip is necessary during Syntaxin 4-based exocytosis events relevant to glucose homeostasis.

Tomosyn and Cab45b: Tomosyn proteins are syntaxin binding factors, with 7 different isoforms expressed from two genes, Tomosyn-1 and Tomosyn-2 (168). b-Tomosyn-1 (b=big), a cytosolic protein, was identified as a Syntaxin 4-binding partner in 3T3-L1 adipocytes, and its over-expression inhibited GLUT4 translocation to the plasma membrane (169). Similarly, in beta cells depletion of an analogous Syntaxin 1A binding isoform of Tomosyn-1 was found to decrease stimulated exocytosis (170). In contrast, depletion of a related m-tomosyn-1 (m=medium) isoform (which also binds to Syntaxin 1A) in clonal beta cells was shown to increase insulin release while over-expression was inhibitory, suggesting that it functions as a negative regulator of insulin exocytosis (171). Although tomosyn-1 knockout mice exist and have enhanced synaptic transmission (172), the mice are not yet characterized for effects upon glucose homeostasis, and it remains unclear which isoforms are ablated.
Cab45b: was recently identified as a soluble 42 kDa calcium binding protein associated with Munc18b in pancreatic islet beta cells (22). In clonal INS-1E beta cells, antibody-mediated interference of endogenous Cab45b or RNAi-knockdown of Munc18b expression reduced depolarization-evoked membrane capacitance, implicating potential roles for each protein in insulin exocytosis.

1.9 Novel Roles for Munc18 and Syntaxin Proteins in Granule Mobilization and Pool Refilling

New evidence suggests that non-traditional roles exist for SM and syntaxin proteins in exocytosis. Both Munc18-1 and Munc18c (-/+) knockout mouse models reveal the necessity of these proteins in granule localization to the plasma membrane (56,108). Munc18-1-depleted clonal beta cells also exhibit defective docking of insulin granules to the plasma membrane (105). Although this might suggest that the soluble fraction of SM proteins somehow directs granule mobilization through the cytoskeletal matrix, preliminary *in vitro* F-actin binding studies argue against Munc18c protein as a direct binding factor of F-actin (Kalwat and Thurmond, unpublished results). Syntaxin 1A can co-immunoprecipitate with F-actin in beta cell lysates and dissociate transiently in response to glucose stimulation (29). Syntaxin 4 can also associate with α-fodrin, an F-actin binding factor, in primary rat adipocytes (173). Given that Syntaxin 4 and Munc18c in particular, are required for the mobilization phase of insulin exocytosis, and are also responsible for the relatively long-range trafficking of GLUT4 vesicles in adipocytes and myocytes, future exploration regarding their interactions with cytoskeletal elements is required. However, it is important to note that stimulus-induced actin remodeling appears to be different for exocytosis in beta cells than it is in adipocytes and myocytes. Current data suggest that disruption of the actin cytoskeleton using agents such as Latrunculin in beta cells potentiates insulin exocytosis, but in adipocytes inhibits GLUT4 vesicle exocytosis (29,174-177).

1.10 HYPOTHESIS

Type 2 diabetes involves specific defects of glucose-stimulated insulin secretion from the pancreatic beta cells in addition to defects in peripheral tissue insulin action required for glucose uptake. Both of these processes, insulin secretion and glucose uptake, are mediated by SNARE protein core complexes composed of Syntaxin, SNAP-23/25, and VAMP proteins. The SNARE core complex is regulated by the Sec1/Munc18 (SM) family of proteins, which

selectively bind to their cognate Syntaxin isoforms with high affinity. The process of insulin secretion utilizes multiple Munc18-Syntaxin isoform pairs, whereas insulin action in the peripheral tissues appears to utilize only the Munc18c-Syntaxin 4 pair. Importantly, recent reports have linked obesity and Type 2 diabetes in humans with changes in protein levels and single nucleotide polymorphisms (SNPs) of Munc18 and Syntaxin isoforms relevant to these exocytotic processes, although the molecular mechanisms underlying the observed phenotypes remain incomplete (85,178,179). Given the conservation of these proteins in two seemingly disparate processes, and the need to design and implement novel and more effective clinical interventions, it will be vitally important to delineate the mechanisms governing these conserved SNARE-mediated exocytosis events. Thus, the central hypothesis proposed in this thesis is that Syntaxin 4-Munc18c complexes are modulated by post-translational modifications and novel interactions. This hypothesis was tested by using complementary *in vitro*, cell-based approaches, and animal tissue extracts to detail protein modifications and protein-protein interactions that impact SNARE core complex assembly and vesicle exocytosis mechanisms. The rationale for the proposed research is that once the mechanisms regulating the function of Munc18c in Syntaxin 4-mediated vesicle exocytosis are established, it will become possible to modulate the complex for therapeutic purposes, either pharmacologically or through molecular based strategies.

CHAPTER 2: THE TYROSINE PHOSPHORYLATION OF MUNC18C INDUCES A SWITCH IN BINDING SPECIFICITY FROM SYNTAXIN 4 TO DOC2β

Some of the text in this Chapter is reproduced from:

Jewell JL, Oh E, Bennett SM, Meroueh S, and Thurmond DC. (2008) The Tyrosine Phosphorylation of Munc18c Induces a Switch in Binding Specificity from Syntaxin 4 to Doc2β. *J Biol. Chem* 283: 21734-46

Author Contributions: Oh E generated data for Figures 2-2B, 2-2C and 2-7C. Bennett SM produced data for Figure 2-9. Meroueh S produced data for Figures 2-9 and 2-10. The rest of the Figures and text were generated by Jewell JL.

2.1 INTRODUCTION

While genetic models of Munc18c over-expression (53) and under-expression (54,55) have both unequivocally substantiated Munc18c as a key and physiologically-relevant regulator of glucose homeostasis by its impact upon Syntaxin 4-mediated exocytosis, how it transiently interacts with Syntaxin 4 in a stimulus-dependent manner remains unclear. For example, it remains to be resolved just what contacts of the Syntaxin molecule are sufficient to confer its interaction with Munc18. There is general consensus that the N-terminal 20-30 residues of syntaxins are important for fostering interaction with Munc18 proteins (97,180,181), and it is suggested that it is through this region that Munc18 proteins remain associated with the SNARE core complex (114). However, that this N-terminal region of Syntaxin 4 can independently confer binding specificity to the Munc18c isoform, as opposed to binding Munc18a or Munc18b (Munc18a and Munc18b specifically bind Syntaxin isoforms 1-3) has been disputed. Thus, it has been suggested there are likely alternate or additional residues required to support and specify the association (114,115).

Consistent with the dissociation model put forth by Zilly *et al* (130), Munc18c-Syntaxin 4 association can be significantly reduced upon the stimulus-induced phosphorylation of residue Y219 of Munc18c (95). We have since determined that a region of Munc18c containing this particular residue is sufficient to confer binding to the C2 domain-containing protein Doc2β, which is localized at the plasma membrane in islet beta cells and adipocytes (146). Syntaxin 4 was excluded from the Munc18c-Doc2β complex, suggesting that some type of “switch mechanism” occurs for transitions between Munc18c-Doc2β and Munc18c-Syntaxin 4 complex formation. In the present study we have examined the minimal binding region of Syntaxin 4 as well as the protein-protein interactions amongst Munc18c and its binding partners Syntaxin 4 and Doc2β to test the validity of such a ‘switch mechanism.’

2.2 MATERIALS AND METHODS

2.2.1 Materials

Rabbit anti-Munc18c antibody was generated as previously described (81). Rabbit polyclonal anti-Syntaxin 4 and N-terminal Syntaxin 4 peptide (residues 2-23) were obtained from Chemicon (Temecula, CA). Antibodies raised against SNAP-23, VAMP2, and phosphotyrosine (4G10) were obtained from Affinity BioReagents (Golden, CO), Synaptic Systems (Göttingen, Germany) and Upstate Biotechnology (Lake Placid, NY), respectively. Rabbit polyclonal anti-Doc2β antibody was a generous gift from Dr. Matthijs Verhage (Vrije Universiteit, Netherlands). Rabbit and mouse anti-GFP antibodies were acquired from Abcam (Cambridge, MA) and Clontech Laboratories (Mountain View, CA), respectively. Protein G plus agarose was obtained from Santa Cruz Biotechnology (Santa Cruz, CA). The MIN6 beta cells were a kind gift from Dr. John Hutton (University of Colorado Health Sciences Center). Goat anti-mouse and anti-rabbit horseradish peroxidase secondary antibodies and Transfectin lipid reagent were acquired from Bio-Rad (Hercules, CA). Monoclonal Flag antibody, radioimmunoassay grade bovine serum albumin and D-glucose were purchased from Sigma (St. Louis, MO). Enhanced chemiluminescence (ECL) and SuperSignal West Femto reagents were obtained from Amersham Biosciences (Pittsburgh, PA) and Pierce (Rockford, IL), respectively. The human C-peptide RIA kit was purchased from Linco Research Inc (St. Charles, MO).

2.2.2 Plasmids

The generation of pcDNA3.1-flag-Munc18c, pET28a (+)-His-Munc18c and pGEX-Munc18c plasmids has been previously described (81,146,157). The TAP-Munc18c DNA constructs were generated by subcloning a PCR-generated Munc18c fragment into the XhoI and ClaI sites of the pNTAP and pCTAP shuttle vectors (Stratagene) for adenoviral particle production by Viraquest (North Liberty, IA). The pGEX-4T1-Syntaxin 4-(1-193), -(1-112), and -(1-70) DNA constructs were generated by subcloning PCR-generated rat Syntaxin 4 fragments into the SalI and XhoI restriction sites of the pGEX-4T1 expression

vector (GE Healthcare). The pGEX-4T1-Syntaxin 4-(1-273), -(39-273), -(118-193), -(71-273), and -(113-273) DNA constructs were made by subcloning PCR-generated rat Syntaxin 4 fragments into the EcoRI and XhoI sites of the pGEX-4T1. The pEGFP-C2-Syntaxin 4-(118-193) DNA construct was generated by digesting the fragment from pGEX-4T1-Syntaxin 4-(118-193) with EcoR1 and XhoI and subcloning into the EcoRI and SalI sites of the pEGFP-C2 vector (BD Biosciences Clontech, San Jose, CA).

2.2.3 Cell Culture, Transient Transfection and Secretion Assays

MIN6 beta cells were cultured in Dulbecco's modified Eagle's medium (DMEM with 25 mM glucose) supplemented with 15% fetal bovine serum, 100 units/ml penicillin, 100 µg/ml streptomycin, 292 µg/ml L-glutamine, and 50 µM β -mercaptoethanol as described previously (146). MIN6 beta cells at 50-60% confluence were transfected with 40 µg of plasmid DNA per 10 cm^2 dish using Transfectin (Bio-Rad) to obtain ~50% transfection efficiency. After 48 h of incubation, cells were washed twice with and incubated for 2 hours in freshly prepared modified Krebs-Ringer bicarbonate buffer (MKRBB; 5 mM KCl, 120 mM NaCl, 15 mM Hepes pH 7.4, 24 mM $NaHCO_3$, 1 mM $MgCl_2$, 2 mM $CaCl_2$ and 1 mg/ml RIA-grade BSA). Cells were stimulated with 20 mM glucose or 0.1 mM pervanadate for the times indicated in the figures. Cells were subsequently lysed in Nonidet NP-40 lysis buffer (25 mM HEPES pH 7.4, 1% NP-40, 10% glycerol, 50 mM sodium fluoride, 10 mM sodium pyrophosphate, 137 mM sodium chloride, 1 mM sodium vanadate, 1 mM phenylmethylsulfonyl fluoride, 10 µg/ml aprotinin, 1 µg/ml pepstatin and 5 µg/ml leupeptin), and lysates were cleared by microcentrifugation for 10 min at 4^oC for subsequent use in co-immunoprecipitation experiments. For measurement of human C-peptide release, MIN6 beta cells were transiently co-transfected with each plasmid plus human proinsulin cDNA, (gift from Dr. Chris Newgard, Duke University), using Transfectin with 2 µg of each DNA per 35 mm dish of cells. Forty-eight hours following transfection, cells were pre-incubated for 2 hours in MKRBB buffer and

stimulated with 20 mM glucose for 1 hours and buffer collected for quantitation of human C-peptide released.

CHO-K1 cell stocks were purchased from the American Type Culture collection (Manassas, VA) and cultured in Ham's F-12 medium supplemented with 10% fetal bovine serum, 100 U/ml penicillin, 100 µg/ml streptomycin and 292 µg/ml L-glutamine. At 80-90% confluence, cells were electroporated with 40 µg DNA as previously described (81) and incubated for 48 hours. Detergent cell lysates were prepared by harvesting in 1% NP40 lysis buffer and lysates cleared by centrifugation at 14,000 x g for 10 min at 4^{o}C for use in co-immunoprecipitation experiments.

2.2.4 Tandem Affinity Purification (TAP)

The InterPlay Adenoviral TAP System (Stratagene, La Jolla, CA) was used for precipitation of Munc18c-associated proteins from MIN6 beta cells. NTAP-Munc18c contained two N-terminal affinity tags: a streptavidin binding peptide (SBP) and a calmodulin binding peptide (CBP), the same tags were present at the C-terminus of CTAP-Munc18c. MIN6 beta cells were transduced using pNTAP-Munc18c or pCTAP-Munc18c CsCl-purified adenoviral particles as described previously (182). Cells were harvested in the manufacturer's lysis buffer containing 0.1% Triton X-100, or in this buffer containing additional detergent (1% Triton X-100 final concentration). The cells were subjected to three successive rounds of freeze-thawing and centrifuged at 16,000 x g for 10 min for collection of supernatant. Supernatants were incubated with streptavidin resin followed by washes with lysis buffer (0.1% Triton X-100) and elution. Eluates were then subjected to a second purification over calmodulin resin. Column flow-through was collected (FT). Purified TAP-Munc18c and associated proteins were eluted and resolved by 12% SDS-PAGE for immunoblotting.

2.2. 5 Subcellular Fractionation

Briefly, MIN6 beta cells at 80-90% confluence were harvested into 1 ml of homogenization buffer (20 mM Tris-HCl, pH 7.4, 0.5 mM EDTA, 0.5 mM EGTA,

250 mM sucrose, 1 mM DTT and 1 mM sodium orthovanadate containing the protease inhibitors leupeptin (10 µg/ml), aprotinin (4 µg/ml), pepstatin (2 µg/ml) and PMSF (100 µM). Cells were disrupted by 10 strokes through a 27 gauge needle and homogenates were centrifuged at 900 x g for 10 min. Plasma membrane fractions (PM) were obtained by mixing the postnuclear pellet with 1 ml of Buffer A (0.25 M Sucrose, 1 mM $MgCl_2$ and 10 mM Tris-HCl, pH 7.4) and 2 volumes of Buffer B (2 M sucrose, 1 mM $MgCl_2$ and 10 mM Tris-HCl, pH 7.4). The mixture was overlaid with Buffer A and centrifuged at 113,000 x g for 1 h to obtain an interface containing the plasma membrane fraction. Interface was collected and diluted to 2 ml with homogenization buffer for centrifugation at 6,000 x g for 10 min, and the resulting pellet was collected as the plasma membrane fraction. Pellets were resuspended in 1% NP-40 lysis buffer to solubilize membrane proteins.

2.2.6 Co-immunoprecipitation and Immunoblotting

MIN6 beta cells were pre-incubated in MKRBB for 2 hours followed by glucose stimulation or treatment with 0.1 mM pervanadate. Pervanadate was made immediately prior to use by combining 1 mM sodium orthovanadate with 3 mM hydrogen peroxide for 15 minutes. Cells were subsequently lysed in 1% NP-40 lysis buffer. MIN6 beta cell cleared detergent lysates (2-4 mg) were combined with primary antibody for 2 hours at 4^{o}C followed by a second incubation with protein G Plus-agarose for 2 hours. The resultant immunoprecipitates were subjected to 10% or 12% SDS-PAGE followed by transfer to PVDF membranes for immunoblotting: Munc18c and VAMP2 antibodies were used at 1:5,000; Syntaxin 4, Doc2β, SNAP-23, and 4G10 antibodies were used at 1:1,000; Flag and EGFP antibodies were used at 1:2,000 and 1:800, respectively. Secondary antibodies conjugated to horseradish peroxidase were diluted at 1:5,000 for all except for phosphotyrosine, which was used at 1:2,000 for visualization by ECL for detection using a Chemi-Doc documentation imaging system (Bio-Rad).

2.2.7 Recombinant Proteins and Interaction Assays

The pGEX fusion constructs were transformed into *E. coli* for expression of all GST fusion proteins and purified by glutathione-agarose affinity chromatography as described previously (163). Recombinant fragments of Syntaxin 4 were obtained following thrombin cleavage and capture (Novagen). Recombinant His-tagged Munc18c was expressed in *E. coli* and purified by Ni-NTA nickel-chelating resin (Invitrogen) under native conditions (50 mM NaH_2PO_4, 0.5 M NaCl). Eluted protein was further dialyzed overnight in 50 mM Tris pH 8.0 supplemented with 1 mM DTT. *In vitro* GST interaction assays were conducted by incubating GST-fusion proteins linked to sepharose beads with recombinant purified proteins for 2 hours at 4°C in NP-40 lysis buffer, followed by three stringent washes with lysis buffer, and interacting proteins eluted from the beads and resolved on 10% or 12% SDS-PAGE followed by transfer to PVDF membrane for immunoblotting. The Syntaxin accessibility assay using GST-VAMP2 was performed similarly but using cleared detergent cell lysates instead of recombinant protein.

2.2.8 Surface Plasmon Resonance

The binding kinetics for the interaction between Syntaxin 4-(1-273) and Syntaxin 4-(118-194) with Munc18c was determined by surface plasmon resonance using a BIAcore3000 instrument (Biacore AB, Uppsala, Sweden). Syntaxin 4-(1-273) and Syntaxin 4-(118-194) were diluted in acetate buffer at pH 4.5 and immobilized on a CM5 sensor chip with amine coupling. The surface was activated by injecting a solution containing 0.4 M N-ethyl-N'-dimethylaminopropyl carbodimide (EDC) and 50 mM N-hydroxysuccinimide (NHS) for a 7 minutes flow rate of 5 µl/min (183). Syntaxin 4 was then injected and the surface was subsequently blocked with 1 M ethanolamine at pH 8.5 for 7 minutes. The target for final immobilization levels was 1,000 resonance units (RUs), corresponding to approximately 1 ng of Syntaxin 4/mm^2 (184). Munc18c was injected over the flow cell at 30 µl/minutes for 2 minutes and allowed to dissociate for 3 minutes. To determine the association (k_{on}) and dissociation (k_{off})

rate constants, Munc18c was injected at seven concentrations (0, 1.7, 3.3, 6.7, 13.3, 26.7, and 53.3 nM) ranging from 0 to 53.3 nM. Between cycles, the surface was regenerated with 10 µl of 0.15 M acetic acid, 0.5 M NaCl. The data was then fitted to a 1:1 (Langmuir) binding model using the BiaEvaluation software. It was found that mass transfer was not a factor in Munc18c binding to Syntaxin 4. All experiments were conducted in HBS-EP running buffer (0.01 M HEPES, pH 7.4, 0.15 M NaCl, 3 mM EDTA, 0.005% surfactant P20) with Munc18c storage buffer added to a 1:50 dilution at 25°C.

2.2.9 Computer Modeling

The three-dimensional structure of the Syntaxin 4/Munc18c complex was guided by the crystal structure of the Syntaxin 1A/Munc18 complex (PDB code 1DN1) and the crystal structure of Munc18c (PDB code 2PJX). A homology model of Syntaxin 4 was constructed using SwissModel based on the crystal structure of Syntaxin 1a. The Syntaxin 4/Munc18c complex was constructed by superimposing these proteins onto their homologs in the Syntaxin 1A/Munc18 complex. This was carried out with the computer program PyMol. All representations of three dimensional structures in the manuscript were generated with PyMol.

2.2.10 Statistical Analysis

All data are expressed as mean ± S.E. Data were evaluated for statistical significance using an unpaired two-tailed Student's t test.

2.3 RESULTS

2.3.1 Munc18c-Syntaxin 4 Binary Complexes Predominate in Detergent Lysates

Recent studies performed *in vitro* report that under low-detergent conditions (0.1% Triton X-100) Munc18 proteins are capable of associating with the SNARE core complex (129,185-187). However, under higher stringency conditions (1% Triton X-100), Munc18c was only able to associate with the SNARE complex when SNAP-23 was GST-tagged (Figure 2-1A, Lane 6), consistent with other similarly performed studies (129,169). However, GST-Munc18c pulldowns revealed a different outcome, Munc18c associated only with Syntaxin 4 and not the SNARE core complex (Figure 2-1B, Lane 8). These results are consistent with other reports pointing to differential association of Munc18 proteins with the SNARE complex depending upon location of epitope tags and detergent stringency in binding buffers (69,80,188,189). The Munc18-SNARE association of endogenous proteins within cells has yet to be demonstrated. MIN6 cells were harvested in 1% NP-40 membrane protein solubilizing buffer and cleared detergent lysates used in immunoprecipitation reactions with anti-Munc18c, anti-VAMP2 or an IgG control (Figure 2-2A). Three independent experiments showed that Munc18c co-immunoprecipitated only with Syntaxin 4 and not with SNAP23 or VAMP2. Munc18c was never seen to bind to Syntaxin 4 when Syntaxin 4 was complexed with other SNAREs. This was observed using lysates prepared from both unstimulated and glucose-stimulated MIN6 cells.

This inability to detect Munc18c association with binary (Syntaxin 4-SNAP23) or ternary (Syntaxin 4-SNAP23-VAMP2) SNARE complexes was reminiscent of results from some of the original immunoprecipitation studies conducted using detergent cell/tissue lysates (128,188,189). Possible reasons for this may be that in beta cells the Munc18c-Syntaxin 4 predominates to the extent that detection of the other complexes was limiting. Alternatively, antibodies used in co-immunoprecipitation may have induced steric hindrance and disallowed association of SNAP23 or VAMP2. A third possibility is that use

of 1% NP-40 detergent to solubilize endogenous membrane-associated proteins disrupted Munc18c-ternary SNARE complex association. In fact, data supporting the existence of Munc18 binding to SNARE complexes was collected in binding studies utilizing 5-10 times less detergent in lysis and reaction/wash buffers than detergent levels used in studies reporting only Munc18c-Syntaxin binding.

To address the issue of antibody interference in the co-immunoprecipitation we generated tandem affinity (TAP)-tagged Munc18c protein for adenoviral expression in MIN6 cells as 'bait' for Syntaxin 4 and associated SNARE proteins (Figure 2-2B). Two versions of tagged Munc18c were tested, with TAP tags added to either the N- or C-terminus of Munc18c to randomize for potential effects due to tag location. TAP tags consist of streptavidin binding peptide and calmodulin binding peptide (CBP), and input lysates containing the TAP-Munc18c were passed over streptavidin resin and subsequently calmodulin resin to yield Munc18c in the eluate, as determined by CBP immunoblotting (Figure 2-2B). In addition, this system was further utilized to test the effect of detergent level in lysis buffers upon Munc18c binding to Syntaxin 4, SNAP23 and VAMP2. TAP purification under either buffer condition resulted in similar yields of TAP-tagged Munc18c, as seen by immunoblotting for the CBP tag (Figure 2-1B, lanes 3 and 6). Syntaxin 4 was precipitated by TAP-Munc18c, detected by relative differences in input and flow-through (FT), and its strong presence in eluates. However, TAP-tagged Munc18c precipitated ~65% less Syntaxin 4 protein from lysates prepared with 0.1% versus 1% NP40 detergent. Furthermore, neither SNAP23 nor VAMP2 protein was found to co-elute with this complex from lysates prepared under either detergent condition. The levels of SNAP23 and VAMP2 in input lysates was comparable to that in FT, consistent with lack of co-precipitation with TAP-Munc18c-Syntaxin 4 complexes (Figure 2-2B, lanes 1-2 and 4-5). In addition, elution using high salt conditions (450 mM NaCl) failed to yield SNAP23 or VAMP2; C-terminal TAP-tagged Munc18c results were identical to N-terminal TAP-Munc18c (Figure 2-2C). These data suggest that the Munc18c-SNARE complex is labile under conditions required to adequately solubilize endogenous SNARE proteins.

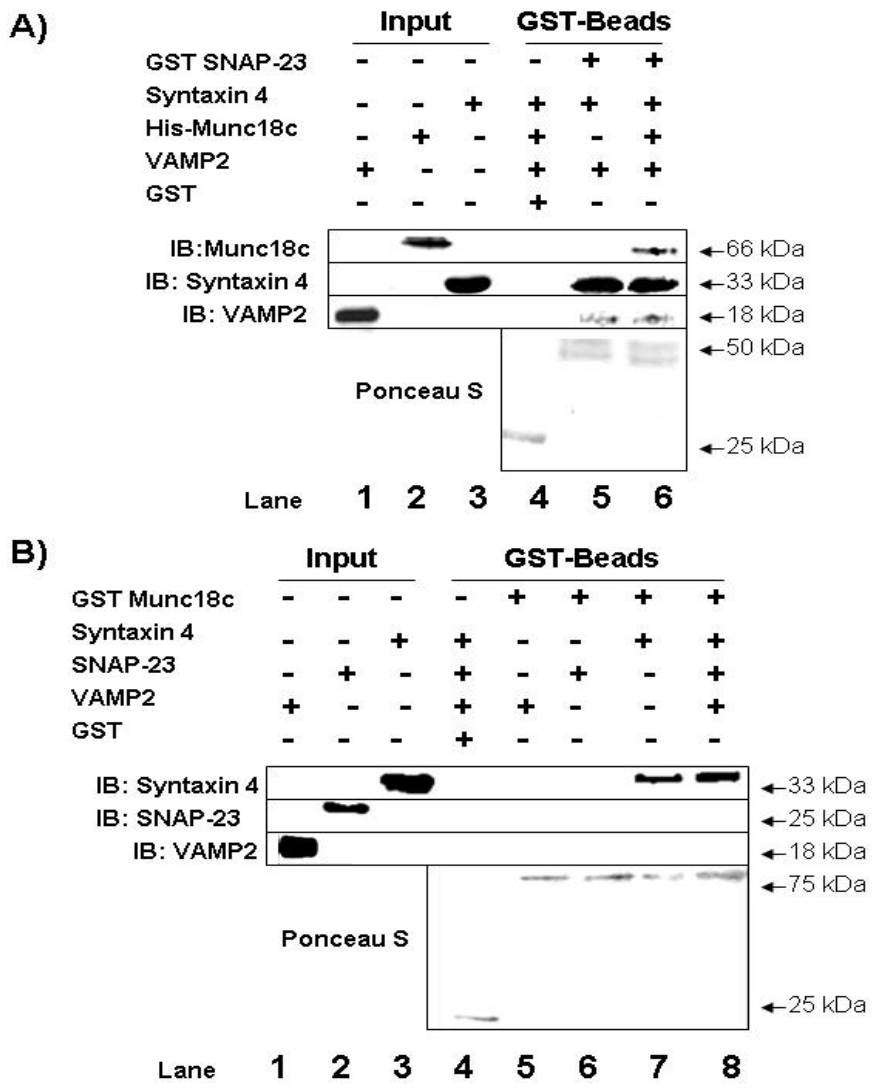

Figure 2-1 Munc18c Associates with the SNARE Complex *In Vitro* Depending On Which Protein is Tagged. A) Bacterially expressed GST-SNAP-23 or GST proteins were purified and linked to beads for *in vitro* binding studies with bacterially-expressed His-Munc18c, and soluble forms of Syntaxin 4 and VAMP2. The Syntaxin 4 and VAMP2 GST fragments were thrombin cleaved to remove the GST tag. Bound Proteins were subjected to a 12% SDS-PAGE for immunoblotting (IB) with anti-Munc18c, anti-Syntaxin 4, and anti-VAMP2 antibodies. B) Bacterially expressed GST-Munc18c or GST proteins were purified and linked to beads for *in vitro* binding studies with bacterially-expressed Syntaxin 4, SNAP-23, and VAMP2. The Syntaxin 4, SNAP-23, and VAMP2 GST fragments were thrombin cleaved to remove the GST tag. Bound Proteins were subjected to a 12% SDS-PAGE for immunoblotting (IB) with anti-Munc18c, anti-Syntaxin 4, and anti-VAMP2 antibodies. Ponceau S staining shows input of GST fusion proteins.

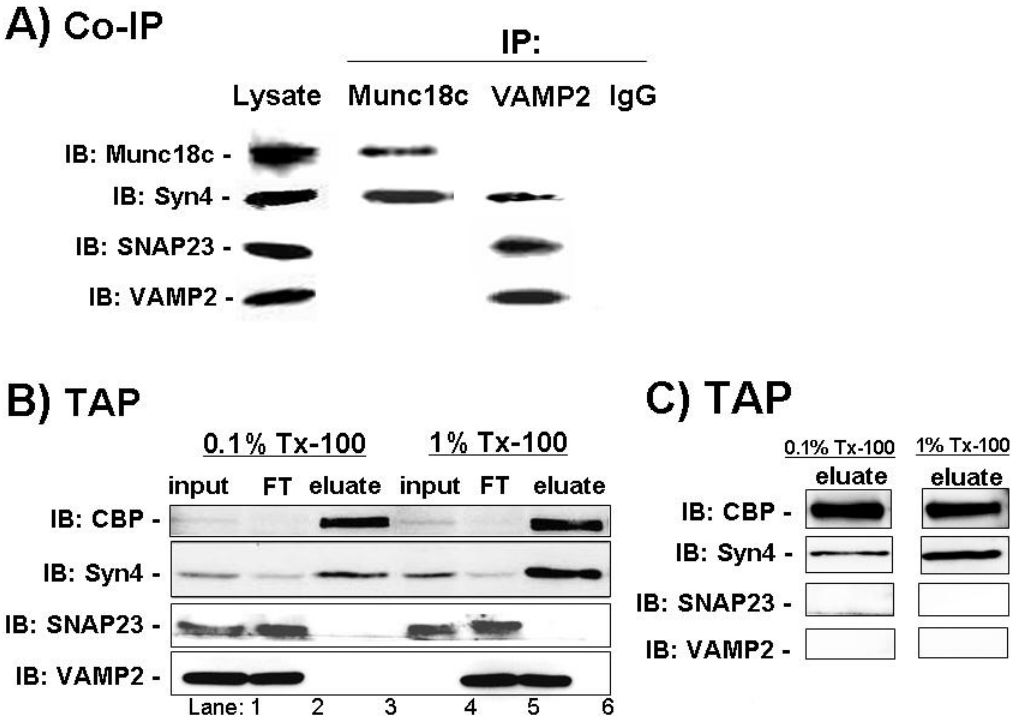

Figure 2-2 Munc18c Does Not Co-immunoprecipitate with VAMP2 in Detergent Solubilized MIN6 Cell Lysates. A) MIN6 beta cells were incubated in MKRBB for 2 hours and harvested in 1% NP40 containing lysis buffer. Lysates were divided into two portions and ~2 mg protein used for immunoprecipitation (IP) with anti-Munc18c or anti-VAMP2 antibodies. Lysate (lane 1) and immunoprecipitated proteins (lanes 2-4) were subjected to a 12% SDS-PAGE for immunoblotting (IB). TrueBlot anti-Rabbit Ig IP beads were substituted in for Protein G plus agarose to facilitate detection of SNAP-23. B) MIN6 cells were transduced with NTAP-Munc18c adenovirus (MOI=100). Lysates were subsequently prepared in buffer containing 0.1% Triton X-100 (lanes 1-3), or 1% Triton X-100 (lanes 4-6). SBP-CBP column eluates were subjected to 12% SDS-PAGE for immunoblotting (IB) and comparison with input lysate (50 µg/lane) with an equivalent volume of CBP column flow-through (FT). C) Same as B) but eluted with higher salt (450mM NaCl).

2.3.2 Doc2β Preferentially Associates with Tyrosine Phosphorylated Munc18c

We have previously shown that treatment of MIN6 cells with the protein tyrosine phosphatase inhibitor pervanadate (pV) results in accumulation of tyrosine-phosphorylated Munc18c, which corresponds to a decrease in Munc18c-Syntaxin 4 interaction (95). The region of Munc18c bound by Doc2β contains a key stimulus-induced phosphorylation site, Y219 (146). To determine if the binding of Doc2β was related to the phosphorylation state of Munc18c, cells were treated for 5 minutes with 0.1 mM freshly-prepared pervanadate and detergent (1% NP-40 unless otherwise specified) cell lysates prepared for use in co-immunoprecipitation experiments. Pervanadate treatment resulted in a ~1.5 ± 0.06-fold increase in phospho-Munc18c (P<0.01) as detected by anti-Munc18c immunoprecipitation from detergent lysate followed by 4G10 antibody immunoblotting (Figure 2-3A, lanes 1-2), with a 60 ± 3% decrease in Syntaxin 4 co-precipitation (P<0.01), consistent with previous results (95). Interestingly, pV treatment resulted in a coordinate 1.8 ± 0.09-fold increase in co-precipitation of Doc2β compared to untreated cell lysates (P<0.01). This pattern of binding with phospho-Munc18c was fully recapitulated using detergent-solubilized plasma membrane (PM) fractions (Figure 2-3A, lanes 3-4), implicating the PM as the principal cellular locale of these events (1.5 ± 0.06-fold increase in phospho-Munc18c, P<0.01; 60 ± 5% decrease in Syntaxin 4 co-precipitation, P<0.01; and 2.2 ± 0.2-fold increase in co-precipitation of Doc2β, P<0.01). As an additional approach, detergent lysates prepared from MIN6 cells over-expressing recombinant flag-Munc18c treated with or without pV were immunoprecipitated using anti-flag antibody for subsequent immunodetection of tyrosine-phosphorylated Munc18c and co-precipitation of Syntaxin 4 and Doc2β (Figure 2-2B). Nearly identical results were obtained (1.5 ± 0.04-fold increase in phospho-Munc18c, P<0.01; 60 ± 8% decrease in Syntaxin 4 co-precipitation, P<0.01; and 1.8 ± 0.09-fold increase in co-precipitation of Doc2β, P<0.01) suggesting that the selective binding of Doc2β to the region of Munc18c containing the pivotal Y219 residue was enhanced by phosphorylation at this site.

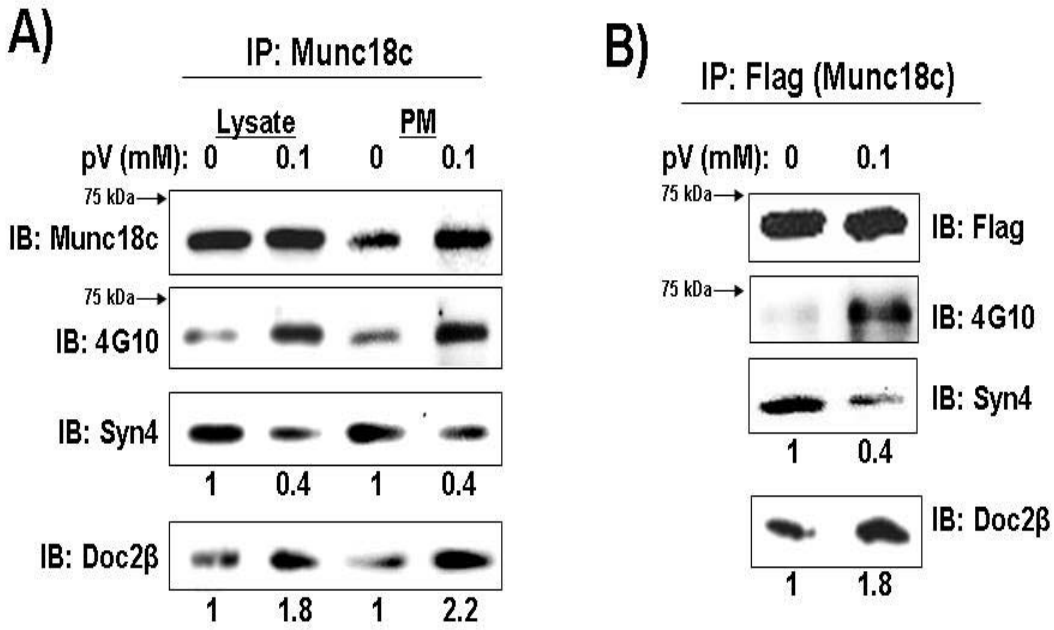

Figure 2-3 An Inverse Correlation Between Syntaxin 4 and Doc2β Association withTyrosine Phosphorylated Munc18c. A) MIN6 beta cells were incubated in MKRBB for 2 hours prior to 15 minutes treatment with or without freshly prepared 0.1 mM pervanadate. Detergent solubilized (1% NP40) cleared cell lysates or plasma membrane (PM) fractions were immunoprecipitated (IP) with anti-Munc18c and proteins resolved on 12% SDS-PAGE for immunoblotting (IB). B) Lysates were prepared from MIN6 cells transfected with pcDNA3-Flag-Munc18c and incubated 48 hours prior to pervanadate treatment. Anti-flag antibody was used for immunoprecipitation, and proteins resolved on 12% SDS-PAGE for immunoblotting. Band intensities were quantified using the BioRad Chemi-Doc system and normalized to untreated (no pV) bands in either Syntaxin 4 (Syn4) or Doc2β immunoblots; data represent the average of 3 experiments, $P<0.05$.

2.3.3 The Hc-linker Region of Syntaxin 4 (Amino Acids 118-194) Confers Binding to Munc18c

Recent structural data have shown that the N-terminal 19 amino acids of Syntaxin 4 constitute an important contact region for Munc18c binding, but that other contacts must contribute to its specificity of binding to Munc18c (114). To investigate additional contact regions that were both necessary and sufficient to confer binding to Munc18c, truncated forms of Syntaxin 4 were used in GST interaction assays *in vitro*. First, GST-Syntaxin 4 truncation proteins were expressed in *E. coli* and purified by glutathione sepharose precipitation, and subsequently thrombin-cleaved from GST. Pure Syntaxin 4 mutant proteins were captured for use in binding assays with GST-Munc18c linked to beads. As shown in Figure 2-4A, four C-terminal truncation mutants of Syntaxin 4 were generated, with sequential deletion of the H3 domain (containing residues 1-194), up to the Hb domain (containing residues 1-112), and up to the Ha domain (containing residues 1-70). Removal of the H3 domain failed to eliminate Syntaxin 4 binding to GST-Munc18c compared with binding of the full-length soluble Syntaxin 4 (1-273, no transmembrane domain) (Figure 2-4A, lanes 1-2). However, further deletion of the Hc-linker and Hb domains eliminated all binding to GST-Munc18c (Figure 2-4A, lanes 3-4). This lack of binding did not result from insufficient Syntaxin 4 protein input (Figure 2-4A, lanes 7-8). Further increases in input of the 1-70 protein failed to permit detection of association with GST-Munc18c (data not shown).

To determine the requirement for the Hc-linker region of Syntaxin 4 in mediating contact with Munc18c, N-terminal deletions of Syntaxin 4 were made. GST-Syntaxin 4 N-terminal deletion mutants were expressed and purified as described above, but were retained on sepharose beads for interaction studies with recombinant His-Munc18c protein. His-Munc18c protein was expressed in *E. coli* and purified for use as previously described (146). As depicted in Figure 2-4B, GST-Syntaxin 4 N-terminal deletions were generated by removal of the first 38 residues (GST-39-273), deletion through the Ha domain (GST-71-273), deletion through the Hb domain (GST-113-273), or removal of all but the

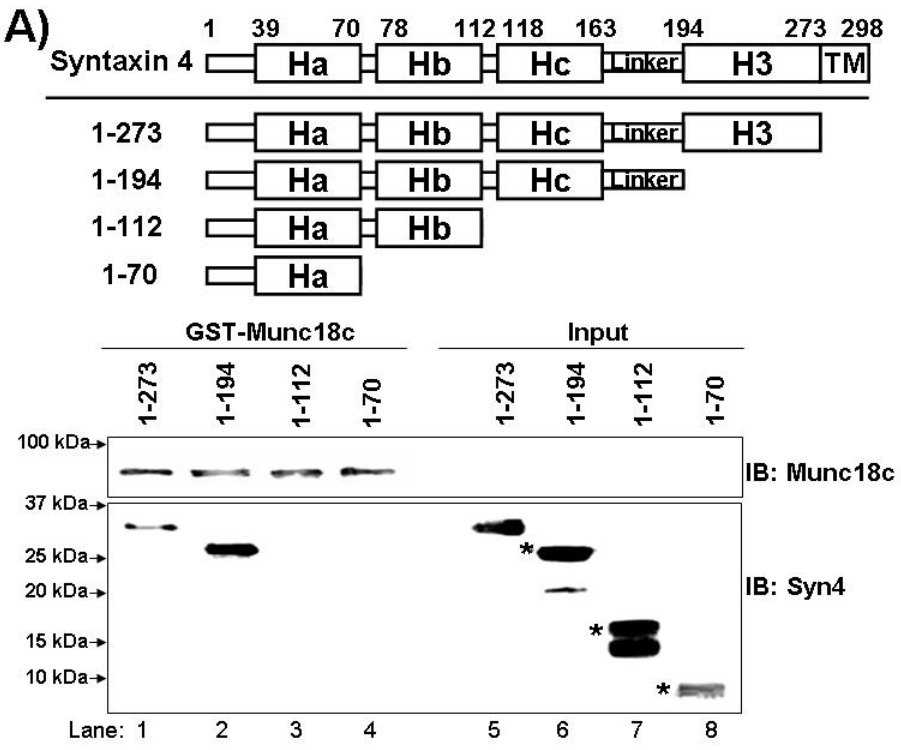
A)
Syntaxin 4
1 39 70 78 112 118 163 194 273 298
Ha
Hb
Hc
Linker
H3
TM
1-273
1-194
1-112
1-70
GST-Munc18c
Input
100 kDa
37 kDa
25 kDa
20 kDa
15 kDa
10 kDa
IB: Munc18c
IB: Syn4
Lane: 1 2 3 4 5 6 7 8

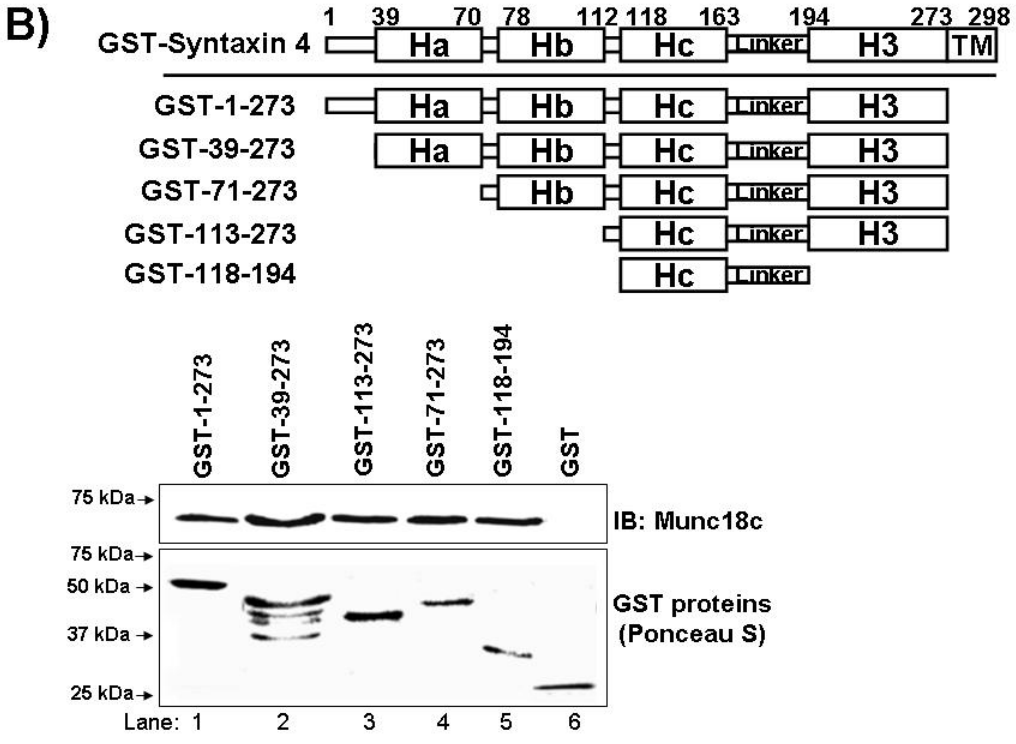
B)
GST-Syntaxin 4
1 39 70 78 112 118 163 194 273 298
Ha
Hb
Hc
Linker
H3
TM
GST-1-273
GST-39-273
GST-71-273
GST-113-273
GST-118-194
GST
75 kDa
50 kDa
37 kDa
25 kDa
IB: Munc18c
GST proteins
(Ponceau S)
Lane: 1 2 3 4 5 6

Figure 2-4 The Region Containing the HC and Linker Domains (118-194) of Syntaxin 4 Binds Directly to Munc18c *In Vitro*. A) Bacterially expressed GST-Munc18c or GST proteins were purified and linked to beads for in vitro binding studies with bacterially-expressed full length or C-terminal truncations of soluble Syntaxin 4. The Syntaxin 4 fragments (1-70, 1 -112, 1-194, and 1-273) were thrombin cleaved to remove the GST tag and were prepared at the concentration 1 mg/ml. Bound Proteins were subjected to 18% SDS-PAGE for immunoblotting (IB) with anti-Munc18c and anti-Syntaxin4 antibodies. Asterisks denote band of expected MW. B) Bacterially expressed N-terminal truncations GST-Syntaxin 4 (1-273, 118-194, 71-273, 113-273, and 39-273) or GST proteins were purified and linked to beads for *in vitro* binding studies with bacterially-expressed full length His-Munc18c. Bound proteins were subjected to 12% SDS-PAGE for immunoblotting with anti-Munc18c antibody. Ponceau S staining shows input of GST-Syntaxin 4 truncation proteins.

Hc-linker region (GST-118-194). All three Syntaxin 4 N-terminal deletion mutants bound to His-Munc18c, as did the isolated Hc-linker region, while GST alone failed to precipitate the His-Munc18c protein (Figure 2-4B, lanes 1-6). Thus, these data delineated the minimal region of Syntaxin 4 that was both necessary and sufficient to confer binding to Munc18c.

Alignment of this Hc-linker region of Syntaxin 4 with other mammalian PM-localized syntaxin isoforms was performed using ClustalW (http://ca.expasy.org). Syntaxin 4 and Syntaxin 1A share 53% and 37% identity in their Hc and linker regions, respectively (Figure 2-5). Residues 155-163 at the C-terminal end of the Hc domain are highly conserved, arguing against this region functioning in Syntaxin binding specificity for its cognate Munc18 protein. However the N-terminal 6 residues of the linker region (amino acids 164-169) of Syntaxin 4 vary considerably from those of Syntaxins 1A, 2 and 3. These data suggest that non-conserved residues present in the Hc-linker region of Syntaxin 4 may participate in conferring its specificity for binding to Munc18c.

2.3.4 The Hc-Linker Region (118-194) of Syntaxin 4 Competitively Inhibits Munc18c-Syntaxin 4 Association

Next we sought to determine whether the Hc-linker region of Syntaxin 4 was capable of competing with full-length soluble Syntaxin 4 for binding to Munc18c. Either GST alone or GST-Munc18c proteins linked to Sepharose beads were preincubated with recombinant purified Syntaxin 4 (residues 1-273) and centrifuged to eliminate unbound Syntaxin 4 protein. Syntaxin 4 binding was dose-dependent and specific, as determined by lack of interaction with GST alone or GST-nSec1 (neuronal Sec1/Munc18-1) (Figure 2-6A, lane 2 and Figure 2-6B lane 5). Subsequent addition of Hc-linker protein to reactions containing pre-bound GST-Munc18c-Syntaxin 4 complexes decreased Syntaxin 4 binding to the GST-Munc18c (Figure 2-6B, lanes 2-4). Because of its small molecular weight (~8 kDa), the Hc-Linker region of Syntaxin 4 protein was difficult to visualize by Coomassie or Ponceau S staining, and lacks the epitope for Syntaxin 4 antibody

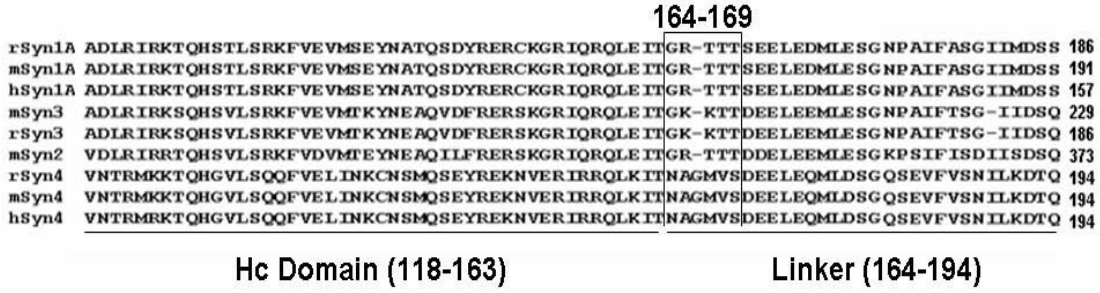

Figure 2-5 Sequence Alignment of Hc-Linker Regions Amongst Mammalian Plasma Membrane-localized Syntaxin Isoforms. ClustalW was used to align sequences of different Syntaxin proteins relative to amino acids 118-240, Hc-Linker domains of rat Syntaxin 4 (http://ca.expasy.org/tools/#align). R, rat; m, mouse; h, human. Boxed region amino acids 164-169 shows region of highest heterogeneity amongst syntaxin isoforms.

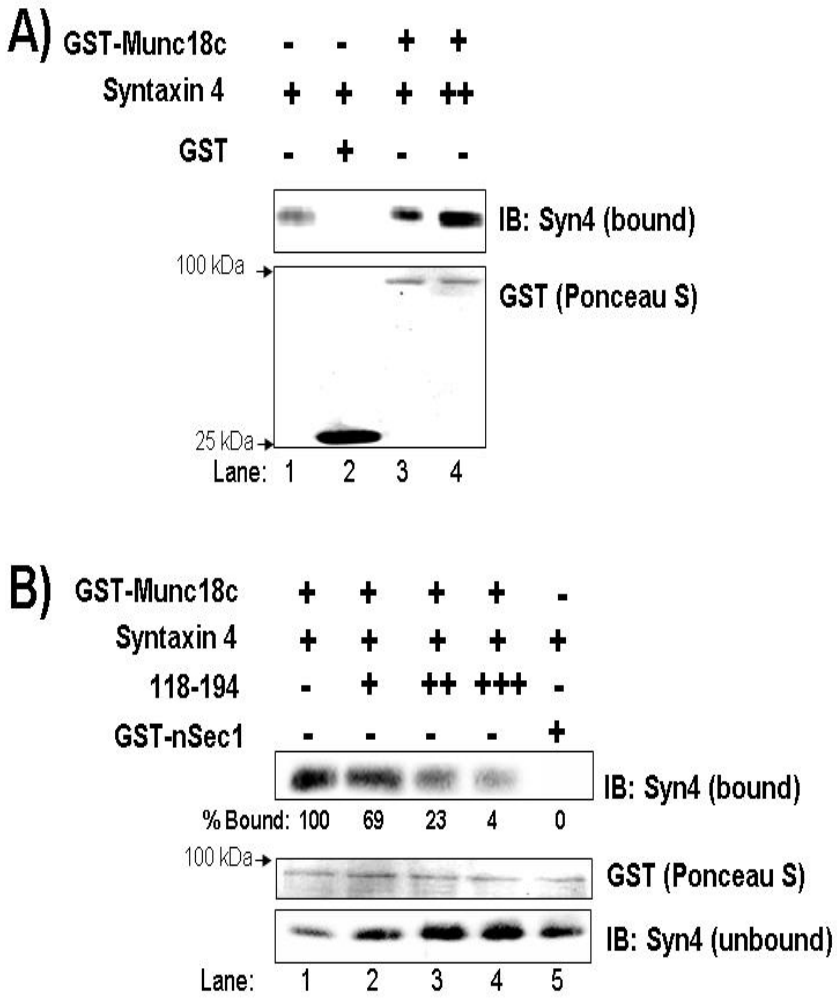

Figure 2-6 The Hc-linker Region of Syntaxin 4 Effectively Competes with Full Length Soluble Syntaxin 4 for Binding of Munc18c *In Vitro*. *A)* Bacterially expressed GST-Munc18c or GST proteins were purified and linked to beads and incubated at 4°C for 2 hours with bacterially-expressed soluble Syntaxin 4 (residues 1-273, 10 µg). Bound proteins were subjected to 12% SDS-PAGE for immunoblotting. Ponceau S staining shows input of GST fusion proteins. *B)* Bacterially expressed GST-Munc18c or GST-nSec1 proteins were purified and linked to beads and incubated at 4°C for 2 hours with recombinant soluble Syntaxin 4 protein (10 µg). The GST-Munc18c-Syntaxin 4 complex was pelleted for subsequent addition of thrombin-cleaved competitor protein (residues 118-194 of Syntaxin 4) and incubated for an additional 2 hours. Bound proteins were subjected to 12% SDS-PAGE for immunoblotting (IB). Ponceau S staining shows input of GST fusion proteins.

recognition. Thus, the Hc-linker region was fused to the C-terminus of EGFP for confirmation of its binding to Munc18c and use in cell studies (schematic in Figure 2-7A).

To determine if the Hc-Linker region bound to Munc18c in cells, pEGFP-(118-194) or pEGFP-C2 vector were co-electroporated with pcDNA3-Flag-Munc18c into CHO-K1 cells and detergent lysates were prepared for use in immunoprecipitation reactions. CHO-K1 cells transfect with very high efficiency, as evidenced by EGFP and Flag immunoblotting of lysates in Figure 2-7B (lanes 1-2), but fail to express detectable levels of endogenous Munc18c. Anti-Flag immunoprecipitation specifically co-precipitated the EGFP-(118-194) and not EGFP alone (Figure 2-7B, lanes 3-4). The pEGFP-(118-194) construct was then transfected into MIN6 cells to determine its ability to bind to endogenous Munc18c (Figure 2-7C). Anti-Munc18c selectively co-immunoprecipitated EGFP-(118-194) with endogenous Munc18c, similar to results obtained in CHO-K1 cells. These data indicated that the interaction of EGFP-(118-194) with Munc18c was specific, and that this region of Syntaxin 4 was sufficient to confer binding in a relevant cell type.

2.3.5 Functional Impact of Hc-Linker Region (Amino Acids 118-194) Expression Upon Insulin Exocytosis

Two types of proteins are known to interact with the N-termini of Syntaxin proteins: Munc18 and Munc13 (80,151). Of these, only Munc18c is known to bind to Syntaxin 4. Munc13-1 binds to the second helix, known as Hb, of Syntaxins 1-3, but it is not yet known whether it associates with Syntaxin 4. Given this selectivity of binding, we predicted that the EGFP-(118-194) could be used in MIN6 cells to determine the functional impact of dissociating endogenous Munc18c-Syntaxin 4 complexes. Transfection of MIN6 cells with the pEGFP-(118-194) or pEGFP constructs resulted in ~30-50% cells exhibiting EGFP fluorescence. Expression of the EGFP-(118-194) protein reduced coimmunoprecipitation of Syntaxin 4 with Munc18c by 25 ± 5% (P<0.01) compared to EGFP expression alone (Figure 2-8A).

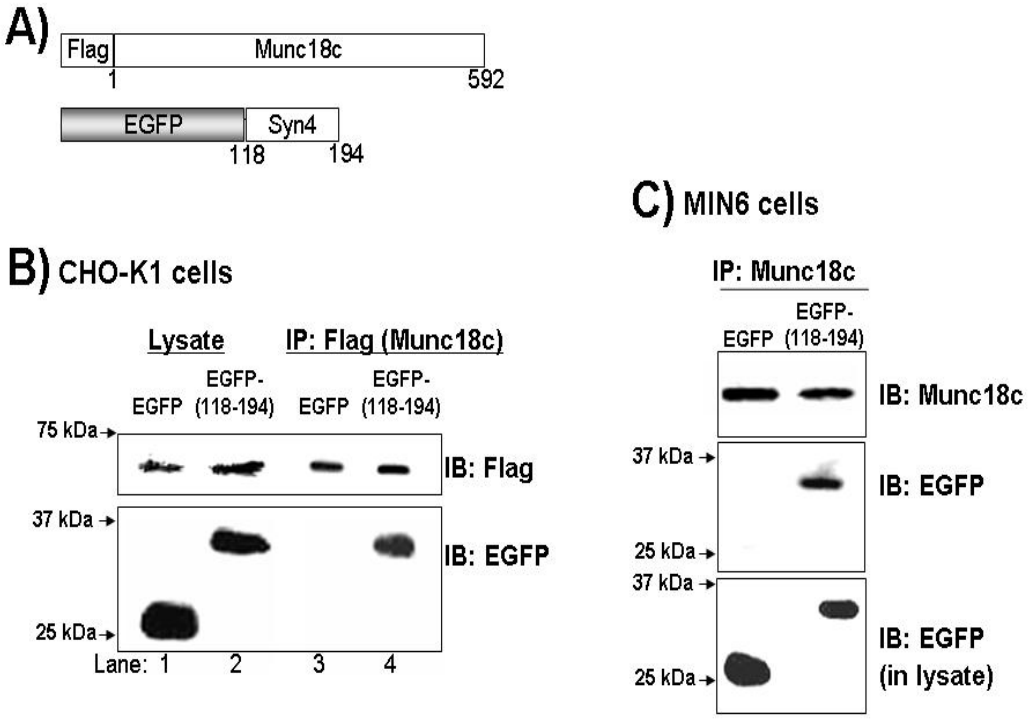

Figure 2-7 Residues 118-194 of Syntaxin 4 Bind to Munc18c in CHO-K1 and MIN6 Beta Cells. A) Schematic of constructs used: Full length Munc18c with a Flag tag at the N-terminus and the Hc-Linker region (118-194) of Syntaxin 4 with a GFP tag at the N-terminus. B) pEGFP-118-194 and pcDNA3-flag-Munc18c were co-electroporated into CHO-K1 cells, and 48 hours later detergent lysates were prepared for immunoprecipitation (IP) with anti-Flag antibody. Proteins were subjected to a 12% SDS-PAGE and immunoblotted (IB) with anti-flag and anti-EGFP antibodies. Lysates (50 µg) were included to show expression and correct migration of each recombinant protein. C) pEGFP-118-194 and pEGFP were transfected into MIN6 beta cells and resulting detergent lysates used for immunoprecipitation with anti-Munc18c. Proteins were subjected to a 12% SDS-PAGE and immunoblotted with anti-EGFP, and anti-Munc18c. Lysates show expression of EGFP and EGFP-118-194 proteins.

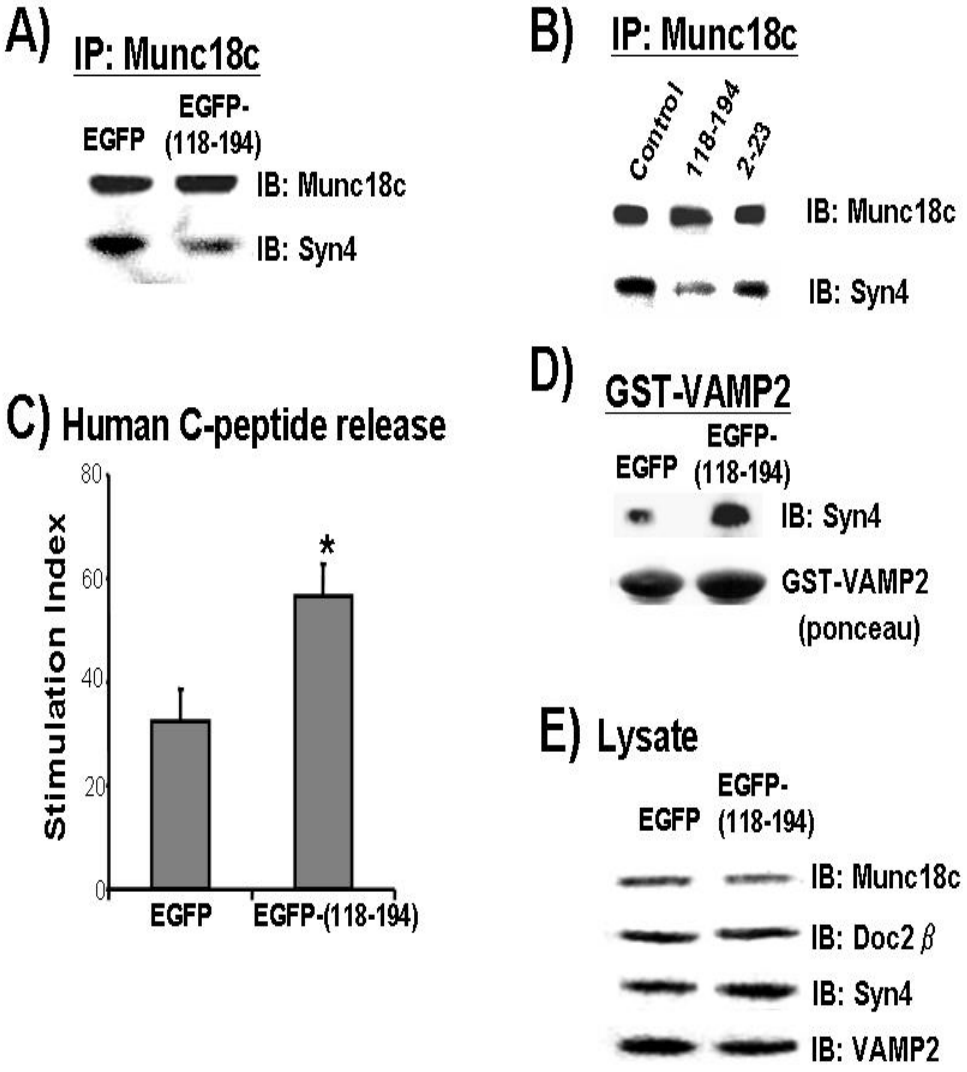

Figure 2-8 The Hc-linker Region (118-194) of Syntaxin 4 Interacts with Endogenous Munc18c and is Important for Insulin Exocytosis. A) Over-expression of Syntaxin 4 (118-194) in MIN6 cells inhibits the association of endogenous Syntaxin 4 with Munc18c. Detergent cell lysates prepared from MIN6 cells transiently transfected to express EGFP-Syntaxin 4 (118-194) or vector control were used in immunoprecipitation (IP) reactions with anti-munc18c antibody. Immunoprecipitated proteins were resolved on a 12% SDS-PAGE and immunoblotted (IB) with anti-Munc18c and anti-Syntaxin 4. Munc18c immunoblotting confirms equal precipitation in each reaction. B) Detergent cell lysates (2.5 mg) from MIN6 cells were incubated with 500 ng of recombinant Syntaxin 4 (118-194) or Syntaxin 4 (2-23) peptides for 2 hours at 4°C and used in immunoprecipitation reactions with anti-Munc18c. Immunoprecipitated proteins

were resolved on a 10% SDS-PAGE for immunoblotting. C) MIN6 cells were transiently transfected with either EGFP vector or EGFP-(118-194) plus human pro-insulin DNA, which served as a reporter of secretion specifically from transfectable cells. After 48 hours of incubation, cells were preincubated in MKRBB for 2 hours and were stimulated with 20 mM glucose. Human C-peptide secreted into the media was measured by RIA and normalized for total cellular protein content. D) Detergent cell lysates prepared from MIN6 cells transfected to express EGFP-Syntaxin 4 (118-194) or vector control were incubated with purified GST-VAMP2 linked to beads. Bound proteins were subjected to 12% SDS-PAGE for immunoblotting. Ponceau S staining shows input of GST fusion proteins. E) Fifty µg MIN6 lysate prepared from EGFP- or EGFP-(118-194)-expressing cells were resolved on 12% SDS-PAGE for immunoblotting to show lack of effect upon SNARE protein expression.

Using a second approach, recombinant peptide was added to anti-Munc18c immunoprecipitation reactions to evaluate the ability of the free peptide to disrupt endogenous Munc18c-Syntaxin 4 protein complexes. The advantages of this approach were the ability to control peptide input level as well as obviate concern over EGFP-peptide cellular localization or differential susceptibility to proteasomal degradation. As seen in Figure 2-8B, the Hc-linker region (residues 118-194) effectively disrupted endogenous Munc18c-Syntaxin 4 complexes by 50 ± 1% (P<0.005), whereas an identical quantity of the N-terminal Syntaxin 4 peptide (residues 2-23) had no significant impact (97 ± 6% of control). Taken together, these assays indicated that the 118-194 residue region of Syntaxin 4 had the capacity to function as a competitive inhibitor of endogenous Munc18c-Syntaxin 4 association in MIN6 cells.

To evaluate its effect upon glucose-stimulated secretion, EGFP-(118-194) was co-transfected with human proinsulin cDNA into MIN6 cells. The human C-peptide derived from expression of human pro-insulin is immunologically distinct from the mouse C-peptide produced by MIN6 cells, and thus serves as a reporter of secretion only from transfected cells. In control EGFP-expressing MIN6 cells, glucose induced a 38% increase in human C-peptide secretion (Figure 2-8C), similar to that in other reports (190,191). However, expression of the EGFP-(118-194) significantly increased glucose-stimulated secretion to nearly 60%. As seen in Figure 2-8D, this secretory increase paralleled a 67 ± 3% increase in the capacity of endogenous Syntaxin 4 to bind to exogenous GST-VAMP2, compared with EGFP expression alone (P<0.01). Over-expression of EGFP-(118-194) had no effect upon expression of endogenous cognate interacting proteins (Figure 2-8E). These data are consistent with recent Doc2β over-expression studies (146) showing that partial disruption of Munc18c binding to Syntaxin 4 results in enhanced glucose-stimulated insulin release via enhancing Syntaxin 4 accessibility for docking.

2.3.6 The 118-194 Region Does Not Associate with Phosphorylated Munc18c

Having identified the 118-194 region of Syntaxin 4 as a functional binding site for Munc18c in a relevant cell system, we next focused upon determining the relationship between the complexation of Munc18c with Syntaxin 4 and the tyrosine-phosphorylation of Munc18c in MIN6 cells. Cells transiently expressing EGFP control protein or EGFP-(118-194) were briefly treated with pV and cleared detergent lysates prepared for immunoprecipitation of tyrosine-phosphorylated proteins using anti-4G10 antibody (Figure 2-9). While the EGFP-containing lysate showed typical phospho-Munc18c and Doc2β co-immunoprecipitation, the EGFP-(118-194)-containing lysates revealed 50 ± 5% less phospho-Munc18c (P<0.01) associated and 75 ± 9% less Doc2β (P<0.01). Importantly, EGFP-(118-194) binding to Munc18c was fully abolished by the tyrosine-phosphorylation of Munc18c. This was not due to reduced expression of EGFP-(118-194) or increased expression of endogenous Syntaxin 4, as expression levels of each were similar to that of EGFP (Figure 2-9, lysate panels). This suggests that the 118-194 fragment may trap Munc18c in a conformation which prevents Munc18c's phosphorylation at Y219, and hence abolishes its ability to coprecipitate Doc2β.

2.3.7 Modeling the Munc18c-Syntaxin 4 Complex Interaction Sites

Although it is assumed that Munc18c will bind to Syntaxin 4 with high affinity, based upon similarity to Munc18-1 interaction with Syntaxin 1A (188), kinetic measurements of the Munc18c-Syntaxin 4 interaction are lacking. To address this, Surface Plasmon Resonance (SPR) data was collected using recombinantly expressed and purified His-Munc18c, Syntaxin 4 (1-273), and Syntaxin 4 (118-194) proteins (Figure 2-10). Analysis of SPR data revealed an association rate constant (k_a) of 9.22 x 10^5 and a dissociation rate constant (k_d) of 2.96 x 10^{-2} with Munc18c-Syntaxin 4 (1-273), as shown in Figure 2-9A. From these data, the calculated equilibrium dissociation constant ($K_D = k_d/k_a$) was 32 nM. The fast association rate, which approaches the diffusion limit, is suggestive

of a small free energy barrier for association of Munc18c with Syntaxin 4. The slow dissociation rate suggests a steeper barrier for the reverse process indicating that the complex formation is exergonic. Munc18c binding to the 118-194 region of Syntaxin 4 resulted in association and dissociation rate constants of 473 s^{-1} and 2.4 x 10^{-3} s^{-1}, respectively (Figure 2-10B). These values led to a dissociation equilibrium constant of 5 x 10^{-6} M^{-1}, which is nearly three orders of magnitude lower than that of full-length soluble Syntaxin 4. The lower affinity for the fragment is mostly attributed to its significantly slower association rate to Munc18c, suggesting a larger free energy barrier that the complex must overcome to bind. While different from that of full-length soluble Syntaxin 4, these data clearly demonstrate the ability of the 118-194 region to confer Syntaxin 4 binding to Munc18c.

To model this high-affinity interaction we used the three-dimensional crystal structures of Munc18c-Syntaxin 4 (114) and nSec1-Syntaxin 1A complex (110) to compile a structure of the Munc18c-Syntaxin 4 complex. More specifically, the crystal structure of Munc18c was used and a homology model of Syntaxin 4 was constructed by using the crystal structure of Syntaxin 1A. The structure is likely highly accurate in light of the high (80%) sequence identity between Syntaxin 4 and Syntaxin 1A (110). We modeled the Munc18c-Syntaxin 4 complex illustrating how Syntaxin 4 anchors it to the plasma membrane through a carboxyl-terminal transmembrane helix (Figure 2-11A). Munc18c is shown in blue and the Doc2β binding site on Munc18c, the N-terminal region residues 173-255 (146), is in orange. The short red region next to the Doc2β binding site corresponds to the first 19 amino acids of Syntaxin 4 that has been crystallized in complex with Munc18c (114). Syntaxin 4 N-terminal domains Ha, Hb, Hc and linker (residues 39-193) regions are shown in red (right) and Syntaxin 4 C-terminal domain H3 (residues 194-273), also known as the SNARE binding domain, is shown in yellow. The absence of the region between residues 1-19 and 39-273 of Syntaxin 4 suggests that this region is highly dynamic in solution. The N-terminal region of Syntaxin 4 (1-19) is remarkably close to the Doc2β and the Y219 residue of Munc18c known to undergo phosphorylation (95). More

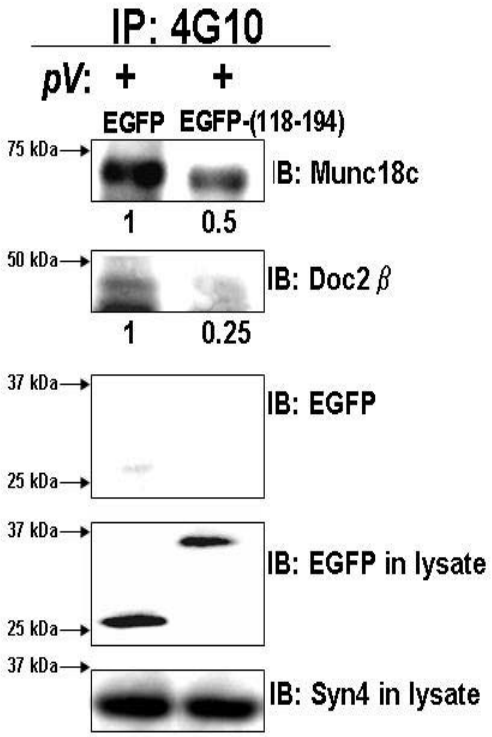

Figure 2-9 Syntaxin 4 (118-194) Does Not Bind to Phosphorylated Munc18c. MIN6 beta cells were transfected with pEGFP-118-194 and pEGFP, and 48 hours later were incubated in MKRBB for 2 hours prior to 15 minutes treatment with freshly prepared 0.1 mM pervanadate. Cleared detergent cell lysates were prepared for immunoprecipitation (IP) with anti-4G10 antibody. Proteins were resolved on 10% SDS-PAGE and immunoblotted (IB) with anti-Munc18c, anti-Doc2β, anti-EGFP, and anti-Syntaxin 4 antibodies.

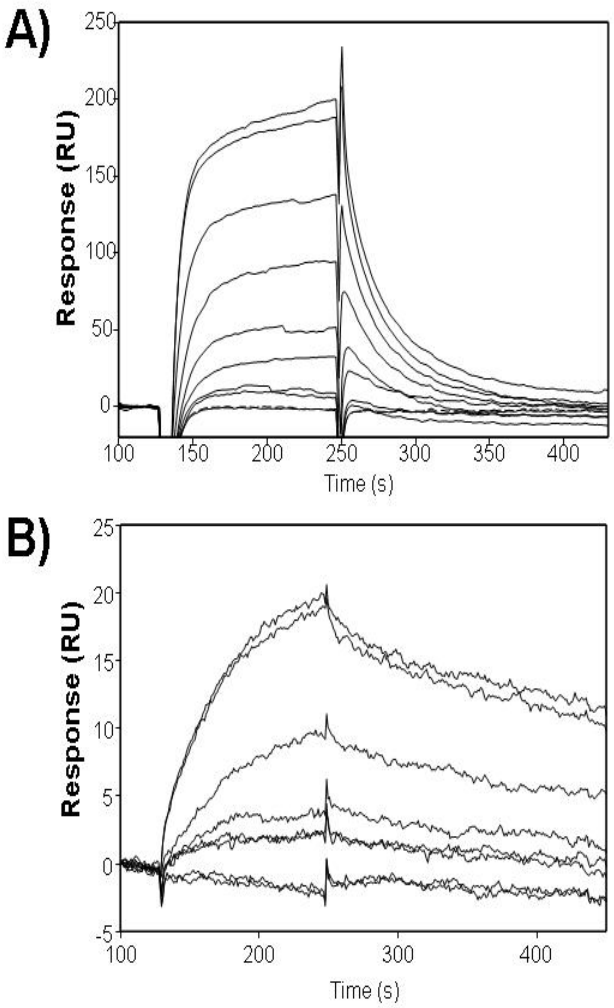

Figure 2-10 Sensorgram Depicting the Kinetic Analysis of Munc18c Binding to Syntaxin 4. Munc18c protein was injected at concentrations of 0, 1.7, 3.3, 6.7, 13.3, 26.7, and 53.3 nm, respectively. Dissociation was monitored for 3 minutes: A) soluble Syntaxin 4 (residues 1-273), B) region containing residues 118-194 of Syntaxin 4. The association data and dissociation data were fit to a 1:1 binding model to determine kinetics of binding.

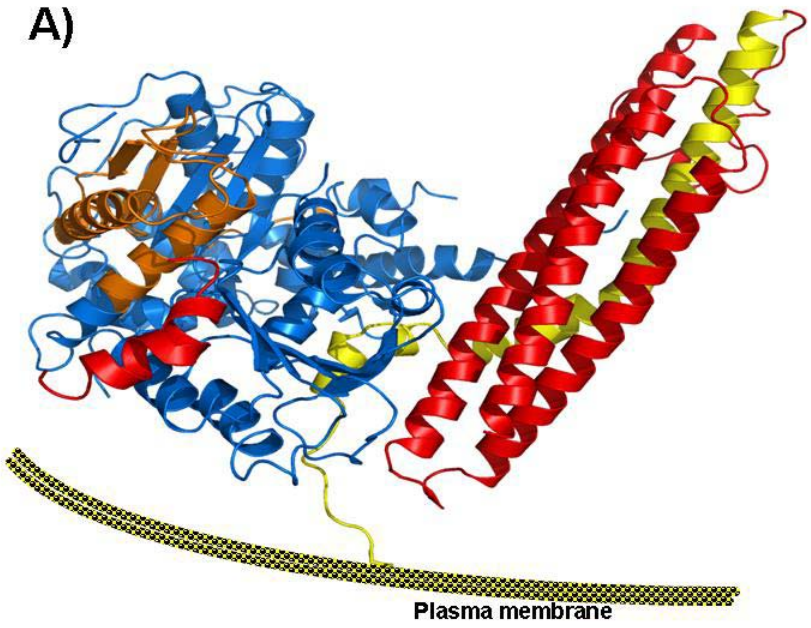
A)
Plasma membrane

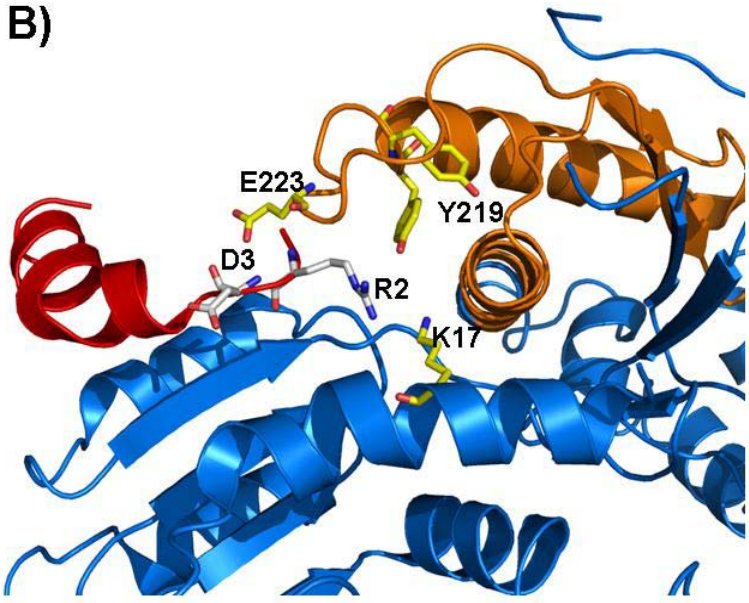
B)
E223
Y219
D3
R2
K17

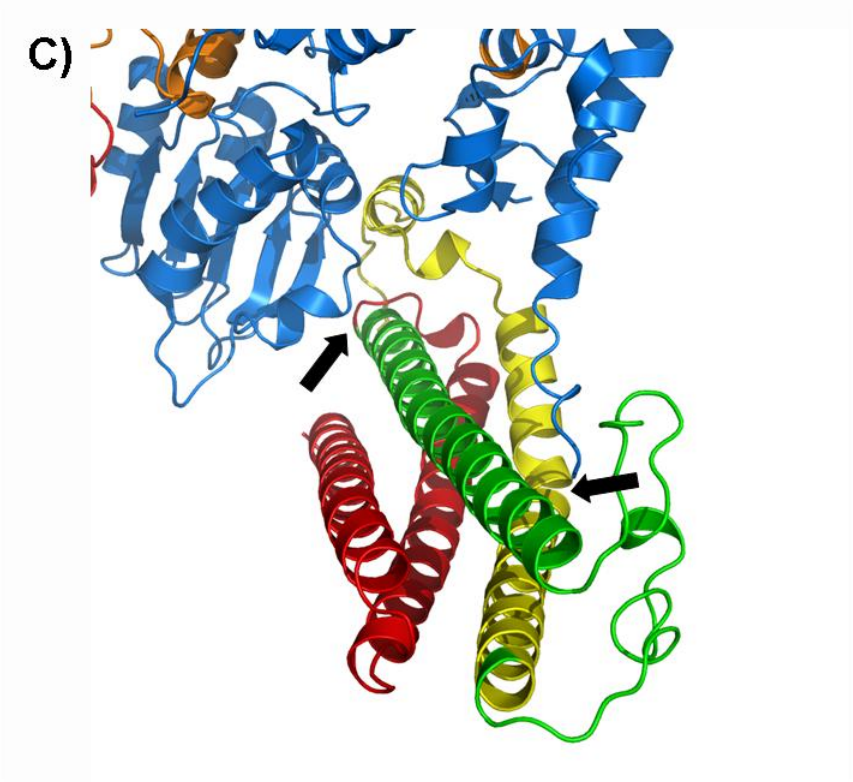

Figure 2-11 Ribbon Representation of the Munc18c-Syntaxin 4 Complex. A) Overall illustration of Syntaxin 4 interacting with Munc18c in close proximity to the plasma membrane (PM). Munc18c is shown in blue, Doc2β binding site on Munc18c in brown, and Syntaxin 4 N-terminus (amino acids 1-19) to the left in red. To the right in red is Syntaxin 4 N-terminal domains Ha, Hb, and Hc. The Syntaxin 4 C-terminal domain H3 (SNARE binding domain) is illustrated in yellow. B) A close up view illustrating Syntaxin 4 R2 interacting with full length Munc18c and Munc18c E223 interacting with a nitrogen in the backbone of Syntaxin 4 which results in a strong hydrogen bond. C) A close up illustration showing two contact sites between Munc18c (blue) and the Hc-Linker domain (green) of Syntaxin 4. Arrows point to the two contact regions between Munc18c and Syntaxin 4 (118-194).

specifically, Figure 2-11B shows that interactions between Syntaxin 4 and Munc18c close to Y219 are mediated by R2 located on Syntaxin 4 and appears to be a water-mediated interaction with Munc18c. Another interaction occurs between K17 and E223 on Munc18c that are found to interact with a backbone nitrogen in Syntaxin 4. Collectively, these interactions would contribute to the introduction of sufficient stability to the Munc18c-Syntaxin 4 complexes so as to maintain Munc18c in the conformation where Y219 is buried and unable to be phosphorylated, and may underlie the binding preference of Syntaxin 4 for unphosphorylated Munc18c. Furthermore, upon dissociation of Syntaxin 4 from Munc18c, a loop that holds the Y219 residue might more easily flip open to expose Y219 for phosphorylation and Doc2β binding.

The Hc-linker region of Syntaxin 4 (residues 118-194) shown in green interacts with Munc18c in two distinct areas as indicated by the arrows (Figure 2-11C). One interaction (right arrow) includes possible hydrophobic interactions between Syntaxin 4 residues V118, M122, Q126, V129, Q132, and Q133 and Munc18c. This is intriguing given that M122, Q132 and Q133 are found only in the Syntaxin 4 isoform and not in Syntaxin isoforms 1-3, whereas Q126 is conserved amongst all isoforms. The other hydrophobic interaction region of Syntaxin 4 contains a conserved R149. Future crystallographic analyses of these regions or the entire soluble Syntaxin 4 protein will be required to validate these proposed contacts.

2.4 DISCUSSION

In an effort to reconcile discrepancies in models of Munc18c-Syntaxin 4 complex dynamics derived primarily from *in vitro* data, we used the islet beta cell as model system of regulated exocytosis that is known to require Munc18c-Syntaxin 4 interaction. Herein, we demonstrate that the induction of Munc18c tyrosine phosphorylation is an important trigger for Munc18c to switch its binding specificity from Syntaxin 4 to Doc2β in the beta cell. Modeling studies showed a putative role for the N-terminal peptide of Syntaxin 4 in this switch mechanism,

given its close proximity to the Y219 site lying within the Doc2β binding site on Munc18c. However mutagenesis studies further revealed the necessity of the Hc-linker region of Syntaxin 4, which was also found to be sufficient to confer binding to Munc18c. Binding of the novel Hc-linker binding site was confirmed by SPR, and its expression in MIN6 cells was found to effectively disrupt endogenous Munc18c-Syntaxin 4 complexes. Functionally, this enhanced glucose-stimulated insulin exocytosis via increasing Syntaxin 4 accessibility to VAMP2. Moreover, phosphorylation of Munc18c reduced its association with Hc-linker, suggesting that the Hc-linker region is involved in the switching mechanism. These data represent a new and important region of Syntaxin 4 on which to focus in our efforts to delineate the dynamic conformational changes and associated functional modes of the Munc18c-Syntaxin 4 complex as it pertains to regulated exocytosis.

In contrast to some recent reports of preferential Munc18 interaction with Syntaxins engaged in SNARE core complex assembly using *in vitro* paradigms, our results were obtained using endogenous proteins present in MIN6 beta cell lysates, and demonstrate the predominance of binary Munc18c-Syntaxin 4 complexes in cells, with no detection of Munc18c-SNARE complexes. Although it is certainly possible that Munc18c-SNARE complexes might exist transiently, our data combined with the current literature suggest that in endocrine cells such as pancreatic beta cells and 3T3L1 adipocytes Munc18c mostly associates with monomeric Syntaxin 4 (114). The rationale behind Munc18c binding to and facilitating formation of Syntaxin-SNARE complexes has been founded upon *in vitro* data. However, we show here that the N-terminal peptide is dispensable for conferring Syntaxin 4 binding in cells, and rather that the association is conferred by the Hc-linker region. Moreover, the N-terminal peptide failed to competitively inhibit endogenous Munc18c-Syntaxin 4 association, while Hc-linker was an effective competitor and SPR data supported its ability to stably interact with Munc18c. Concomitant with these findings, other reports demonstrate that the 99N-terminal peptide of Syntaxin 1A or Syntaxin 4 is insufficient to confer the binding interaction (115,116). Most recently, Weis and Fasshauer (192) used

isothermal titration calorimetry and fluorescence spectroscopy to confirm that the binary interaction between Munc18-1 and Syntaxin 1A for the 'closed conformation' did require contact sites which included the N-terminal peptide, but show that removal of the first 24 residues of Syntaxin 1A only reduces the K_d from 1 nM to 8 nM, indicating that there is only a small contribution of the N-peptide.

Our modeling studies indeed support the concept that the N-terminal peptide of Syntaxin 4 binds to Munc18c, but also expand upon this by further speculating that this peptide might actively participate in the dissociation mechanism involving exposure of Y219 of Munc18c, along with participation of the Hc-linker region of Syntaxin 4. Evidence supportive of Hc-linker function in this phosphorylation-dissociation mechanism stems from the loss of Hc-linker binding to phosphorylated Munc18c, contrasting with its otherwise robust binding to Munc18c *in vitro* and in unstimulated MIN6 cells. One possible explanation for this is that the 118-194 fragment held Munc18c in a conformation that is unfavorable for Munc18c to become phosphorylated. Alternatively, Munc18c phosphorylation may have triggered dissociation of Hc-linker, as it does with full-length endogenous Syntaxin 4. However our data do not fully support this latter scenario, given the 50% loss of Munc18c phosphorylation detected in EGFP-118-194-expressing cells. Thus while the first explanation seems more plausible, future conformational studies of the phosphorylated form of Munc18c will be required to confirm or dispute this concept.

A recent NMR study demonstrated that Munc18-1 binds to and prevents the opening of Syntaxin 1A, and that an additional factor helps to transition Syntaxin into the open conformation (193). Doc2β would seem a suitable candidate for the 'additional factor', given our finding that it preferentially bound the tyrosine-phosphorylated form of Munc18c, and that the increase in binding to Doc2β was proportional to the decrease in Syntaxin 4 association. Our modeling studies revealed a close proximity of the Syntaxin N-terminal peptide to a solvent-exposed Doc2β binding site on Munc18c which contains the Y219 phosphorylation site. Incorporation of Doc2β into the binding model with

Munc18c-Syntaxin 4 provides new insight into the mechanism by which Munc18c dissociates, whether partially or fully, from Syntaxin 4. However, it is predicted that this protein triad is further impacted by proteins such as Munc-13 and Tomosyn, which like Doc2β have been shown to regulate and inhibit Munc18-Syntaxin complexes. Although Munc13-1 has not yet been shown to participate in Syntaxin 4-based complexes, the UNC-13 homolog from *C. elegans* was shown to displace Syntaxin from the Munc18-Syntaxin (UNC-18-Syntaxin) complex by competing for binding to Munc18 (194). In addition, Munc13-1 can bind directly to an N-terminal region of Doc2β and also to the Hb domain of Syntaxin 1A, which was later shown to stabilize Syntaxin in its open conformation (195). Tomosyn binds to Syntaxin 1A and Syntaxin 4 through their H3 domains, the same region bound by VAMP2 and SNAP25 (113,169). Thus, it may be that the presence of these and other proteins in cell lysates in combination with stimulus-induced post-translational modifications such as the tyrosine-phosphorylation of Munc18c is the reason for the discrepant results gained by *in vitro* studies as opposed to those conducted using mammalian cell systems.

Assigning a role to Munc18c as either a positive SNARE complex interacting protein as opposed to a negative closed Syntaxin 4 'clamping' protein has also varied as a function of detergent conditions used. For example, titration studies demonstrated the ability of Munc18 to displace SNAP-25 and VAMP2 from Syntaxin 1, coordinate with the ability to co-immunoprecipitate only Syntaxin 1 with anti-Munc18 antibody but not SNAP-25 or VAMP2 from detergent-solubilized (1% Triton X-100) synaptosomal membranes (80,127,128). However, more recent studies show that while the Munc18-Syntaxin binary complex does predominate, under *in vitro* conditions containing little (0.1% Triton X-100) or no detergent, SNARE complexes bound by Munc18 were detected (116,129,186,196). Using a novel immunofluorescent approach, it was shown that Syntaxin 1 bound to Munc18-1 could also bind SNAP-25, but that addition of VAMP2 displaced Munc18-1 (130). The current general consensus is therefore that Munc18-1-Syntaxin 1 complexes predominate and likely function in regulating vesicle docking (197). The molecular mechanism of Munc18c function

is equally controversial. For example, Munc18c reduced the binding of SNAP23 to Syntaxin 4 in a concentration-dependent manner when evaluated in 1% Triton X-100 solubilized cell lysates (69), yet under low-stringency detergent conditions Munc18c binding to Syntaxin 4-bound SNARE core complexes was detected (129). Indeed the benefit of using low-stringency buffers was the ability to detect the otherwise elusive transient docking complex. However, biochemical validation of the formation of this complex by endogenous proteins in cells awaits further investigation.

In summary, the model presented in this paper provides a new base/scaffold for building in these additional Syntaxin4-Munc18c-Doc2β interacting proteins, and serves to explain in part the mechanistic role for Munc18c in stimulus-induced Syntaxin 4 engagement in exocytosis. In addition to tyrosine phosphorylation, other modifications such as glycosylation and serine/threonine phosphorylation of Munc18c still need to be incorporated into this model. Munc18c becomes O-linked glycosylated in 3T3L1 adipocytes to inhibit insulin-stimulated GLUT4 vesicle translocation (143). Serine/threonine phosphorylation of Munc18c by PKC has been suggested to dissociate it from Syntaxin 4 and facilitate SNARE complex assembly in pancreatic acinar cells (136). Very recently, S-nitrosylation of Syntaxin 1 was shown to alter affinity for Munc18-1 (142). Therefore, further studies of various post-translational Munc18c modifications will be important for fully understanding its impact upon Syntaxin 4 conformation and role in exocytosis in physiologically relevant exocytosis events.

CHAPTER 3: IDENTIFICATION OF AN INSULIN-STIMULATED MUNC18C TYROSINE KINASE IN ADIPOCYTES AND SKELETAL MUSCLE

Some of the text in this Chapter will be submitted for publication:

Jewell JL, Tagliabracci VS, Oh E, Elmendorf JS and Thurmond DC. 2010. Identification of an Insulin-stimulated Munc18c Tyrosine Kinase in Adipocytes and Muscle.

Author Contributions: Tagliabracci VS generated data for Figures 3-1B, 3-2B, and 3-6. Oh E. assisted in the mice work, generation of the Munc18c Phospho-Tyrosine 219 antibody, and microscopy. The rest of the data and text was generated by Jewell JL.

3.1 INTRODUCTION

Insulin-stimulated GLUT4 vesicle translocation is mediated by Syntaxin 4-based SNARE protein complexes (reviewed in (7,198)). The GLUT4 vesicle-associated SNARE protein (VAMP2) complexes with the binary cognate receptor complex at the target membrane composed of SNAP23 and Syntaxin 4 proteins (t-SNAREs) to form a SNARE heterotrimeric complex (9,25,49,70,199,200). The Munc18c isoform of the Sec1/Munc18 secretory protein family further regulates this SNARE core complex through its ability to directly bind to Syntaxin 4 at the plasma membrane in 3T3L1 adipocytes and skeletal muscle (1,26,53,55,81,93,95,146,157,201). Reductions in the endogenous protein level of Munc18c in mice and humans are implicated in the incidence of insulin resistance and Type 2 diabetes, presumed to be necessary for facilitating Syntaxin 4 function in GLUT4 vesicle translocation and fusion, although the detailed molecular mechanistic action(s) of this regulatory protein are perplexing.

It has recently been determined by our laboratory and others that Munc18c-Syntaxin 4 complexes undergo numerous phosphorylations in response to a variety of stimuli, leading to confusion as to its differing actions when compared across tissues. For example, Syntaxin 4 becomes tyrosine phosphorylated in adipocytes upon stimulation by insulin (140), while in islet beta cells Syntaxin 4 does not undergo phosphorylation in response to glucose (95). However in adipocytes and islet beta cells, we and others have shown that the Munc18c isoform undergoes stimulus-induced phosphorylation at residues Tyr 521 and Tyr 219 respectively. The identification of a common mechanism, if targeted therapeutically, could simultaneously improve insulin release from the beta cell and glucose clearance from the muscle and adipose tissue, which would be of great value for the treatment of Type 2 diabetes. However, the kinase(s) responsible for phosphorylating Munc18c are unknown.

In the present study, we have identified the first known tyrosine kinase for Munc18c, the Insulin Receptor (IR). Further investigations using 3T3L1 adipocytes and skeletal muscle extracts indicate that Munc18c interacts with the IR tyrosine kinase in an insulin-dependent manner resulting in phosphorylation of

Munc18c, coordinate with the timing of its dissociation from Syntaxin 4. Finally, knockdown of endogenous Munc18c decreased GLUT4 translocation to the plasma membrane in 3T3L1 adipocytes.

3.2 MATERIALS AND METHODS

3.2.1 Materials

Rabbit anti-Munc18c antibody was generated as previously described (81). Anti-phosphotyrosine monoclonal antibody (4G10) was obtained from Upstate Biotechnology. Monoclonal PY20 and clathrin were purchased from BD Biosciences. Rabbit polyclonal antibodies anti-phospho AKT (T308) and AKT (pan) were purchased from Cell Signaling. Rabbit polyclonal anti-Syntaxin 4 was obtained from Chemicon (Temecula, CA), rabbit polyclonal anti-IR and anti-IR HRP from Santa Cruz Biotechnology, and monoclonal anti-IRS-1 from Millipore. The rabbit polyclonal Munc18c phosphotyrosine 219 peptide antibody was generated by PhosphoSolutions (Aurora, CO). Mouse anti-Myc was from Santa Cruz Biotechnology and rabbit anti-Myc antibody was from Upstate. Goat anti-mouse and anti-rabbit horseradish peroxidase secondary antibodies were acquired from Bio-Rad (Hercules, CA). Monoclonal Flag antibody, bovine serum albumin were purchased from Sigma (St. Louis, MO). The insulin, insulin like growth factor (IGF-1), and wortmannin used in the cell culture studies were obtained from Sigma. Protein G plus agarose was obtained from Santa Cruz Biotechnology (Santa Cruz, CA). Enhanced chemiluminescence (ECL) and SuperSignal West Femto reagents were obtained from Amersham Biosciences (Pittsburgh, PA) and Pierce (Rockford, IL), respectively. The IR inhibitor HNMPA-$(AM)_3$ used for these studies was from Biomol International.

3.2.2 Plasmids

The generation of pcDNA3.1-flag-Munc18c, pGEX4T1-Syn4 (1-273), pET28a(+)-His-Munc18c, pGEX-Munc18c, pSilencer 1.0-siControl, and pSilencer 1.0-siMunc18c #2 plasmids has been previously described (56,81,146,157). The siRNA resistant pcDNA3-Munc18c-WT, -Y219F and -Y521F constructs were

made using the Quick-Change II site-directed mutagenesis kit (Stratagene) according to the manufacturer's protocol, and DNA sequencing used for validation.

3.2.3 Cell Culture and Transient Transfection

Murine 3T3-L1 preadipocytes were cultured in DMEM that contained 25 mM glucose, 10% calf serum, 100 units/ml penicillin, 100 µg/ml streptomycin, and 292 µg/ml L-glutamine at 37°C in an 8% CO_2 atmosphere. Confluent cultures were fully differentiated into adipocytes as previously described (143,202). All studies used adipocytes that were between 8 and 12 days after differentiation, upon full differentiation. Differentiated adipocytes were co-electroporated (0.16 kV and 960 microfarads) with 50 µg of Myc-GLUT4-EGFP, 200 µg of additional plasmid DNA. After electroporation the cells were allowed to adhere to coverslips in 35-mm tissue culture dishes for 48 hours and were used for confocal microscopy.

3.2.4 Co-immunoprecipitation and Immunoblotting

Adipocytes - Whole cell detergent extracts were prepared by solubilization in NP-40 lysis buffer (1 M HEPES, pH 7.4, 1% Nonidet P-40, 10% glycerol, 50 mM sodium fluoride, 10 mM sodium pyrophosphate, 137 mM sodium chloride, 1 mM sodium vanadate, 1 mM phenylmethylsulfonyl fluoride, 10 µg/ml aprotinin, 1 µg/ml pepstatin, 5 µg/ml leupeptin) rotating for 10 minutes at 4°C. Insoluble material was removed by microcentrifugation for 10 minutes at 4°C. Cleared whole cell detergent lysate (2–4 mg) was combined with primary antibody for 2 hours at 4°C followed by a second incubation with protein G Plus-agarose for 2 hours. The resultant immunoprecipitates were subjected to a 10% or 12% SDS-PAGE followed by transfer to PVDF membranes for immunoblotting: Munc18c and Syntaxin 4 antibodies were used at 1:5000, IRS-1, IR, Clathrin, 4g10, PY20, and AKT were used at 1:1000, and PAKT used at 1:500. Secondary antibodies conjugated to horseradish peroxidase were diluted at 1:5,000 for visualization by ECL for detection using a Chemi-Doc documentation imaging system (Bio-Rad).

Skeletal Muscle – Mice were fasted 8am-12pm (male, 3-4 months, C57BL/6J), then injected intraperitoneally with 10 U/kg of insulin (Humulin R, Eli Lilly Indianapolis IN, diluted in saline); control mice were injected with a similar volume of saline. After 5 minutes mice were sacrificed by cervical dislocation and hind limb skeletal muscle was excised immediately and frozen in liquid nitrogen. Frozen tissues were subsequently pulverized under liquid nitrogen and stored at -80°C until use. All subsequent steps were performed at 4°C: frozen powdered tissue samples were homogenized in 10 volumes (w/v) of a buffer containing 50 mM Tris-HCl (pH 7.5), 0.5 mM EDTA, 2 mM EGTA, 1% Triton X-100, 0.1 mM N-p-tosyl-L-lysine chloromethyl ketone, 2 mM benzamidine, 0.5 mM phenylmethylsulfonyl fluoride, 10 µ/mL leupeptin and 1mM Na_3VO_4 using a tissue tearer (Biospec Products Inc.). Homogenates were then centrifuged at 3600 ×g for 10 minutes, and resultant supernatants used in anti-Munc18c immunoprecipitation reactions. Briefly, 2-3 mg of skeletal muscle lysate was combined with anti-Munc18c antibody for 2 hours at 4^{o}C followed by incubation with protein G Plus-agarose for 2 hours. Beads were extensively washed using lysis buffer and co-immunoprecipitated proteins resolved on a 10% SDS-PAGE.

3.2.5 In Vitro Kinase Assays

In vitro protein kinase activity assays were performed by quantifying the incorporation of [^{32}P] phosphate from [γ^{32}P] ATP into recombinantly expressed and purified His-Munc18c protein, using the activated β-subunit of the IR as the source of the kinase (Millipore). The reaction contained 50 mM Tris HCl (pH 7.5), 0.1 mM EGTA, 0.1 mM Na_3VO_4, 0.1% β-mercaptoethanol, 10 mM $MnCl_2$, 50 µM [γ^{32}P] ATP with a specific radioactivity of 2000 cpm/pmol, and of His-Munc18c protein substrate for the time points indicated. Reactions were stopped by the addition of Laemmli sample buffer and boiling for 5 minutes. Proteins were separated by 10% SDS-PAGE and gels then stained with Coomassie Blue, and dried. The phospholabeled proteins were detected by autoradiography, and bands subsequently excised from gels and quantitation of γ^{32}P incorporation by scintillation counting. The IRS-1 (Y608) peptide substrate (Biomol International

Inc.) was incubated in the presence of [γ^{32}P] ATP with or without the recombinant β-subunit of the IR in the same reaction buffer and spotted on filter paper. The peptide was then precipitated with 1% phosphoric acid, washed with acetone, dried, and incorporation of radioactivity determined by scintillation counting.

In addition, *in vitro* kinase assays were performed with non-radiolabled [γ^{32}P] ATP, using instead GST-Munc18c, GST-Munc18c-Y219F, or GST-Munc18c-Y521F with or without the recombinant activated β-subunit of the IR in a reaction buffer (described above) for 30 minutes. The reaction was stopped with Laemmli sample buffer and subjected to 10% SDS-PAGE followed by transfer to PVDF membrane for immunoblotting. The phosphorylation of Munc18c was determined by the anti-phosphotyrosine monoclonal antibody 4G10.

3.2.6 Computer Modeling

The three-dimensional crystal structure of the Munc18c complex (PDB code 2PJX) was used to illustrate the locations of 219 and 521. This was carried out with the computer program PyMol.

3.2.7 Myc-GLUT4-EGFP Translocation Analysis

Forty-eight hrs following transfection, 3T3-L1 adipocytes were fixed with 4% formaldehyde in phosphate-buffered saline (PBS, pH 7.4) on coverslips for 20 minutes at RT, washed three times with PBS and permeabilized (only in cells co-transfected with pFlag-Munc18c DNA) in 0.2% Triton X-100 at RT for 15 minutes. Fixed cells were rinsed with PBS three times (if permeablized) and blocked (1% bovine serum albumin and 5% donkey serum in PBS) at 4°C overnight. Coverslips were incubated with anti-Myc monoclonal or polyclonal antibody (1:50, when co-transfected with pFlag-Munc18c DNA) for 1 hour and the Alexa555-conjugated secondary (1:50) antibody for 1 hour. Anti-Flag monoclonal antibody (1:50) was used to detect Flag Munc18c and Flag Munc18c mutants for 1 hour and the Alexa405-conjugated secondary antibody for 1 hour.

3.2.8 Confocal Microscopy

Fully differentiated non-transfected 3T3L1 adipocytes were incubated in serum free media for 2 hours, treated with pervanadate (0.1 mM) for 15 minutes, followed by fixation with 4% formaldehyde in PBS on coverslips for 20 minutes at RT, washed three times with PBS and permeabilized in 0.2% Triton X-100 at RT for 15 minutes. Fixed cells were rinsed with PBS three times (if permeablized) and blocked. Coverslips were incubated with anti-Munc18c phospho-tyrosine 219 primary antibody (1:50) for 1 hour with the addition of the peptide competitor (500 ng) in its non-phosphorylated or phosphorylated state. FITC-conjugated anti-secondary antibody was then applied for 1 hour for subsequent confocal immunofluorescent microscopy analysis.

3.2.9 Statistical Analysis

All data are expressed as mean ± S.E. Data were evaluated for statistical significance using an unpaired two-tail Student's t test.

3.3 RESULTS

3.3.1 Insulin Stimulates Munc18c-IR Association Concurrent with Munc18c Tyrosine Phosphorylation in Adipocytes and Skeletal Muscle.

We and others have previously reported the rapid tyrosine phosphorylation of Munc18c in 3T3L-1 adipocytes in response to insulin stimulation (95,140,141). To better define the temporal pattern of Munc18c phosphorylation in fully differentiated 3T3L-1 adipocytes, the cells were stimulated with 100 nM insulin for 5, 15, or 30 minutes and the cell lysates were prepared (Figure 3-1A). While unstimulated adipocytes contained a low but detectable level of tyrosine-phosphorylated Munc18c, within 5 minutes of insulin stimulation Munc18c tyrosine phosphorylation levels rose more than two-fold (2.1 ± 0.01-fold, $p<0.05$). However, after 10 minutes of insulin stimulation, no detectable Munc18c tyrosine phosphorylation remained.

In general the GLUT4 translocation mechanisms are conserved in skeletal muscle and adipocytes, but Munc18c tyrosine phosphorylation has yet to be reported for skeletal muscle. Therefore, mouse hindlimb muscle homogenates were prepared for anti-Munc18c immunoprecipitation reactions (Figure 3-1B). Twelve C57BL/6J male mice, matched for body weight (3-4 months age), were fasted for four hours (8am-12pm) in clean feed-free cages, and injected intraperitoneally with 10 U/kg of insulin or with a similar volume of saline. After a 5 minutes incubation, mice were sacrificed and entire hindlimb muscles rapidly excised for preparation of cleared detergent extracts for use in immunoprecipitations and detection of insulin-stimulation of tyrosine phosphorylation. Consistent with the adipocyte data, Munc18c tyrosine phosphorylation increased by nearly two-fold (1.82 ± 0.09-fold, $p<0.05$) in insulin stimulated skeletal muscle extracts. As a positive control for the action of insulin, phospho-AKT detection was analyzed, clearly showing the expected downstream activation of AKT. Taken together, these data show that the rapid insulin-stimulation of Munc18c tyrosine phosphorylation is a conserved event in adipocytes and skeletal muscle.

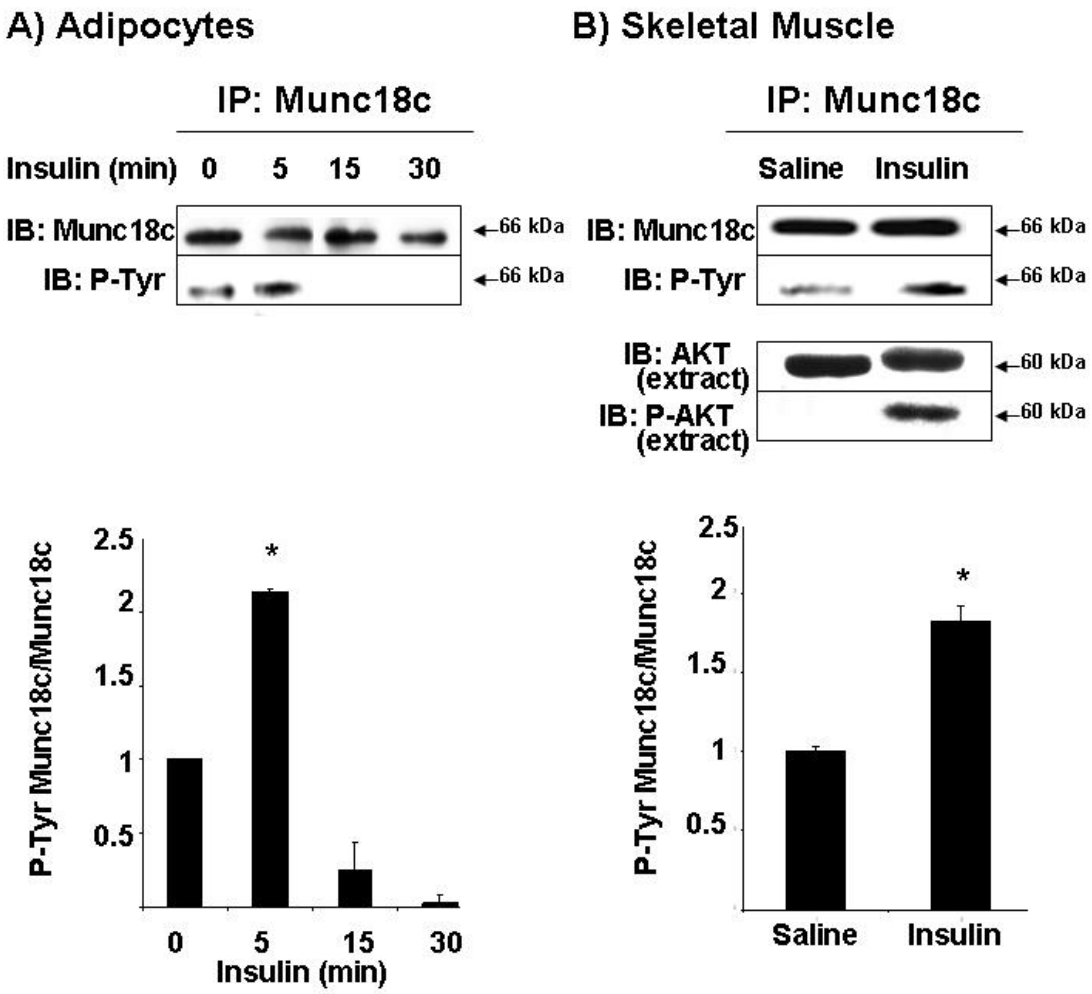

Figure 3-1 Insulin Stimulation Increases Munc18c Tyrosine Phosphorylation. A) Munc18c was immunoprecipitated (IP) from 3T3L1 adipocytes with or without insulin (100nM) for the indicated time points. Proteins were subjected to a 10% SDS-PAGE and immunoblotted (IB) with anti-Munc18c and striped for detection of P-Tyr Munc18c using the tyrosine antibody 4G10. Quantitation of 3 independent experiments below panel, *$p<0.05$ significance for Munc18c tyrosine phosphorylation under basal conditions vs. insulin stimulation. B) Munc18c was IP from mouse muscle hindlimb homogenates with or without insulin (10U/kg, for 5 min) stimulation for the indicated time points. Proteins were subjected to a 10% SDS-PAGE and IB with anti-Munc18c and stripped for detection of P-Tyr Munc18c using the tyrosine antibody 4G10. The phosphorylation of AKT (T301) in extracts was immunoblotted as validation of insulin activation using this protocol. Quantitation of 12 mice (6 injected with saline and 6 injected with insulin) below panel, *$p<0.005$ significance for Munc18c tyrosine phosphorylation under basal conditions vs. insulin stimulation.

To initiate the identification of the Munc18c kinase, inspection of the Munc18c amino acid sequence by the ExPASy Proteomics Server (NetPhosk 1.0 Server, http://www.cbs.dtu.dk/services/NetPhosK/) and Group-based Prediction System (203) revealed the presence of potential IR tyrosine phosphorylation consensus sites at tyrosine 219 (EKKLEDY**Y**KIDEKGL) and tyrosine 521 (RQKPRTN**Y**LELDRKN). To test this hypothesis, the potential Munc18c-IR interaction was examined in insulin-stimulated adipocytes and muscle (Figure 3-2B and C). Anti-Munc18c antibody effectively co-immunoprecipitated the IR from 3T3L1 adipocytes stimulated with insulin (2 ± 0.1-fold, $p<0.05$) versus unstimulated cells (Figure 3-2B), and similar results were obtained using stimulated muscle extracts by 2.7 ± 0.03-fold ($p<0.0005$, versus unstimulated controls, Figure 3-2C). Specificity for the action of insulin upon IR interaction was confirmed by demonstration of a 1.7-fold increase in the IR association with its well known substrate, the Insulin Receptor Substrate (IRS-1) under similar insulin-stimulated conditions (Figure 3-2A). These data supported the prediction that the IR serves as an insulin-stimulated tyrosine kinase for Munc18c in both adipocytes and skeletal muscle, and suggest that the activated IR preferentially associates with Munc18c.

3.3.2 Pervanadate Mimics the Effects of Insulin

We have previously shown that in β-cells the protein-tyrosine phosphatase inhibitor pervanadate (pV) increases the tyrosine phosphorylation of Munc18c, and correspondingly reduces its association with Syntaxin 4 (95,139). To determine whether this mechanism is conserved in insulin-responsive cell types, 3T3L1 adipocytes were treated with freshly prepared 0.1 mM pervanadate for 15 minutes and resultant detergent lysates used for anti-Munc18c co-immunoprecipitation experiments. In the absence of insulin stimulation, pervanadate treatment resulted in a 1.6 ± 0.07-fold ($p<0.005$) increase in the abundance of tyrosine-phosphorylated Munc18c compared to untreated cells, as detected by 4G10 (P-Tyr) antibody immunoblotting (Figure 3-3A, bar graph).

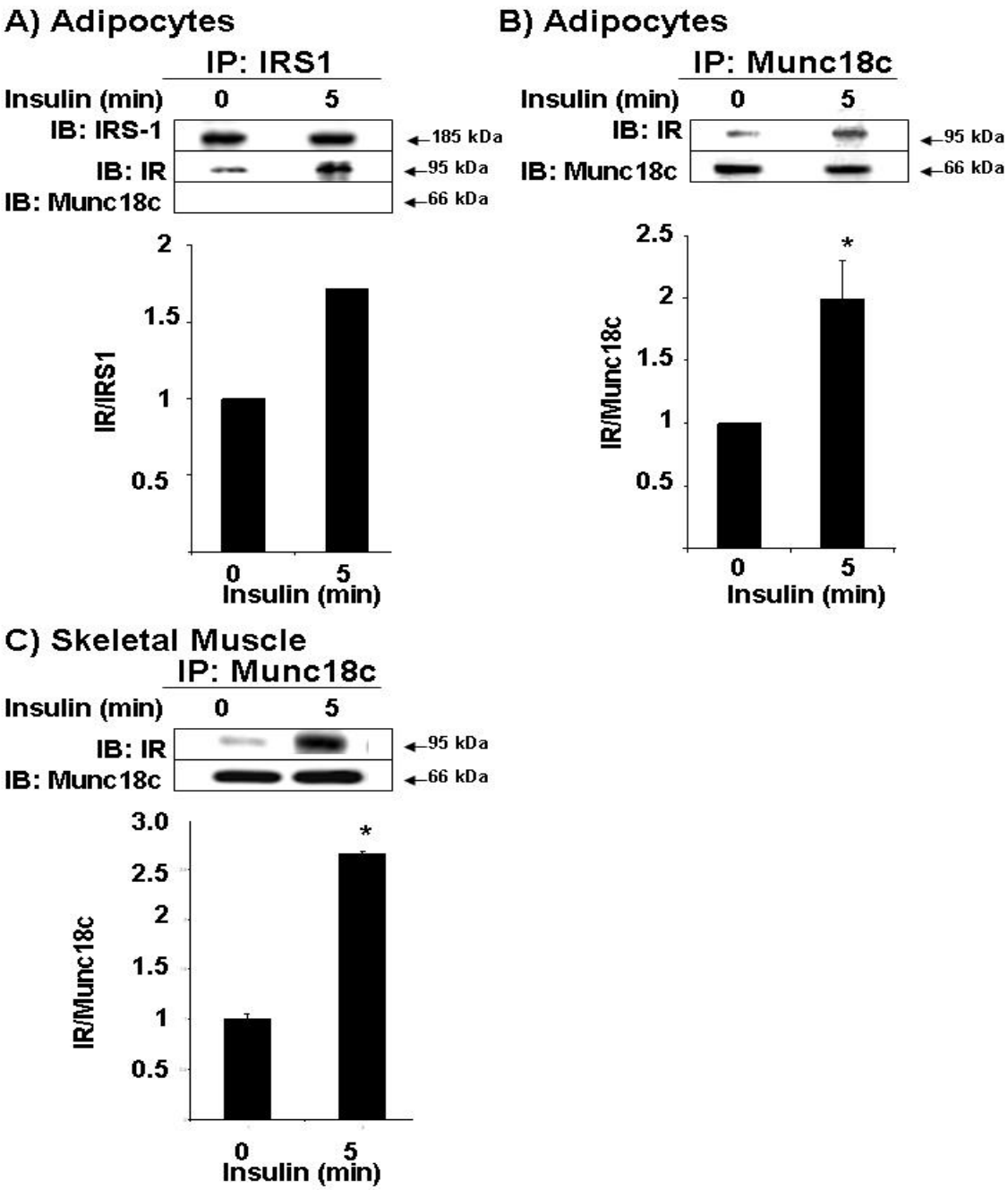

Figure 3-2 Munc18c-IR Association Increases Upon Insulin Stimulation. A) IRS-1 or B) Munc18c was co-immunoprecipitated (co-IP) from 3T3L1 adipocytes for 5 minutes with or without insulin (100nM). C) Munc18c was co-IP from mouse muscle hindlimb homogenates with or without insulin (10U/kg, for 5 minutes). Proteins were subjected to a 10% SDS-PAGE and IB with anti-Munc18c, anti-IRS-1, and anti-IR.

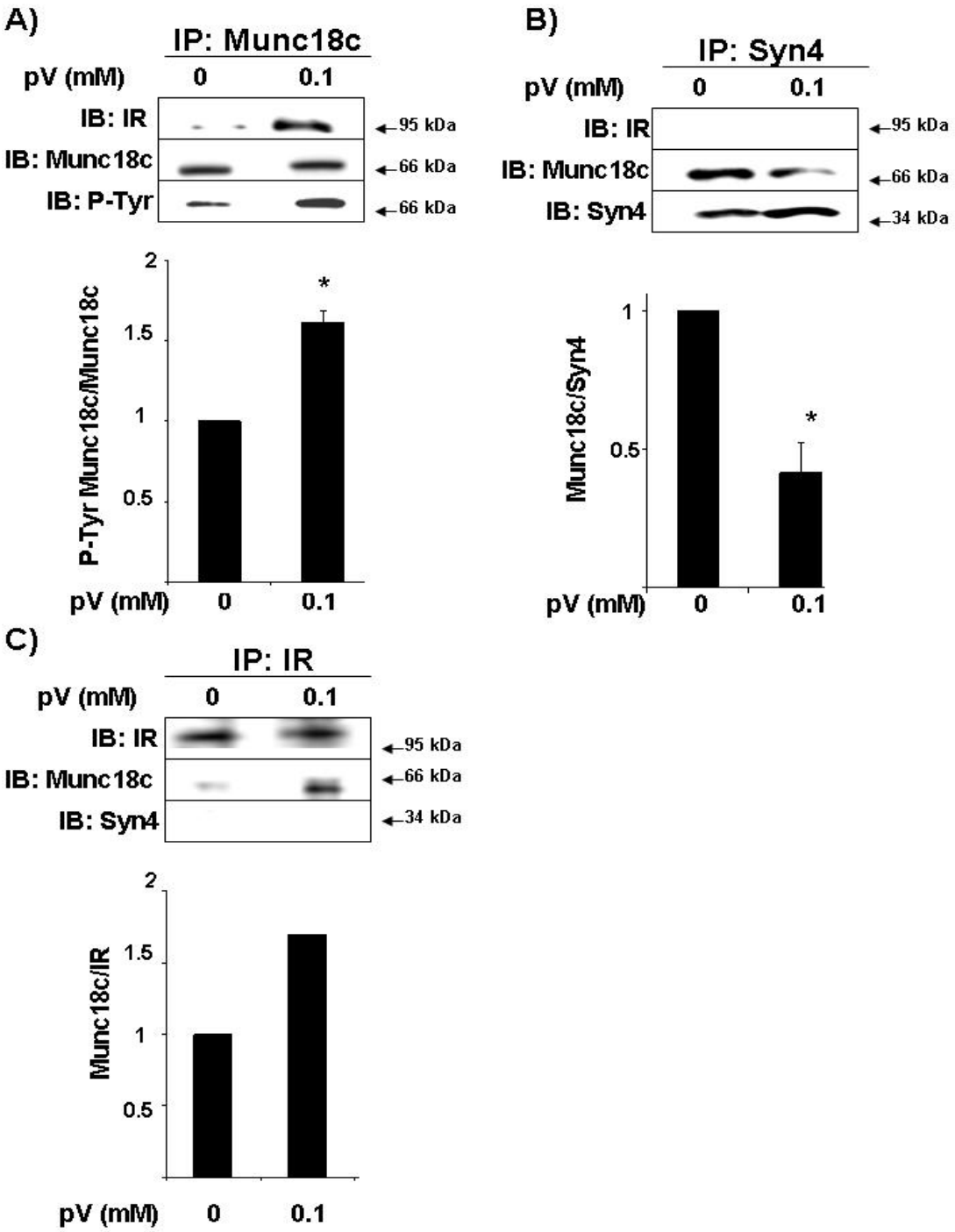

Figure 3-3 <u>IR-Munc18c Complexes Are Mutually Exclusive of Syntaxin 4-Munc18c Complexes.</u> Lysates prepared from 3T3L1 adipocytes treated with or without freshly prepared pervanadate (pV, 0.1mM) were used for co-immunoprecipitations (co-IP) with A) anti-Munc18c, B) anti-Syn4, or C) ant-IR. Co-IP proteins were resolved by a 10% SDS-PAGE and for immunoblotting (IB) with anti-Munc18c, anti-phospho tyrosine 4G10 (P-Tyr), anti-IR, and anti-Syn4. Data are representative of at least three independent cell studies.

Also similar to insulin stimulation, pervanadate treatment increased the amount of IR co-immunoprecipitating with Munc18c. Concurrently, pervanadate-stimulated tyrosine phosphorylation of Munc18c resulted in a 59 ± 1% (p<0.005) decrease in Munc18c-Syn4 association (Figure 3-3B). Strikingly, anti-Syntaxin 4 failed to co-immunoprecipitate the IR from pervanadate treated or untreated lysates (Figure 3-3B). Reciprocal IR co-immunoprecipitation experiments confirmed the absence of Syntaxin 4 from IR-Munc18c association complexes (Figure 3-3C). However, IR co-immunoprecipitation experiments clearly showed the pervanadate-induced association of Munc18c with IR. These data showed the pervanadate-induced tyrosine phosphorylation of Munc18c to be a conserved mechanism in adipocytes, to mimic the actions of insulin-stimulation, and suggest that Munc18c-IR complexes are mutually exclusive of its binding to Syntaxin 4.

3.3.3 Inhibition of IR Activity Decreases its Association with and Tyrosine Phosphorylation of Munc18c

To determine whether IR kinase activity was indeed required for the tyrosine phosphorylation of Munc18c, the IR-specific inhibitor Hydroxy-2-napthalenylmethylphosphoric acid tris-acetoxy-methyl ester (HNMPA-$(AM)_3$) (204,205) was used. Fully differentiated 3T3L1 adipocytes were pretreated with 100 μM HNMPA-$(AM)_3$ for 1 hour, stimulated with insulin for 5 minutes, and cleared detergent lysates prepared for immunoprecipitation using anti-Munc18c antibody (Figure 3-4). The phosphorylation of AKT (AKT T301) was monitored by immunoblotting to ensure that HNMPA-$(AM)_3$ halted the insulin signaling pathway (Figure 3-4B). Compared to the typical two-fold increase in Munc18c tyrosine phosphorylation triggered by 5 minutes of insulin stimulation (2.3 ± 3-fold, *p<0.01), the HNMPA-$(AM)_3$ fully abolished insulin stimulated Munc18c phosphorylation (Figure 3.4A , bar 2 versus bar 4, **p<0.01). Moreover, IR kinase activity was necessary for its interaction with Munc18c, since complexes were reduced by ~ 50 % (51± 2%, p<0.05) in lysates prepared from HNMPA-$(AM)_3$–treated insulin-stimulated adipocytes (Figure 3-4C). This was specific to IR, since IGF-1 stimulation failed to trigger tyrosine phosphorylation of Munc18c

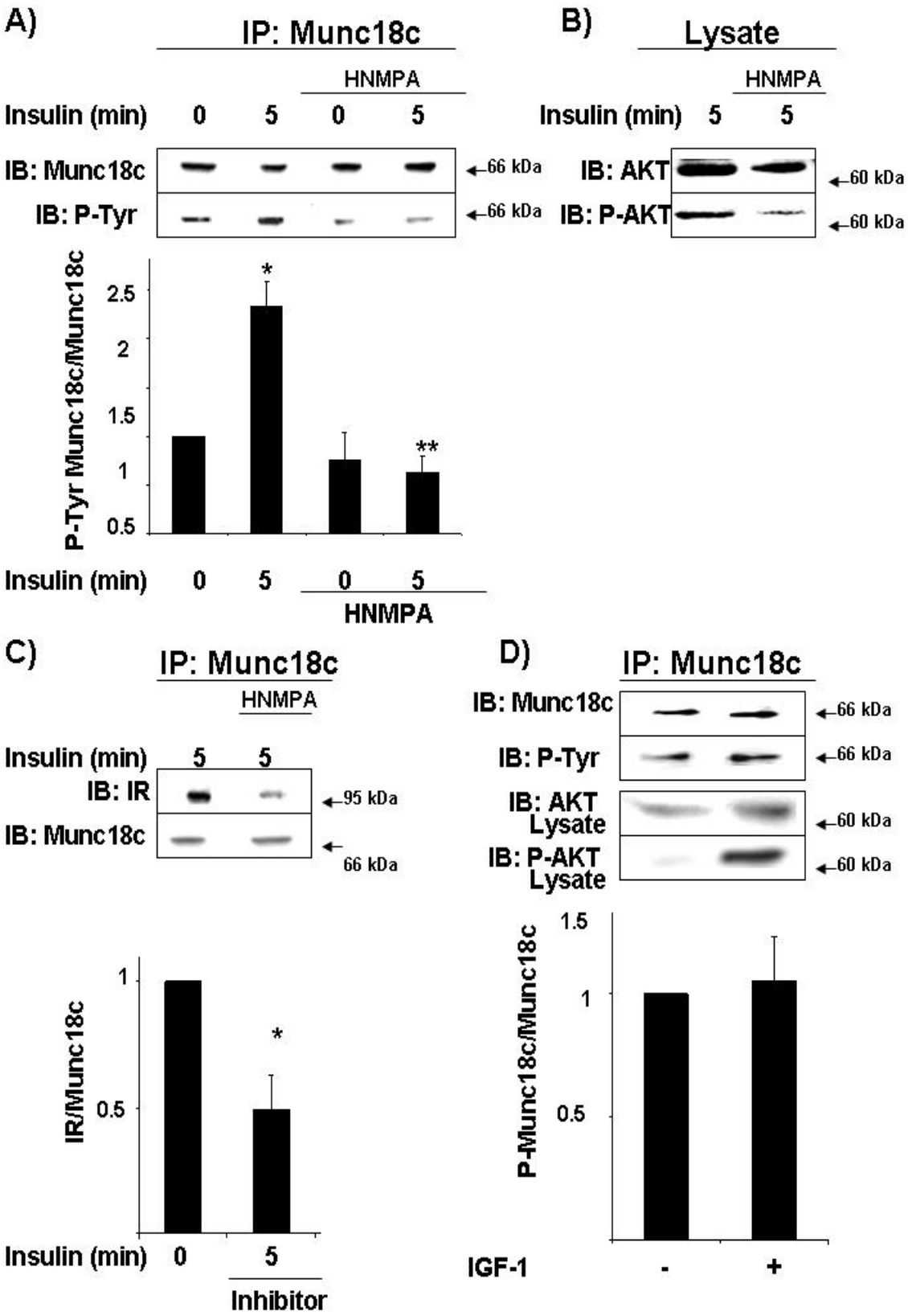
A)
IP: Munc18c
HNMPA
Insulin (min) 0 5 0 5
IB: Munc18c
IB: P-Tyr
66 kDa
66 kDa
P-Tyr Munc18c/Munc18c
2.5
2
1.5
1
0.5
*
**
Insulin (min) 0 5 0 5
HNMPA
B)
Lysate
HNMPA
Insulin (min) 5 5
IB: AKT
IB: P-AKT
60 kDa
60 kDa
C)
IP: Munc18c
HNMPA
Insulin (min) 5 5
IB: IR
IB: Munc18c
95 kDa
66 kDa
IR/Munc18c
1
0.5
*
Insulin (min) 0 5
Inhibitor
D)
IP: Munc18c
IB: Munc18c
IB: P-Tyr
IB: AKT Lysate
IB: P-AKT Lysate
66 kDa
66 kDa
60 kDa
60 kDa
P-Munc18c/Munc18c
1.5
1
0.5
IGF-1 - +

Figure 3-4 Munc18c Tyrosine Phosphorylation and Munc18c-IR Binding was Reduced Following Treatment with the IR Inhibitor HNMPA-$(AM)_3$. A) 3T3L1 adipocytes were pre-incubated in serum free media with or without 100 μM HNMPA-$(AM)_3$ for 1 hour prior to insulin stimulation. Munc18c was immunoprecipitated and co-immunoprecipitated proteins resolved by 10% SDS-PAGE and immunoblotted with anti-Munc18c and anti-4G10 or PY20 B) The phosphorylation of AKT in lysates was IB as validation of the inhibitor working. C) Munc18c was immunoprecipitated and co-immunoprecipitated proteins resolved by 10% SDS-PAGE and immunoblotted with anti-Munc18c anti-IR. D) 3T3L1 adipocytes were pre-incubated in serum free media for 2 hours followed by IGF-1 (100nM) stimulation for 5 minutes. Munc18c was immunoprecipitated, resolved by 10% SDS-PAGE, and immunoblotted with anti-Munc18c, and anti-4G10 or PY20 antibodies. The phosphorylation of AKT (T301) in was IB in lysates as validation of IGF-1 activation using this protocol.

(Figure 3-4D). These results suggest that the tyrosine phosphorylation of Munc18c requires IR kinase activity, as does the Munc18c-IR interaction.

3.3.4 Munc18c Becomes Tyrosine Phosphorylated Independent of PI3K

Insulin-stimulated tyrosine phosphorylation of Munc18c occurred concurrently with that of AKT activation, and AKT phosphorylation occurs downstream of PI3K. To determine whether the IR-kinase dependent phosphorylation of Munc18c occurred in a PI3K-dependent or independent manner, adipocytes were pretreated with or without the PI3K inhibitor wortmannin prior to stimulation with insulin for 5 minutes. Interestingly, wortmannin treatment failed to reduce the level of tyrosine-phosphorylated Munc18c compared to vehicle control (Figure 3-5). Wortmannin action was confirmed by detection of its inhibition of AKT phosphorylation at T301. These data indicate that insulin-stimulated tyrosine phosphorylation of Munc18c occurred in parallel to that of PI3K, in an independent pathway.

3.3.5 The IR Phosphorylates Munc18c at Tyrosine 521 *In Vitro*

To determine whether Munc18c could serve as a substrate for IR's kinase activity, *in vitro* kinase assays were performed. *In vitro* kinase assays used an active IR beta subunit, [γ^{32}P] ATP, and recombinant His-tagged Munc18c as the substrate (Figure 3-6A). Autoradiography of ^{32}P incorporation revealed an increase in Munc18c tyrosine phosphorylation in a time-dependent manner. An IRS-1 peptide was used as a positive control to ensure that the IR beta subunit was active (inclusive of Tyr-608, which is a well known substrate of the IR) and yielded the same increase in phosphate incorporation in a time dependent manner (Figure 3-6B).

The site of Munc18c modification was examined next using a modified *in vitro* kinase assay. Site-directed mutations of tyrosines 219 and 521 of Munc18c to phenylalanine were made and *in vitro* kinase reactions were performed

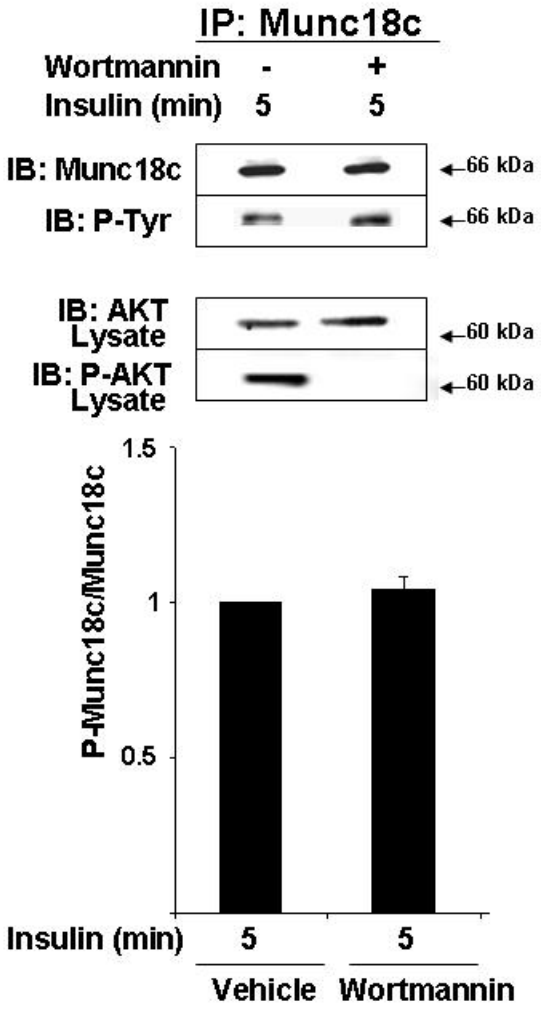

Figure 3-5 <u>Munc18c Becomes Tyrosine Phosphorylated Upstream of PI3K in the Insulin Signaling Pathway.</u> Adipocytes were incubated in serum free media for 2 hr with or without wortmannin (100 nM) before insulin stimulation (100 nM) for 5 minutes. Cleared detergent cell lysates were prepared for anti-Munc18c immunoprecipitation reactions, resolved by 10% SDS-PAGE, and immunoblotted with anti-Munc18c, anti-4G10 or PY20 antibodies. The phosphorylation of AKT (T301) in lysates served as validation of insulin's action and wortmannins inhibition of PI3K-dependent signaling. Data represents three independent experiments.

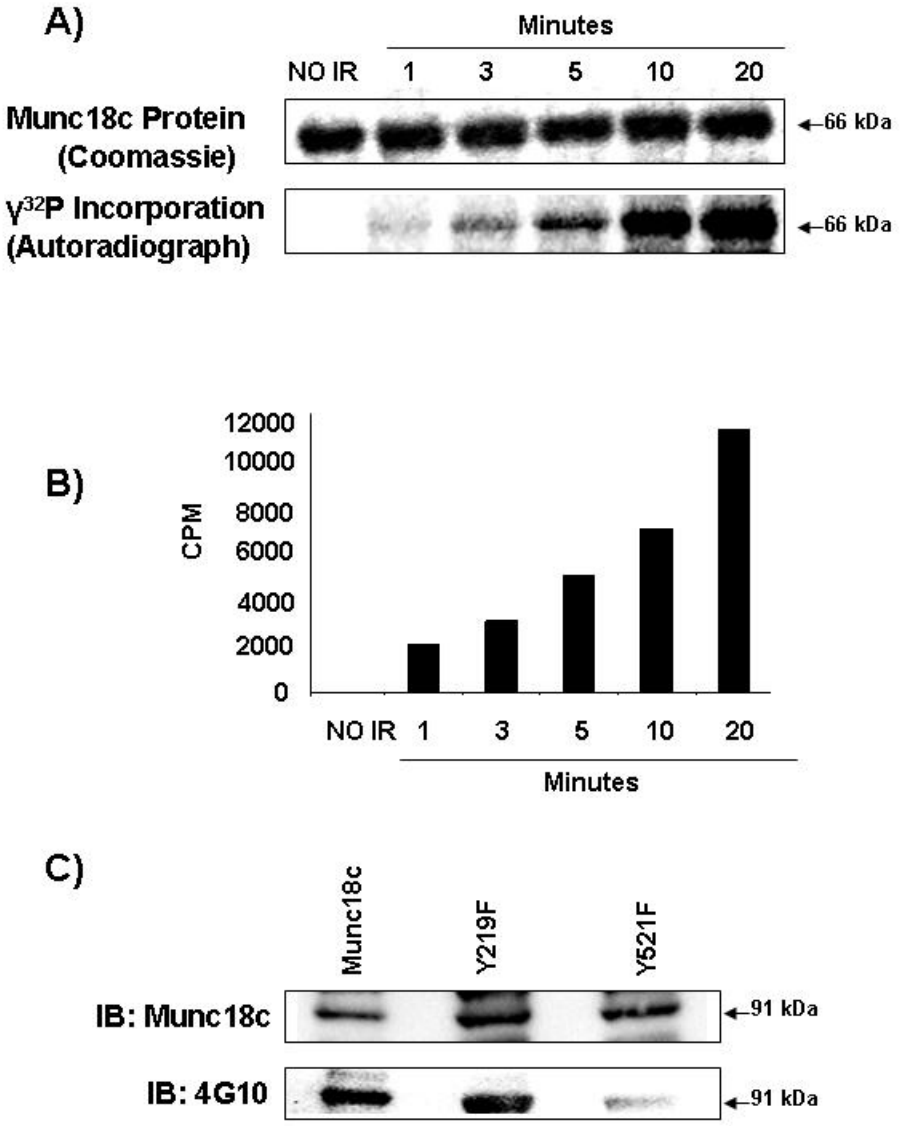

Figure 3-6 <u>The IR Phosphorylates Munc18c on Tyrosine 521 *In Vitro*.</u> A) Recombinant His-Munc18c was incubated in the presence of [γ^{32}P] ATP with or without the active beta subunit of the IR. The reaction was stopped at the indicated time points by addition of SDS loading buffer. B) IRS-1 peptide was incubated in the presence of [γ^{32}P] ATP with or without the active beta subunit of the IR. The reaction was stopped at the indicated time points. C) GST-Munc18c was incubated in the presence of ATP and the active beta subunit of the IR. The reaction was stopped after 30 minutes by addition of Laemmli sample buffer. Phosphorylation was detected using the anti-tyrosine phosphorylation antibody 4G10.

containing the recombinant active IR β subunit, non-labeled ATP, plus either GST-Munc18c-WT, -Munc18c-Y219F, or -Munc18c-Y521F (Figure 3-6C). Consistent with the first *in vitro* kinase assay data, GST-Munc18c-WT incorporated phosphate, as detected by anti-4G10 antibody. Surprisingly, GST-Munc18c-Y219 became phosphorylated similarly to GST-Munc18c-WT. However, Munc18c-Y521F failed to undergo phosphorylation, suggesting that Y521 was the target for the active IR β subunit.

3.3.6 Munc18c Becomes Phosphorylated at Tyrosine 219 in Adipocytes

Having previously shown that Munc18c Y219 is a key phosphorylation site in MIN6 beta cells, we had generated a phosphospecific Munc18c Y219 antibody to detect the cellular localization of tyrosine phosphorylated Munc18c. Consistent with the phospho-tyrosine pattern of Munc18c in plasma membrane fractions of β-cells (95), phospho-Y219-Munc18c specific antibody labeling of pervanadate treated 3T3L1 adipocytes was detected at the plasma membrane (Figure 3-7, panel 1). The specificity of the phospho Y219 antibody was verified by competition with the synthetic phosphorylated antigenic peptide, whereas competition with the non-phosphorylated form of the same peptide was without effect (Figure 3-7, panel 3 versus 1 and 2). Panel 4 verified the presence of adipocytes on the coverslip used to image panel 3. Thus, these data show that Munc18c could be phosphorylated in adipocytes at Y219 in response to pervanadate, in contrast to the *in vitro* kinase data.

3.3.7. Depletion of Munc18c Decreases GLUT4 translocation to the Plasma Membrane

Munc18c heterozygous knockout mice exhibit an impaired insulin-stimulated GLUT4 vesicle translocation in the hindlimb skeletal muscle consistent with their insulin resistance (20). In contrast, a line of MEF-derived differentiated adipocytes from an independent Munc18c (-/-) mouse model shows an increase in GLUT4 abundance in plasma membrane subcellular fractions (57). To reconcile these data using the 3T3L1 adipocyte model, RNAi-mediated depletion

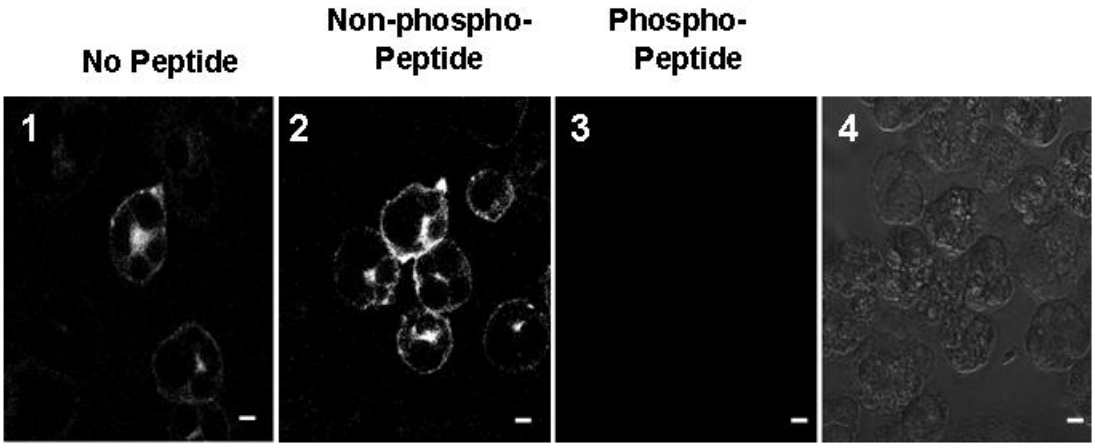

Figure 3-7 <u>Munc18c Tyrosine 219 Becomes Phosphorylated in 3T3L1 Adipocytes.</u> 3T3L1 adipocytes were incubate in serum free media (2 hours) prior to pervanadate treatment (pV), 0.1mM, for 5 minutes followed by fixation and permeabilization and immunostaining with anti-PY219-Munc18c antibody with the addition of the peptide competitor (500 ng) in its non-phosphorylated (Non-phospho-Peptide) or phosphorylated (Phospho-Peptide) state for confocal immunofluorescent microscopy analysis.

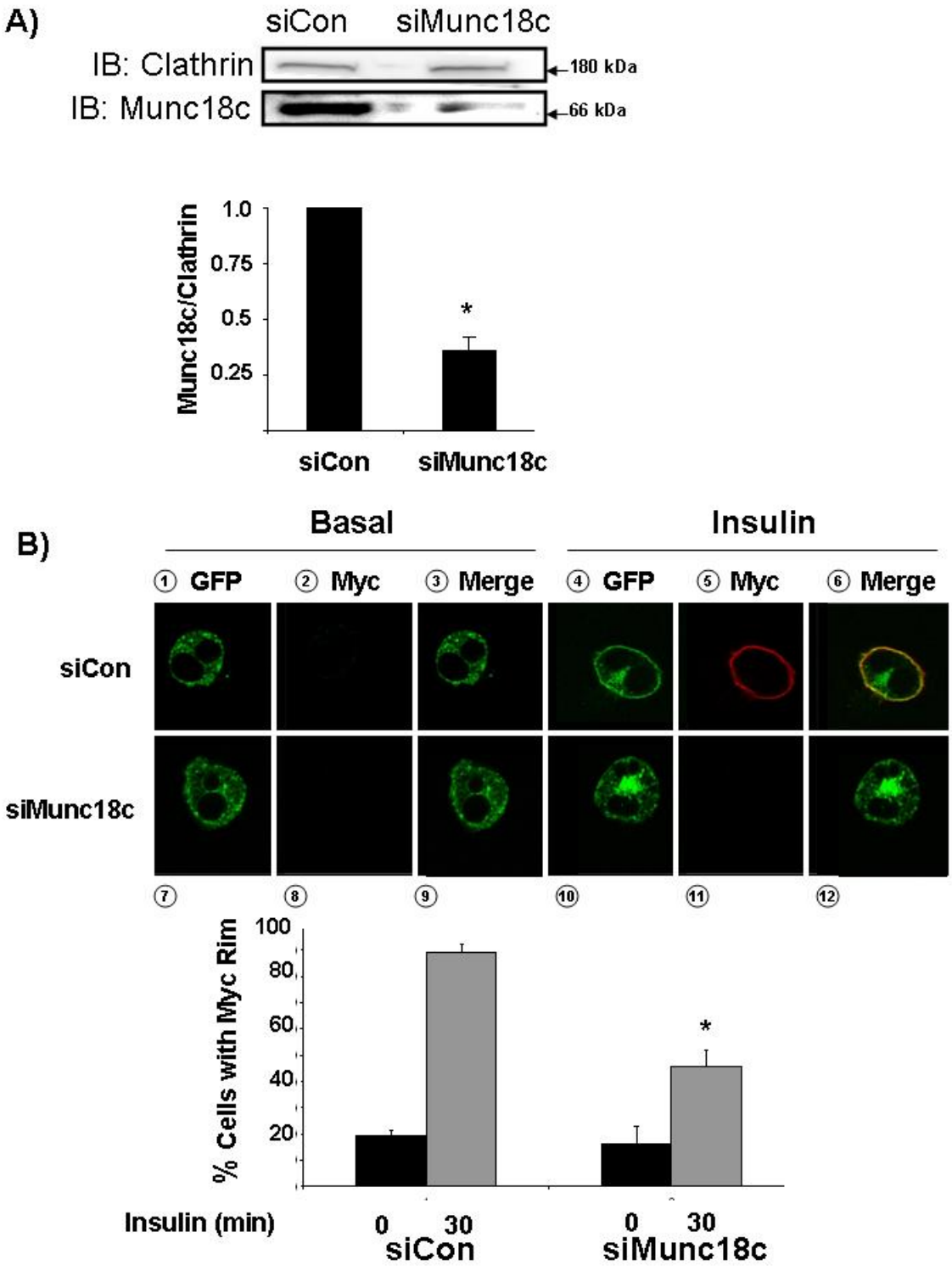
A)
siCon
siMunc18c
IB: Clathrin
IB: Munc18c
180 kDa
66 kDa
Munc18c/Clathrin
1.0
0.75
0.5
0.25
*
siCon
siMunc18c
B)
Basal
Insulin
① GFP
② Myc
③ Merge
④ GFP
⑤ Myc
⑥ Merge
siCon
siMunc18c
⑦
⑧
⑨
⑩
⑪
⑫
% Cells with Myc Rim
100
80
60
40
20
*
Insulin (min)
0
30
0
30
siCon
siMunc18c

Figure 3-8 The Knockdown of Munc18c Decreases Plasma Membrane GLUT4. A) Munc18c shRNA and non-targeting control shRNA constructs were each electroporated into 3T3L1 adipocytes and detergent cell lysates prepared 48 hours later to determine the efficiency of protein depletion achieved by each. Lysates were subjected to 10% SDS-PAGE for immunoblotting with anti-Munc18c and anti-clathrin (loading control) antibodies. Optical density scanning quantitation was used to derive the band density for each clathrin band, which was used to normalize Munc18c bands in each experiment, and the mean ± SE of at least six independent sets of experiments were determined (*$P < 0.005$). B) 3T3L1 adipocytes were transfected with Myc-GLUT4-EGFP plasmid with or without Munc18c shRNA construct. Forty-eight hours later the cells were either left untreated or stimulated with insulin (100nM) for 30 minutes. The cells were then assayed for the plasma membrane translocation of GLUT4 by single cell assays with the confocal microscopy. Fifty cells were blindly counted for a Myc Rim in each condition in three independent experiments.

was carried out using our transient plasmid delivery system (pSilencer1.0-siMunc18c), as previously described (39). The efficiency of the siMunc18c depletion from siMunc18c-expressing adipocytes was 64 ± 6% ($p<0.005$, Figure 3-8A). Adipocytes were co-electroporated with shRNA plasmid and myc-GLUT4-GFP as a reporter of fusion of GLUT4 with the plasma membrane selectively in control or Munc18c depleted cells. Because the myc epitope is inserted into the first exofacial loop of GLUT4, it becomes externalized upon fusion of vesicles containing myc-GLUT4-GFP with the plasma membrane (PM), making it available for labeling with a myc antibody in non-permeabilized cells. Under basal conditions, control-depleted (siCon) cells expressing myc-GLUT4-GFP were identified by their punctuate green fluorescence, with nearly undetectable myc staining, consistent with a low level of fused GLUT4 in the absence of stimulation (Figure 3-8B, panel 1 and 2). In response to insulin, GLUT4 vesicles translocated to the PM to form a continuous GFP rim, concurrent with a rim of externalized myc (Figure 3-8B, panels 4-6), consistent with insulin-induced GLUT4 vesicle fusion with the PM. Cells co-transfected with siMunc18c displayed ~ 40% less membrane localized GLUT4 translocation in response to insulin (Figure 3-8 panels 10-12). The intracellular punctuate pattern of GLUT4 under basal conditions was unaffected by Munc18c depletion (Figure 3-8, panels 7-9). Consistent with the general role of Munc18c as a positive effector of vesicle fusion, and with the role of Munc18c in skeletal muscle, these data indicate the requirement for Munc18c in insulin-stimulated GLUT4 translocation in 3T3L1 adipocytes.

Preliminary studies reveal that in adipocytes co-electroporated with myc-GLUT4-GFP, Munc18c shRNA, and shRNA resistant Flag-Munc18c, insulin-stimulated GLUT4 translocation is rescued approximately 67% (Figure 3-9 A). Interestingly, similar studies using shRNA resistant Munc18c-Y219F and Munc18c-Y521F showed less rescue of GLUT4 translocation (Figure 3-9A and B). Studies are now underway to confirm these results.

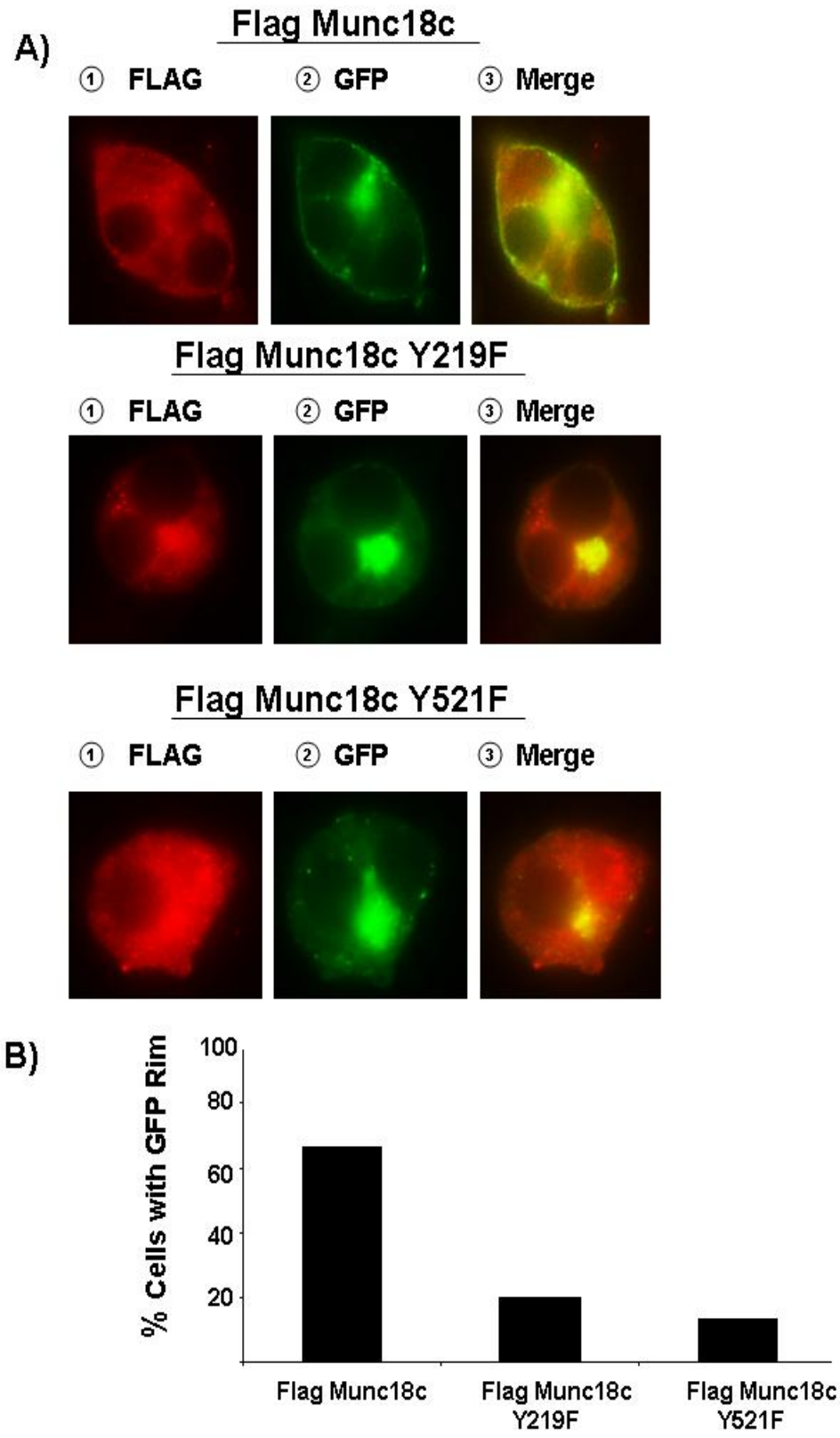
A)
Flag Munc18c
① FLAG
② GFP
③ Merge
Flag Munc18c Y219F
① FLAG
② GFP
③ Merge
Flag Munc18c Y521F
① FLAG
② GFP
③ Merge
B)
% Cells with GFP Rim
100
80
60
40
20
Flag Munc18c
Flag Munc18c Y219F
Flag Munc18c Y521F

Figure 3-9 <u>The Effect of Munc18c Tyrosines 219 and 521 in Insulin-Stimulated GLUT4 Translocation.</u> A) 3T3L1 adipocytes were transfected with Myc-GLUT4-EGFP plasmid, Munc18c shRNA construct, and Flag Munc18c (Top), Flag Munc18c Y219F (Middle), or Flag Munc18c Y521F (Bottom). Forty-eight hours later the cells were stimulated with insulin (100nM) for 30 min. The cells were then assayed for the plasma membrane translocation of GLUT4 by single cell analysis with confocal microscopy. Thirty cells were blindly counted for a GFP Rim in one experiment.

3.4 DISCUSSION

In this study, we found that in 3T3L1 adipocytes and mouse skeletal muscle, insulin triggers the tyrosine phosphorylation of Munc18c concomitant with its association with the IR, and disruption of Munc18c-Syntaxin 4 complexes. IR kinase activity is required for these events, further implicating the IR as a novel Munc18c tyrosine kinase. *In vitro* kinase assays and Y219-phospho specific antibody labeling point to Y219 and Y521 as target sites for modification in adipocytes. Moreover, these sites are in close proximity within the Munc18c crystal structure (Figure 3-10), suggesting that this region is of particular importance in the transient and stimulus-coupled regulation of Munc18c-Syntaxin 4 complexation. Importantly, our data support a model whereby insulin-stimulated phosphorylation of one or both of these tyrosine residues is required for normal insulin-stimulated GLUT4 translocation.

This is the first report of a tyrosine kinase that phosphorylates Munc18c, that being IR. IR-Munc18c association and Munc18c tyrosine phosphorylation supports the existence of parallel pathways for IR-mediated Munc18c tyrosine phosphorylation and the classic IR-IRS-1-PI3K dependent signaling cascade. In fact, IR has numerous substrates besides IRS-1, such as insulin receptor substrate proteins (IRS2–IRS4), Shc, Gab-1, Cbl, APS, and caveolin 1 (206,207). However, since SNARE-mediated GLUT4 vesicle translocation has usually been considered the most distal event of the insulin-signaling cascade in adipocytes and skeletal muscle, we and others had predicted that the kinase mediating the dissociation of Munc18c-Syntaxin 4 complexes was downstream of PI3K, and likely PI3K-dependent. To the contrary, our data instead suggest a new model, in which IR orchestrates the preparation of Syntaxin 4 for subsequent incoming insulin-stimulated GLUT4 vesicles in parallel to its signaling to mobilize those vesicles. Future studies are required to stringently test this model.

Finally, studies are now underway to determine the importance of Munc18c tyrosine phosphorylation of 219 and 521 with regards to the regulation of insulin-stimulated glucose uptake. Preliminary data suggest that the tyrosine phosphorylation of both of these sites is important for the translocation of GLUT4

to the plasma membrane. This region on Munc18c containing Y219 and Y521 may be a potential target not only for regulating the Munc18c-Syntaxin 4 interaction but also vesicle exocytosis, insulin-stimulated GLUT4 translocation in the peripheral tissues and glucose-stimulated insulin secretion in the pancreatic beta cell.

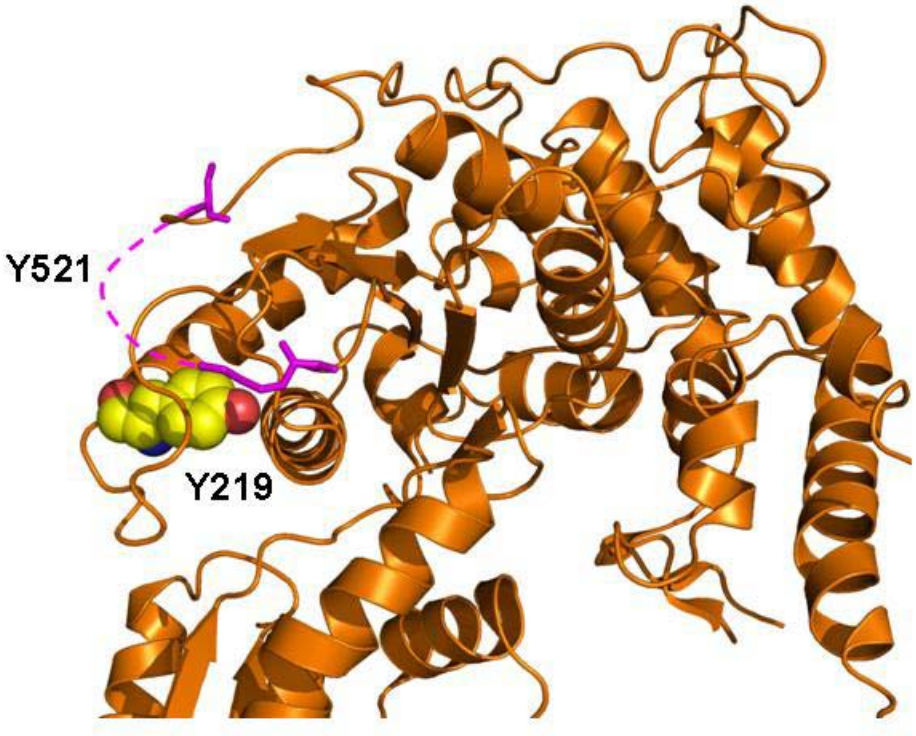

Figure 3-10 <u>Modeling of Munc18c Y219 and Y521 Residues.</u> A depiction of the Munc18c (orange) crystal structure illustrating the close proximity of Y219 and Y521. The Pink dash line represents the disordered and uncrystallized region in which Y521 resides.

CHAPTER 4: FILAMENTOUS ACTIN REGULATES INSULIN EXOCYTOSIS THROUGH DIRECT INTERACTION WITH SYNTAXIN 4

Some of the text in this Chapter is reproduced from:

Jewell JL*, Luo W*, Oh E, Wang Z, and Thurmond DC. (2008). A Direct Association of Filamentous Actin with Syntaxin 4 Functionally Restricts Granule Accessibility to Regulate Insulin Exocytosis. *J Biol Chem* 283: 10716-10726.
**Authors Contributed Equally*

Author Contributions: Oh E generated data for Figure 4-1. Wang Z produced data for Figure 4-7. Luo W generated data for Figures 4-3, 4-4, and 4-5. Jewell JL produced data for Figures 4-2A, 4-5, 4-6C, 4-8 and 4-9.

4.1 INTRODUCTION

Insulin granule exocytosis requires two syntaxin isoforms: Syntaxin 1A and Syntaxin 4. Syntaxin 1A null mouse islets show significantly fewer pre-docked granules which support first-phase insulin release in response to calcium influx, although second-phase secretion is normal (19). Syntaxin 4 heterozygous knockout mouse islets show decreased first-phase secretion and also a slight decrease in second phase secretion (26). In addition, Syntaxin 4 over-expressing transgenic mouse islets have enhanced second-phase secretion (26). Other cell systems that utilize multiple syntaxins show partitioning of interactions and localization to particular membrane compartments to achieve differential modes of vesicle targeting and fusion (208,209). Characterization of unique properties of Syntaxin 1A and Syntaxin 4 will be required before a mechanistic understanding of their different roles in biphasic insulin release can be discerned.

We have previously demonstrated that, in rodent islet beta cells, glucose-induced insulin exocytosis is coupled to the interaction of F-actin with t-SNARE proteins (29). Here, we demonstrate the relevance of this to human islet function, and have expanded upon the underlying mechanism by showing that F-actin bound directly to a novel motif in the N-terminus of Syntaxin 4.

4.2 MATERIALS AND METHODS

4.2.1 Materials

Rabbit polyclonal Syntaxin 4 and mouse monoclonal Syntaxin 1 antibodies were obtained from Chemicon (Temecula, CA) and Upstate Biotechnology (Lake Placid, NY), respectively. The mouse anti-insulin and rabbit anti-actin antibodies were obtained from Sigma (St. Louis, MO). Rabbit anti-GFP antibody was acquired from Abcam (Cambridge, MA). Monoclonal anti-SNAP-25 and anti-GFP antibodies were purchased from BD Biosciences Clontech (San Jose, CA). The mouse monoclonal anti-VAMP2 antibody and recombinant soluble Syntaxin 1A protein were obtained from Synaptic Systems (Gottingen, Germany). Latrunculin B was purchased from Calbiochem (La Jolla, CA). Texas-red conjugated secondary antibody and control mouse and rabbit IgG for immunoprecipitation were purchased from Jackson Immunoresearch Laboratories (West Grove, PA). Radioimmunoassay grade bovine serum albumin and D-glucose were purchased from Sigma. The MIN6 cells were a gift from Dr. John Hutton (University of Colorado Health Sciences Center). Goat anti-mouse and anti-rabbit horseradish peroxidase secondary antibodies and Transfectin lipid reagent were acquired from Bio-Rad (Hercules, CA). ECL reagent was purchased from Amersham Biosciences (Piscataway, NJ). The human C-peptide and rat insulin RIA kits were purchased from Linco Research Inc (St. Charles, MO). The Actin binding spin-down assay (#BK001) and F/G-actin quantitation kits were purchased from Cytoskeleton (Denver, CO).

4.2.2 Plasmids

The pGEX-4T1-VAMP2-(1-94) was generated as previously described (210). The pGEX-4T1-Syntaxin 4-(1-193), -(1-112) and –(1-70) cDNA constructs were generated by subcloning PCR-generated rat Syntaxin 4 fragments into the SalI and XhoI sites of the pGEX-4T1 expression vector. The pGEX-4T1-Syntaxin 4-(1-273) and -(39-273) cDNA constructs were made by subcloning PCR-generated fragments into the EcoRI and XhoI sites of the pGEX-4T1. The pEGFP-Syntaxin 4-(39-112) cDNA construct was generated by subcloning the PCR-generated Syntaxin 4 fragment engineered with 5'EcoRI and 3'XhoI sites

into the 5'EcoRI and 3'SalI sites of the EGFP-C2 vector (Clontech). All constructs were verified by DNA sequencing.

4.2.3 Cell Culture, Transient Transfection and Secretion Assays

MIN6 beta cells were cultured in Dulbecco's modified Eagle's medium (DMEM with 25 mM glucose) supplemented with 15% fetal bovine serum, 100 units/ml penicillin, 100 µg/ml streptomycin, 292 µg/ml L-glutamine, and 50 µM β-mercaptoethanol as described previously (146). MIN6 beta cells at ~60% confluence were transfected with 40 µg of plasmid DNA per 10 cm^2 dish using Transfectin (Bio-Rad) to obtain ~30-50% transfection efficiency. After 48 hours of incubation, cells were washed twice with and incubated for 2 h in freshly prepared modified Krebs-Ringer bicarbonate buffer (MKRBB; 5 mM KCl, 120 mM NaCl, 15 mM Hepes pH 7.4, 24 mM $NaHCO_3$, 1 mM $MgCl_2$, 2 mM $CaCl_2$ and 1 mg/ml RIA-grade BSA). Cells were stimulated with 20 mM glucose for the times indicated in the figures, after which the buffer was collected, microcentrifuged for 5 min at 4^oC to pellet cell debris, and insulin secreted into buffer quantitated using a rat insulin immunoassay kit (Linco Research). Cells were harvested in NP-40 lysis buffer (25 mM HEPES, pH 7.4, 1% NP-40, 10% glycerol, 50 mM sodium fluoride, 10 mM sodium pyrophosphate, 137 mM NaCl, 1 mM sodium vanadate, 1 mM PMSF, 10 µg/ml aprotinin, 1 µg/ml pepstatin and 5 µg/ml leupeptin) containing 60 mM *n*-octylglucoside and lysed for 10 minutes at 4^oC, and lysates cleared of insoluble material by microcentrifugation for 10 minutes at 4^oC for subsequent use in co-immunoprecipitation experiments. For measurement of human C-peptide release, MIN6 beta cells were transiently co-transfected with each plasmid plus human proinsulin cDNA (kind gift from Dr. Chris Newgard, Duke University). Forty-eight hours following transfection, cells were pre-incubated for 2 hours in MKRBB buffer and stimulated with 20 mM glucose for 1 hour. MKRBB was collected for quantitation of human C-peptide released.

4.2.4 Immunofluorescence and Confocal Microscopy

MIN6 cells at 40% confluency plated onto glass coverslips were preincubated in MKRBB in the absence or presence of Latrunculin (10 μM) or vehicle (DMSO) for 1-2 hours followed by stimulation with 20 mM glucose for 5 minutes and immediately fixed and permeabilized in 4% paraformaldehyde and 0.1% Triton X-100 for 10 minutes at 4^{o}C. Fixed cells were blocked in 1% BSA plus 5% donkey serum for 1 h at room temperature, followed by incubation with ant-insulin antibody (1:100) for 1 hour. MIN6 cells were then washed with phosphate buffered saline (PBS, pH 7.4) and incubated with anti-mouse Texas Red secondary antibody for 1 hour. All cells were washed again in PBS, overlaid with Vectashield mounting medium and mounted for confocal fluorescence microscopy using a Zeiss 510 confocal microscope. EGFP and insulin-Texas Red fluorescing cells were imaged using single-channel scanning using a 100x objective.

4.2.5 Electron Microscopy

MIN6 beta cells were grown to ~80% confluence on Thermonox coverslips. Cells were washed twice with and incubated 2 hours in freshly prepared modified Krebs-Ringer bicarbonate buffer followed by addition of either Latrunculin B or DMSO vehicle for an additional 30 minutes. Cells were fixed in a 0.1 M cacodylate buffered mixture of 2% glutaraldehyde and 2% paraformaldehyde for 30 min at room temperature followed by overnight incubation at 4^{o}C, and then post-fixed in 1% OsO_4 in for 1 hour. En bloc staining in 0.5% aqueous uranyl acetate was performed for 3 hours followed by a 10 minute water wash. Dehydration was done in the following sequence, 50% ethanol, 70% ethanol, 95% ethanol, and 100% ethanol each 10 minutes. Infiltration entailed ethanol and resin in the order of 3:1 (1 hour), 1:1 (overnight), 1:3 (1 hour), and 100% resin (2-3 changes each 30 minutes). The Thermonox Coverslips were inverted over a 1.5 ml centrifuge tube filled with resin and polymerized for 48 hours at 60°C. Thick (0.5-2.0 μm) and thin (60-100 nm) sections were cut using the

microtome (Leica Ultracut). The thin sections were stained with uranyl acetate and lead citrate and viewed on the FEI Tecnai G2 Biotwin.

4.2.6 Subcellular Fractionation

Subcellular fractions of beta cells were isolated as described previously (210). Briefly, MIN6 beta cells at ~90% confluence were harvested into 1 ml of homogenization buffer (20 mM Tris-HCl, pH 7.4, 0.5 mM EDTA, 0.5 mM EGTA, 250 mM sucrose, 1 mM DTT and 1 mM sodium orthovanadate containing protease inhibitors. Cells were disrupted by 10 strokes through a 27 gauge needle and homogenates centrifuged at 900 x g for 10 minutes. Postnuclear supernatants were centrifuged at 5,500 x g for 15 minutes and the subsequent supernatant centrifuged at 25,000 x g for 20 minutes to obtain the storage granule (SG) fraction in the pellet. The supernatant was further centrifuged at 100,000 x g for 1 hour to obtain the cytosolic fraction (Cyt). Plasma membrane fractions (PM) were obtained by mixing the postnuclear pellet with 1 ml of Buffer A (0.25 M Sucrose, 1 mM $MgCl_2$ and 10 mM Tris-HCl, pH 7.4) and 2 volumes of Buffer B (2 M sucrose, 1 mM $MgCl_2$ and 10 mM Tris-HCl, pH 7.4). The mixture was overlaid with Buffer A and centrifuged at 113,000 x g for 1 hour to obtain an interface containing the plasma membrane fraction. The interface was collected and diluted to 2 ml with homogenization buffer for centrifugation at 6,000 x g for 10 minutes, and the resulting pellet was collected as the plasma membrane fraction. All pellets were resuspended in 1% NP-40 lysis buffer to ensure solubilization of membrane proteins.

4.2.7 Co-immunoprecipitation and Immunoblotting

MIN6 beta cell cleared detergent homogenates (2-3 mg) were combined with rabbit anti-Syntaxin 4 or mouse anti-Syntaxin 1 antibodies for 2 hours at 4°C followed by a second incubation with protein G Plus-agarose for 2 hours. The resultant immunoprecipitates were subjected to 12% SDS-PAGE followed by transfer to PVDF membranes for immunoblotting. Membranes were blocked in 5% milk/TBS-Tween for 1 hour at room temperature, followed by immunoblotting

(Syntaxin 1A, Syntaxin 4 and SNAP-25 antibodies were used at 1:1000; VAMP2 antibody was used at 1:5000). Proteins were visualized by enhanced chemiluminescence for quantitation using a Chemi-Doc gel documentation system (Bio-Rad).

4.2.8 Recombinant Proteins and Interaction Assays

GST-VAMP2 (1-94) fusion protein was expressed in Escherichia coli and purified by glutathione-agarose affinity chromatography as described (210). GST-VAMP2 was immobilized on sepharose beads and incubated with cleared detergent lysates (~3 mg) prepared from unstimulated cells for 2 hours at 4^{o}C. Following 3 washes with 1% NP40 lysis buffer, proteins were eluted from the sepharose beads and subjected to electrophoresis on 12% SDS-PAGE followed by transfer to PVDF membrane for immunoblotting with anti-Syntaxin 4 antibody. For the F-actin spin-down assays, recombinant VAMP2 and Syntaxin 4 proteins were initially expressed and purified as GST-fusion proteins, after which the GST was removed by thrombin cleavage and remaining protein captured (Novagen kit). Syntaxin 1A protein was purchased from Synaptic Systems. Proteins were concentrated to ~20 μM and centrifuged at 150,000 x g for 1 hour at 4^{o}C immediately prior to use of resulting supernatant in actin binding assay. Purified F-actin stocks (23 μM) were prepared according to manufacturer's instructions. Test proteins were incubated with F-actin stock in actin polymerization buffer at room temperature for 30 minutes. BSA and α-actinin control proteins provided by the manufacturer were used as negative and positive F-actin binding control proteins, respectively, in each experiment for validation of binding. All reactions were centrifuged at 150,000 x g for 1.5 hours at 24^{o}C and supernatants removed into individually labeled new tubes on ice. Both the supernatants and the pellets were subjected to 12-18% SDS-PAGE followed by transfer to PVDF membranes for Coomassie staining or immunoblotting analyses.

4.2.9 Statistical Analysis

All data are expressed as mean ± S.E. Data were evaluated for statistical significance using an unpaired two-tail Student's t test.

4.3 RESULTS

4.3.1 F-actin Function is Conserved Between Human and Rodent Islet Beta Cells

We previously reported that treatment of rat islets with Latrunculin B results in potentiation of glucose-stimulated insulin release (29). Latrunculin is a potent actin monomer-binding and sequestering agent which converts cellular F-actin to G-actin. To establish continuity of function amongst islet model systems, the impact of Latrunculin upon secretion from mouse islets and human islets was evaluated. Similar to rat islets, isolated mouse islets showed a robust response to 2 hours glucose stimulation, which was further potentiated by Latrunculin (Figure 4-1A). Human islets were obtained from three independent non-diabetic human cadaver pancreases through the NIH/ICR/ABCC distribution program. Because of the fragility of these human islets following isolation and shipment, Latrunculin pre-treatment and stimulation time was limited to 1 hour, rather than the 2 hour period used with mouse islets, which cumulatively resulted in a lesser yet still significant secretory response to glucose stimulation (Figure 4-1B). Importantly, each batch of human islets showed the Latrunculin-potentiated effect upon glucose-stimulated insulin release, while basal secretion was comparable to the vehicle (DMSO)-treated islets (Figure 4-1B). Since islets contain multiple cell types, 70-80% of which are insulin-containing beta cells, cultured MIN6 beta cells were used to further confirm that this potentiating effect of Latrunculin was transduced through the beta cells and not one of the other islet cell types. This potentiating effect occurred very rapidly, evident within 5 minutes of stimulation with glucose (Figure 4-1C). Latrunculin also potentiated insulin release from MIN6 cells in response to KCl and PMA, as well as calcium-stimulated secretion from Streptolysin-O-permeabilized cells (21). Moreover, the actin-depolymerizing effect of Latrunculin was validated by analysis of the F:G-actin ratio, converting F-actin:G-actin ratio from ~20%:80% in unstimulated or vehicle-treated cells to ~1%:99% (data not shown). Thus the potentiating effect of Latrunculin was found to be conserved across species and relevant to human islet function.

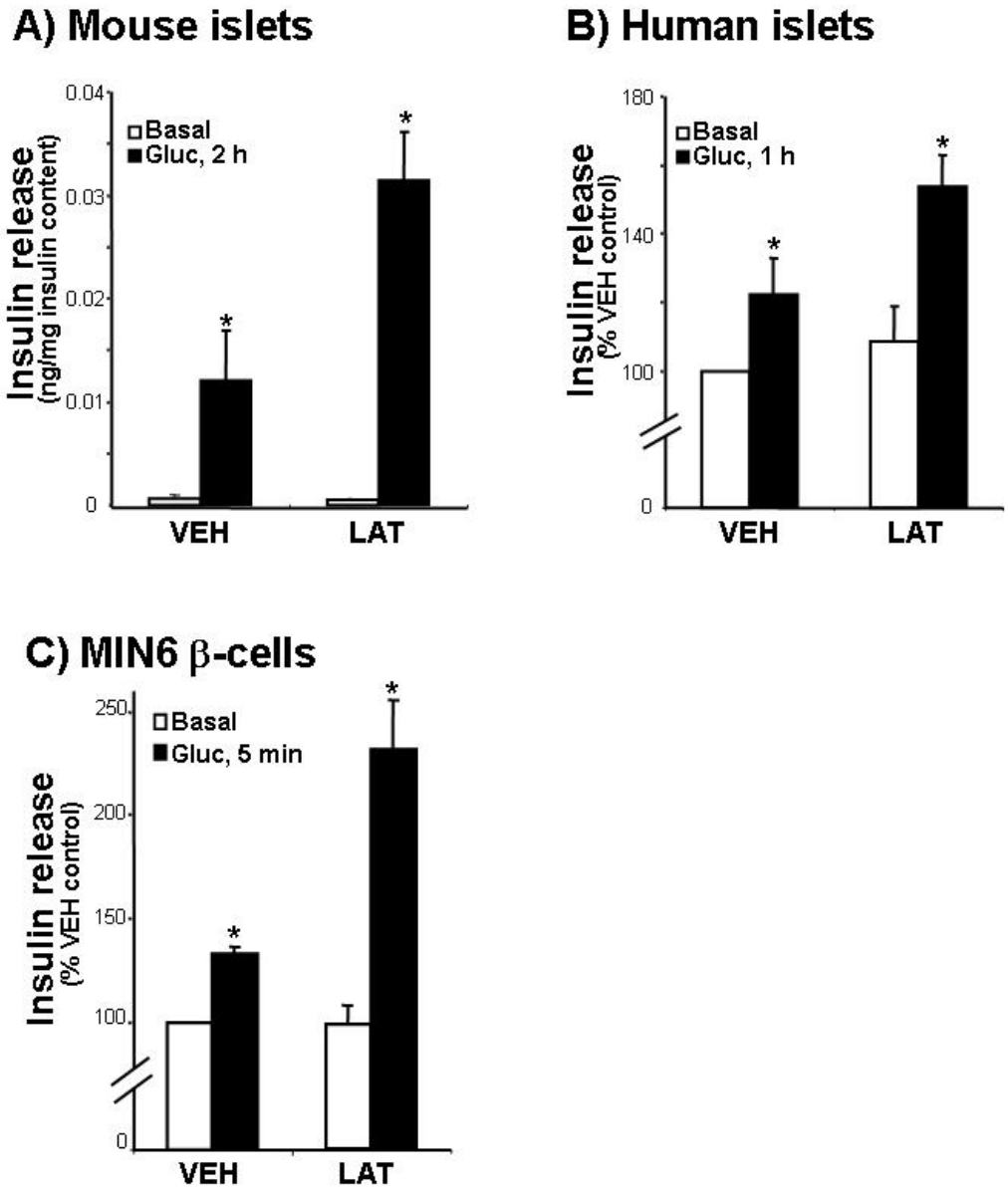

Figure 4-1 Latrunculin Potentiates Insulin Secretion in Human Islets-Conservation of Function with Rodent Islets and Cultured Beta Cells. A) Mouse islets were handpicked for 2 hour pre-incubation in KRB with 2.8 mM glucose ± Latrunculin (10 µM LAT), then 2 hour more under basal or stimulated conditions (20 mM glucose), with 10 islets per condition. Three independent sets of mouse islets were combined and data expressed as insulin secretion normalized to insulin content. *P< 0.05, versus vehicle-basal condition. B) Human islets were isolated from cadaver pancreas at the ICR and shipped for receipt within 48 hours of isolation. Islets were allowed to recover for 3 hours and then handpicked for pre-incubation for 1 hour in KRB containing 2 mM glucose ±

Latrunculin (10 μM LAT) followed by 1 hour incubation under basal (2.8 mM glucose) or stimulated conditions (20 mM). Data represent the average of three independent batches of human islets, normalized for insulin content and expressed as % vehicle-basal secretion set equal to 100%; *P< 0.05, versus vehicle-basal condition. C) MIN6 cells were pre-incubated in glucose-free MKRBB containing vehicle or LAT for 2 hour and then stimulated with 20 mM glucose for 5 minutes. Data represent the average of 6 independent sets of MIN6 cells, normalized for protein content and expressed as % vehicle-basal secretion; *P< 0.02, versus vehicle-basal condition.

Moreover, the MIN6 beta cell line was found to be an appropriate model system in which to pursue mechanistic study of the role of F-actin in beta cell secretion.

To determine how Latrunculin facilitated this potentiation, insulin granule localization was examined. Electron micrograph images of Latrunculin-treated MIN6 cells showed the prevalence of granules localized at the plasma membrane (Figure 4-2A, right panel). In 10 images collected of Latrunculin-treated cells, greater than 90% exhibited this phenotype. In contrast, vehicle-treated cells contained only a few granules at the cell periphery (Figure 4-2A, left panel, arrow denotes plasma membrane between neighboring cells) in all fields. Insulin immunofluorescent confocal microscopy of vehicle- or Latrunculin-treated MIN6 cells confirmed the identity of the granules localized at the PM as insulin-containing (Figure 4-2B). Punctate insulin staining was visible broadly across the expanse of the beta cells under basal conditions, with regrouping of granules closer to the cell periphery after only 5 minutes of glucose stimulation. Latrunculin treatment mimicked this glucose-induced redistribution of granules to the cell periphery, but did so in the absence of glucose. Immunofluorescent images of more than 30 clusters of Latrunculin-treated cells showed the phenotype in Figure 4-2B. In a third approach, subcellular fractions were prepared from MIN6 cells treated with vehicle or Latrunculin to quantify the extent of the granule redistribution induced by Latrunculin. The fractionation procedure was validated in two ways: 1) demonstration of highest insulin content in insulin secretory granule (SG) fraction with lesser but significant levels in PM fraction and none in cytosolic fraction (210-212); 2) the presence of marker proteins in the PM (Syntaxin 4, Syntaxin 1A), in the SG (VAMP2, phogrin), and in the Cyto fraction (Cdc42, Munc18c). In three independent sets of fractions, Latrunculin induced an ~2.5-fold increase in VAMP2-bound insulin granules localized to the PM, with a coordinate ~40% loss from the storage granule (SG) pool (Figure 4-2C and D). Ponceau S staining was used to validate equal loading in each experiment. Thus, Latrunculin-induced F-actin depolymerization allowed flow of insulin granules to the PM in the absence of the glucose stimulus.

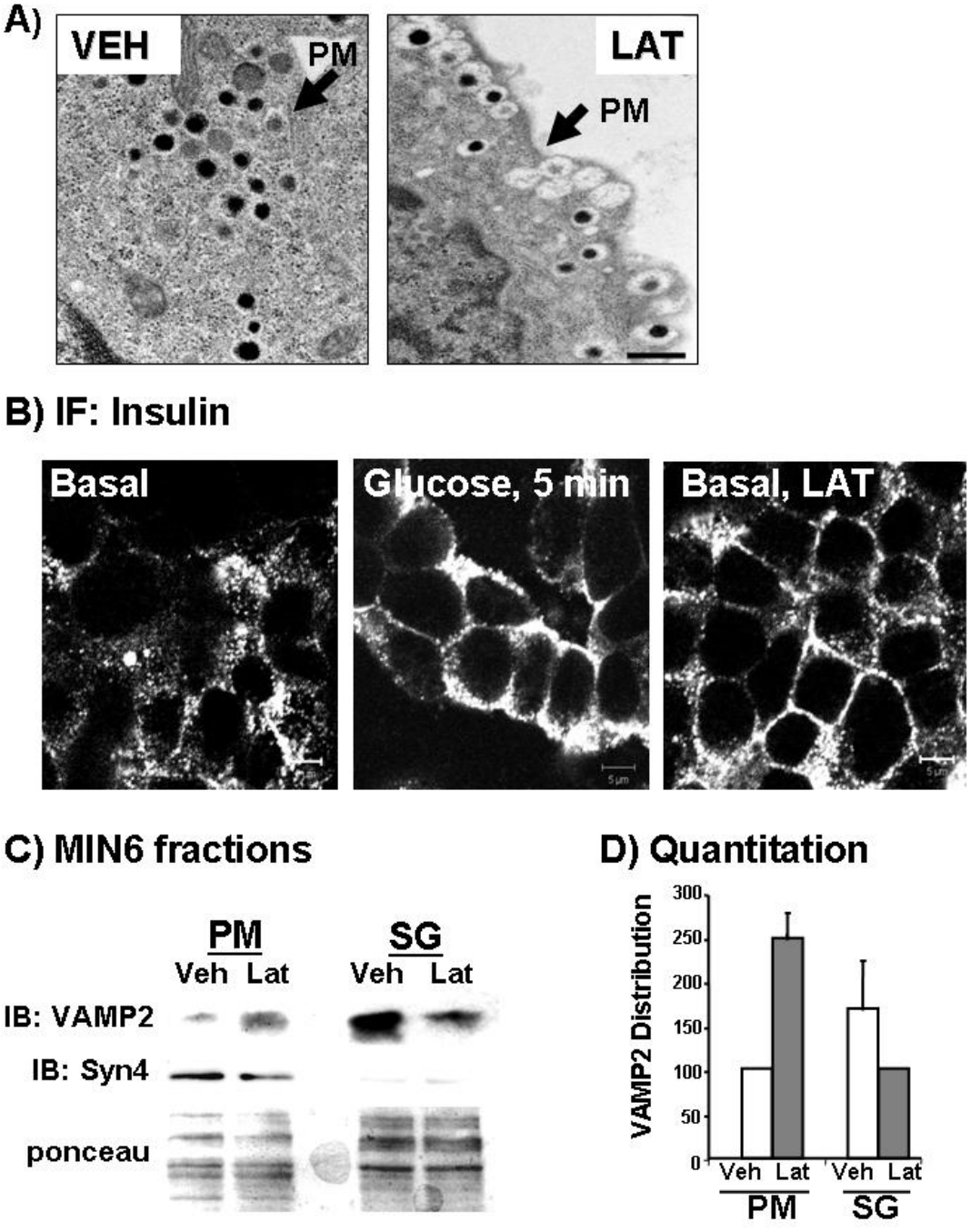

Figure 4-2 Latrunculin Causes Increased Granule Accumulation at the Plasma Membrane in the Absence of Glucose. A) Electron microscopy (TEM) of MIN6 cells treated with vehicle (VEH) or Latrunculin (LAT), bar=500 nm. B) Latrunculin treatment mobilizes granules towards the plasma membrane compartment from the storage granule pool under basal conditions. MIN6 cells were left unstimulated, stimulated with 20 mM glucose for 5 minutes or treated with 10 μM

Latrunculin (LAT) for 2hours, then fixed and permeabilized for anti-insulin immunofluorescent confocal microscopy. Bar, 5μm. C) MIN6 cells were treated with Latrunculin or the DMSO vehicle for 2hours, then subfractionated and 20 μg protein from of plasma membrane (PM) and storage granule (SG) fractions were resolved on 12% SDS-PAGE for immunoblotting. Ponceau S staining used to verify equal loading; Syntaxin immunoblotting used to validate PM fraction integrity in each fractionation. Data are representative of two independent experiments. D) Optical density scanning quantitation (each set of fractions normalized to VEH control=100%) of VAMP2; data shown as average ± S.E. of 3 independent sets of fractions. Ponceau staining used to verify loading in SG and PM fractions each experiment.

4.3.2 Glucose-Induced Dissociation of F-actin from Syntaxin 4

We have previously reported that F-actin is dynamically reorganized in response to glucose stimulation in islet beta cells, and that this phenomenon is coupled to Syntaxin 1 association (29,213). F-actin associated in a specific manner, as IgG alone or VDCC primary antibodies failed to co-immunoprecipitate F-actin. These studies also showed that Syntaxin 1 only associates with F-actin and not G-actin; treatment of cells with actin depolymerizing agents destroyed this association. We have since demonstrated a requirement for a second syntaxin isoform in insulin granule exocytosis, Syntaxin 4 (26). Here we show that like Syntaxin 1, Syntaxin 4 associated with F-actin under basal conditions (Figure 4-3A and B). Also similar is the marked significant reduction of actin association with Syntaxin 4 after 10 minutes of glucose stimulation. Following 30 minutes of glucose stimulation actin re-associated with Syntaxin 4, albeit to a lesser extent than it did with Syntaxin 1. Treatment of cells with Latrunculin abolished ~90% of actin interaction with Syntaxin 4 (Figure 4-3C), indicating that it was F-actin and not G-actin that interacted with Syntaxin 4. These data expand upon the current notion of F-actin serving as a barrier by suggesting that the negative function of F-actin is mediated through its association with multiple plasma membrane-bound Syntaxins.

4.3.3 F-actin Directly Associates with Only the Syntaxin 4 Isoform

To determine how the SNARE proteins might confer interaction with F-actin, sequence analyses of v- and t-SNARE proteins for potential homology with any known actin binding protein motifs were conducted (http://smart.embl-heidelberg.de). While no homologies were identified in VAMP2, SNAP-25 or Syntaxin 1A, Syntaxin 4 was found to have some homology to a motif known as “spectrin-like”. To determine whether Syntaxin 4 might bind in a direct manner to F-actin, an *in vitro* actin sedimentation/spin-down assay was employed. Recombinant soluble forms of each SNARE protein (transmembrane domain deleted) were expressed in *E. coli* and purified were incubated with F-actin in a calcium-containing binding buffer and subsequently centrifuged to pellet F-actin

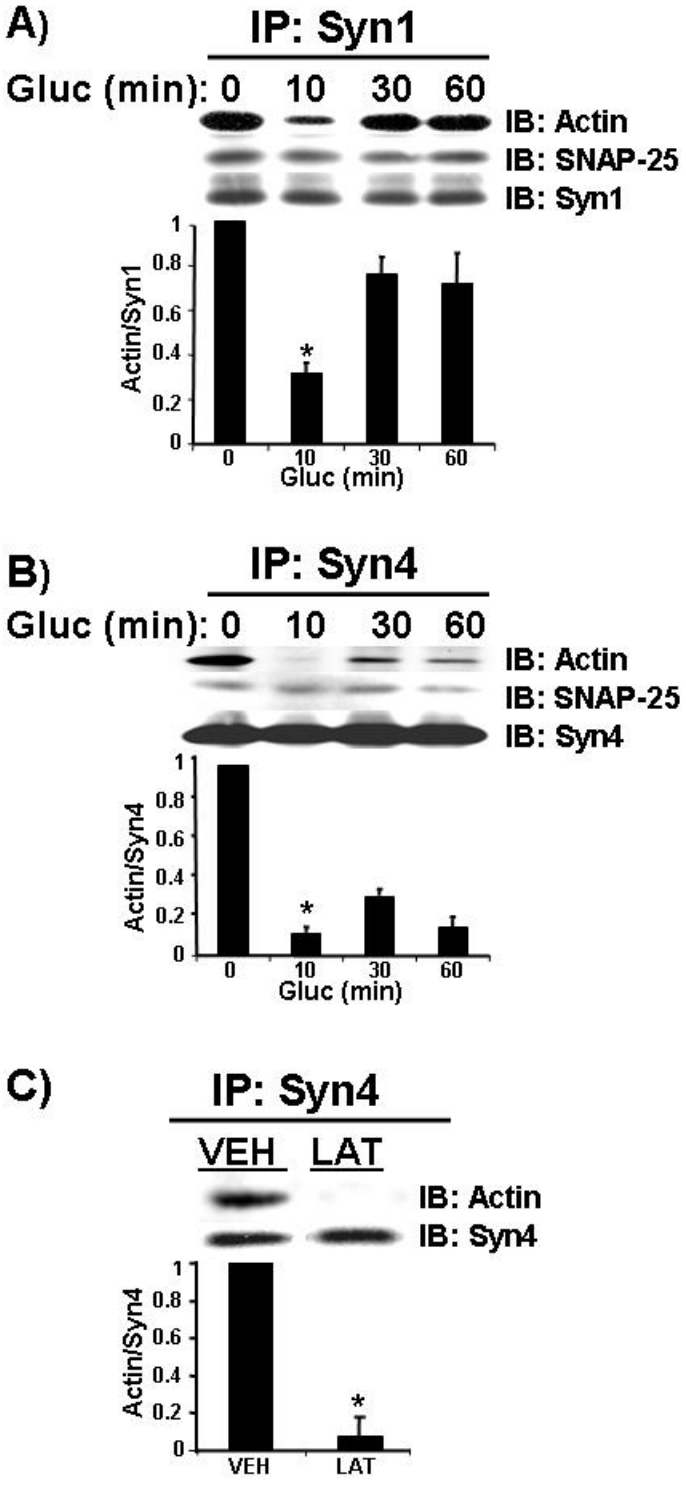
A)
IP: Syn1
Gluc (min): 0 10 30 60
IB: Actin
IB: SNAP-25
IB: Syn1
Actin/Syn1
1
0.8
0.6
0.4
0.2
0
*
0 10 30 60
Gluc (min)
B)
IP: Syn4
Gluc (min): 0 10 30 60
IB: Actin
IB: SNAP-25
IB: Syn4
Actin/Syn4
1
0.8
0.6
0.4
0.2
0
*
0 10 30 60
Gluc (min)
C)
IP: Syn4
VEH LAT
IB: Actin
IB: Syn4
Actin/Syn4
1
0.8
0.6
0.4
0.2
0
*
VEH LAT

Figure 4-3 Glucose-Induced Dissociation of F-actin from Syntaxin 1A and Syntaxin 4. MIN6 cells were pre-incubated in MKRBB for 2 hours and stimulated with 20 mM glucose for 10, 30 and 60 minutes. Detergent cell lysates were prepared by harvesting in lysis buffer containing 1% NP40 and *n*-octylglucoside. Cleared detergent cell lysates (2 mg of protein) were immunoprecipitated with: A) mouse anti-Syntaxin 1, or B) rabbit anti-Syntaxin 4 for 2hours at 4°C. Immunoprecipitates were resolved on 12% SDS-PAGE, and proteins were transferred to PVDF for immunoblotting with mouse anti-Syntaxin 1A or Syntaxin 4, anti-SNAP25 and rabbit anti-actin. C) Lysates prepared from cells pre-treated for 2 hours with vehicle (DMSO, VEH) or Latrunculin (LAT) were used in immunoprecipitation reactions with anti-Syn4 antibody for subsequent immunoblotting for co-immunoprecipitation of actin. Parallel reactions including IgG immunoprecipitation reactions were included to control for non-specific binding as demonstrated previously ((29) not shown here). Data are representative of at least 5 independent co-immunoprecipitation experiments. Optical density scanning quantitation of actin association with Syntaxin is shown directly below each of the three immunoprecipitation studies (each set of lysates normalized to basal=1). Bars represent the average ± S.E. of 3-5 independent experiments normalized to basal=1.0.

and associated proteins. Proteins in each fraction were resolved on SDS-PAGE for detection by Coomassie blue staining. The known F-actin binding protein α-actinin, appropriately localized to the pellet (P) with F-actin (Figure 4-4A, lanes 7-8), while BSA served as the negative control in this assay and localized to the supernatant (S, Figure 4-4A, lanes 5-6). Recombinant Syntaxin 1A also remained strictly in the supernatant (Figure 4-4, lane 4), as did VAMP2 (data not shown). Syntaxin 4 protein was present in both the pellet and supernatant fractions (Figure 4-4A, lanes 1-2). These data indicated that Syntaxin 4 had the ability to interact directly with F-actin, while Syntaxin 1A associated exclusively via an indirect mechanism.

To determine which region of Syntaxin 4 conferred direct interaction with F-actin, a series of C- and N-terminal truncations (Figure 4-5A) were made in the context of GST-Syntaxin 4 (ΔTM, soluble form). Coomassie blue staining showed that all GST-Syntaxin 4 truncation proteins migrated at the correct molecular weight and as single bands (Figure 4-5B). GST was cleaved and remaining Syntaxin 4 fragments purified for use in the F-actin spin down assay. In each assay, recombinant Syntaxin 1A and Syntaxin 4 were used as negative and positive controls for F-actin interaction, respectively (data not shown). C-terminal deletion of domains H3, Hc, or the N-terminal deletion of residues 1-38 failed to abolish Syntaxin 4 interaction with F-actin (Figure 4-5C). Further delineation of the binding region was detected by immunoblotting instead of Coomassie, because of lesser sensitivity due to the small molecular weight of the protein. Immunoblotting increased sensitivity to any interaction, taking advantage of the N-terminal epitope recognized by this particular antibody (epitope is residues 2-23 of Syntaxin 4). Using this, we observed that the C-terminal deletion through the Hb domain did eliminate binding to F-actin (Figure 4-5D). Subsequent truncations of the Ha and Hb domains in the full soluble Syntaxin 4 protein were constructed to determine further importance of the Ha and Hb domains individually, but unfortunately were labile upon cleavage from the GST protein. Since these binding data indicated that the N-terminal Ha-Hb region comprising residues 39-112 as the minimal region sufficient to confer

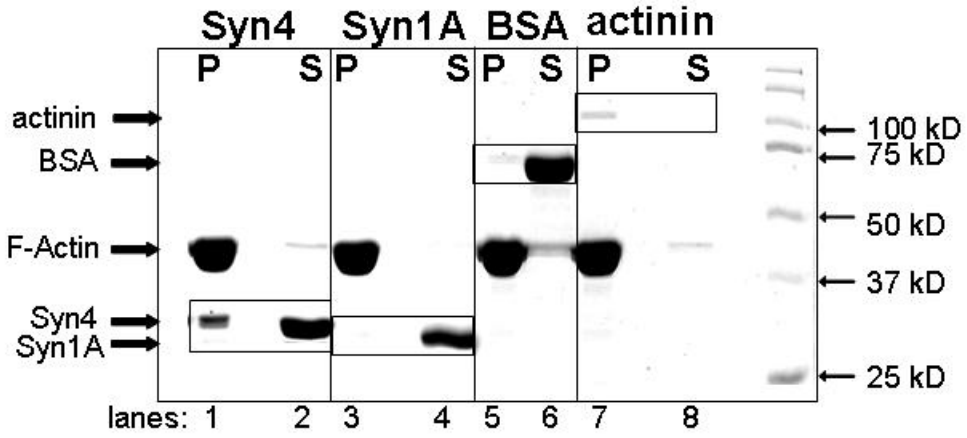

Figure 4-4 Syntaxin 4 but not Syntaxin 1A Binds Directly to F-actin *In Vitro*. Recombinant purified proteins were tested for direct F-actin binding in an *in vitro* sedimentation assay. Following incubation and centrifugation, F-actin and associated binding proteins are recovered in the pellet (P) fraction while non-F-actin binding proteins remain in the supernatant (S). Proteins were resolved on 10% SDS-PAGE and detected by Coomassie blue staining. This reaction was determined to be at saturation for binding (data not shown). Data representative of 6 independent experiments using 4 different preparations of proteins.

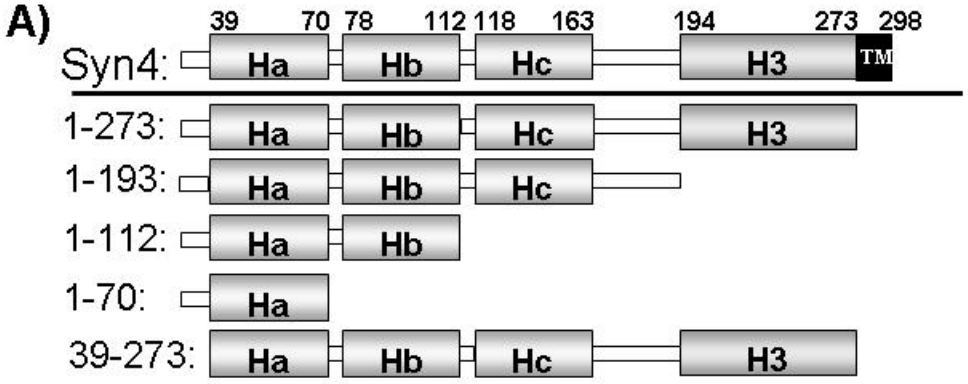
A)
39
70
78
112
118
163
194
273
298
Syn4:
Ha
Hb
Hc
H3
TM
1-273:
1-193:
1-112:
1-70:
39-273:

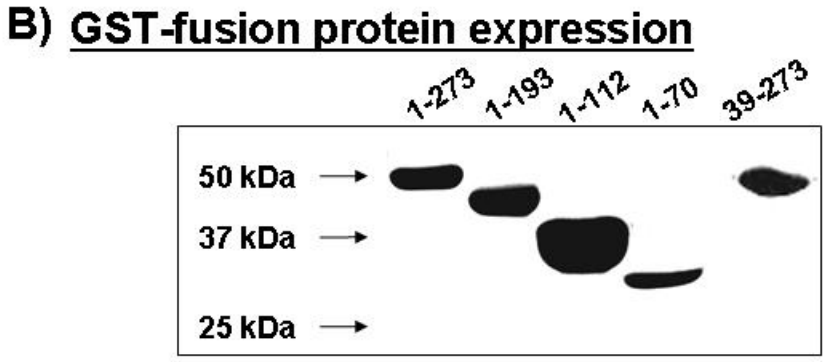
B) GST-fusion protein expression
1-273
1-193
1-112
1-70
39-273
50 kDa
37 kDa
25 kDa

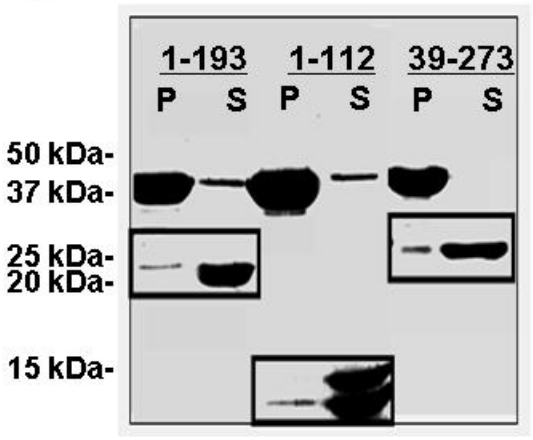
C) Coomassie
1-193
1-112
39-273
P
S
50 kDa-
37 kDa-
25 kDa-
20 kDa-
15 kDa-

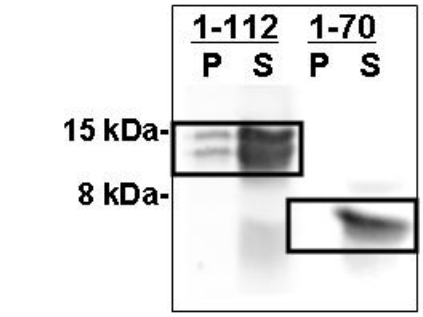
D) IB: Syn4
1-112
1-70
P
S
15 kDa-
8 kDa-

Figure 4-5 The Region Containing the Ha-Hb Domains of Syntaxin 4 is Necessary and Sufficient to Confer Direct Binding to F-actin. A) Four C-terminal truncations and one N-terminal truncation of Syntaxin 4 were generated as GST fusion proteins for expression in *E. coli* and purification on glutathione sepharose. B) Coomassie blue staining showed the expression of GST fusion Syntaxin 4 truncation proteins to be expressed, soluble fragments with high purity. C) Thrombin cleaved Syntaxin 4 N-terminal and C-terminal truncated fragments 1-194, 1-112 and 39-273 were prepared at the concentration 1 mg/ml for use in the *in vitro* actin sedimentation assay. Both the supernatants (S) and the pellets (P) were subjected to 15% SDS-PAGE for Coomassie blue staining. Syn4 and Syn1A reactions were used as positive and negative controls, respectively, in each experiment (see Figure 4). D) Purified Syntaxin 4 C-terminal truncations 1-112 and 1-70 were prepared and tested in the actin sedimentation assay. Both the supernatants and the pellets were subjected to 18% SDS-PAGE followed by transfer to PVDF membranes for immunoblotting with rabbit anti-Syntaxin 4. Data are representative of 2-3 independent sets of proteins.

binding of Syntaxin 4 with F-actin, GST-(39-112) was constructed, but also was labile *in vitro*. The importance of these far N-terminal residues in Syntaxin 4 structure has been reported and likely explains the instability of our constructs lacking this region (114). Thus, the *in vitro* assay data suggested the F-actin interacting region of Syntaxin 4 to be between amino acids 39-112. Notably, this region also contains the predicted spectrin-like motif.

4.3.4 Selective Separation of Syntaxin 4 from F-actin Enhances Granule Mobilization and Exocytosis

To determine the requirement for Syntaxin 4 binding to F-actin in cells, the Syntaxin 4 actin binding region (residues 39-112) was used as a selective competitive inhibitor. This small region was fused to the C-terminus of the EGFP protein as shown in Figure 4-6A, which enabled visualization of its localization within transfected cells and easier detection of its expression by immunodetection on SDS-PAGE (Figure 4-6B, IB: EGFP in lysate). Plasmids encoding EGFP-(39-112) or EGFP vector alone were transfected into MIN6 cells and effects upon Syntaxin 4-F-actin association evaluated by immunoprecipitation with anti-Syntaxin 4 antibody and actin immunoblotting. Because the EGFP-(39-112) fragment did not contain the epitope recognized by the Syntaxin 4 antibody, only endogenous Syntaxin 4 was immunoprecipitated. Indeed, expression of the EGFP-(39-112) resulted in an ~30% decrease in co-precipitation of endogenous Syntaxin 4-F-actin complexes. EGFP-(39-112) action was not due to inadvertent binding to other Syntaxin 4 binding partners, since immunoprecipitation of this fusion protein failed to coprecipitate proteins such as Syntaxin 4, VAMP2, SNAP-25 or Munc18c (data not shown). The analogous region of Syn1A was not used for comparison, since this region of Syntaxin 1A is known to directly interact with another important exocytotic protein, Munc13-1 (151). Despite its ability to dissociate endogenous F-actin-Syntaxin 4 complexes and to bind to F-actin *in vitro*, stable association of the peptide with endogenous F-actin could not be consistently detected. Although EGFP-(39-112) protein expression levels were substantial, conformational changes in

peptide structure due to its fusion to EGFP may have impaired its ability to stably interact with F-actin. Unlike Latrunculin treatment, the EGFP-(39-112) expression had no substantial effect upon global cellular F-actin content (F:G-actin ratio of both was ~25%:75%), such that the action of the inhibitory peptide was more likely through selective separation of F-actin from Syntaxin 4 and not via dispersal of the cortical F-actin network to allow granules to gain access to the plasma membrane.

The EGFP-(39-112) competitive inhibitory fragment was then used to evaluate the functional importance of the endogenous Syntaxin 4-F-actin association in glucose stimulated insulin secretion. Because transfection efficiency was ~50%, the human C-peptide reporter assay was utilized as a means to measure secretion only from transfectable cells. MIN6 cells were co-transfected with EGFP-(39-112) or vector control together with human proinsulin cDNA. Human C-peptide (derived from human proinsulin) is synthesized and packaged in an identical fashion to mouse C-peptide and insulin in granules, but is immunologically distinct from mouse C-peptide and serves as a reporter of secretion from transfectable cells. MIN6 cells transfected with EGFP vector responded to glucose stimulation by a 26% increase in insulin release (Figure 4-6C), similar to levels reported by others using this particular reporter assay (190,191). However, expression of EGFP-(39-112) increased this to ~49%, suggesting that the selective disruption of F-actin binding to Syntaxin 4 enhanced insulin exocytosis. Thus, the potentiating effect of Latrunculin could be recapitulated, at least in part, by competitive inhibition of F-actin binding to Syntaxin 4.

A)

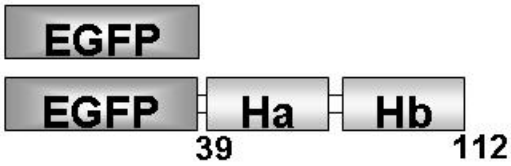

B) IP: Syn4

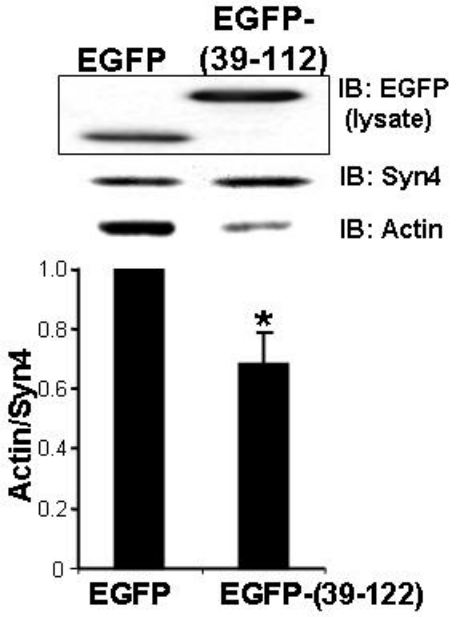

C) Human C-peptide release

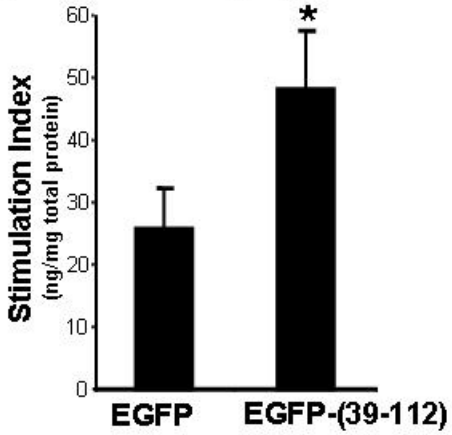

Figure 4-6 Expression of Syntaxin 4 residues 39-112 in MIN6 Cells Results in Dissociation of the Endogenous F-actin-Syn4 Association and Increased Glucose-stimulated Secretion. A) The Ha-Hb region of Syntaxin 4 was fused to the C-terminus of EGFP for expression in mammalian cells. Schematic representation of EGFP and EGFP-(39-112) proteins. B) MIN6 lysates expressing the ~37 kDa EGFP-(39-112) protein were used for immunoprecipitation with Syntaxin 4 antibody and immunoblotted for co-precipitation of actin. EGFP (29 kDa) in lysates served as control; the actin/Syn4 ratio in EGFP-expressing lysates was set equal to 1 for normalization in each of 4 immunoprecipitation experiments,*P< 0.05. C) MIN6 cells were co-transfected with EGFP or EGFP-(39-112) with human proinsulin to report effects upon glucose-stimulated human C-peptide secretion only from transfected cells. MIN6 cells were pre-incubated in glucose-free MKRBB followed by stimulation with 20 mM glucose for 30 min. Data represent the mean ± S.E. from 5 independent experiments, normalized for total protein content. Data normalized to unstimulated level for each construct to obtain stimulation index; *P< 0.05.

4.3.5 Disruption of F-actin Binding to Syntaxin 4 Enhances Granule Mobilization and Syntaxin 4 Accessibility

Given the functional parallels between actions of EGFP-(39-112) with Latrunculin upon insulin secretion, we next sought to determine if the EGFP-(39-112) inhibitor impacted granule localization. MIN6 cells expressing either EGFP of EGFP-(39-112) were subfractionated and VAMP2 accumulation in PM and SG fractions assessed. There was a ~1.6-fold increase in VAMP2 in the PM fraction of EGFP-(39-112) expressing cells compared to cells expressing EGFP alone ($P< 0.0002$, Figure 4-7). This increase occurred under basal conditions, similar to that with Latrunculin treatment, and correlated with a ~30% decrease of VAMP2 from the SG fraction of EGFP-(39-112) cells relative to control ($P< 0.0001$). These data indicated that VAMP2-bound granules were inappropriately mobilized to the PM in the absence of the glucose stimulus.

In addition to increasing granule number at the PM, we speculated that the role of F-actin binding to Syntaxin 4 might be to negatively regulate Syntaxin 4 accessibility by VAMP2. To test this hypothesis, exogenous GST-VAMP2 (soluble form, ΔTM) protein linked to sepharose beads was added to cell lysates to 'probe' for accessible Syntaxin 4, i.e. Syntaxin 4 that was available for binding. From unstimulated MIN6 cells left untreated or treated with vehicle (DMSO), the GST-VAMP2 was able to co-precipitate Syntaxin 4 protein (Figure 8A, lane 1). Interestingly however, GST-VAMP2 co-precipitated significantly more Syntaxin 4 protein (2.4 ± 0.2, $P< 0.0005$) from lysates prepared from Latrunculin-treated cells (Figure 4-8A, lane 2).

However, even though Latrunculin-induced F-actin depolymerization rendered Syntaxin 4 more accessible to VAMP2 and also significantly increased the number of granules juxtaposed to the PM under basal conditions, the amount of endogenous VAMP2 co-immunoprecipitated with Syntaxin 4 was not coordinately increased in Latrunculin treated lysates when compare to vehicle-treated lysates (Figure 4-8B, lanes 1-2). This result argued against a simple inverse relationship between loss of F-actin binding corresponding to increased VAMP2 binding. In addition, Syntaxin 4-VAMP2 association was similar between

EGFP-(39-112) and EGFP-expressing cell lysates (Figure 4-8B, lanes 3-4), even though F-actin binding to Syntaxin 4 was significantly reduced by expression of EGFP-(39-112). Co-immunoprecipitation experiments were also conducted using PM fractions in place of whole cell lysates, similarly showing no increased association of VAMP2 with Latrunculin treatment of EGFP-(39-112) expression (Figure 4-8C). This lack of impact upon VAMP2-Syntaxin 4 association correlates with lack of effect of Latrunculin or the EGFP-(39-112) fragment upon basal insulin release. Thus, these data suggest that F-actin negatively regulates exocytosis via binding and blocking Syntaxin 4 accessibility, but also reveal the necessity for additional signals and/or steps required to trigger vesicle docking and fusion.

4.4 DISCUSSION

The importance of F-actin in insulin exocytosis has long been debated, yet the relevance of this to human insulin release has remained unknown. Here we demonstrate for the first time that the potentiating effect of F-actin depolymerization upon glucose-stimulated insulin secretion is a conserved mechanism in human islets. Syntaxin 4 was found to function as a novel actin binding protein, associating with F-actin via its N-terminal region containing the Ha-Hb domains. This association was specific for Syntaxin 4 as Syntaxin 1A failed to directly bind to F-actin, which represents the first mechanistic evidence to support functionally distinct roles for these seemingly redundant isoforms in insulin granule exocytosis.

Our data show that Syntaxin 4-F-actin complexes were key to the mechanism by which F-actin regulates granule flow/mobilization. One possible role for this complex might be that Syntaxin 4 serves as an attachment site of F-actin to the plasma membrane, such that under basal conditions, Syntaxin 4 might exist in two conformations (Figure 4-9 model, left panel): 1) ‘closed’ and bound by F-actin to block granule docking, consistent with data presented here showing that Syntaxin 4 was more accessible in cells treated with Latrunculin, and 2) ‘open’ and bound by a granule to support first-phase insulin release.

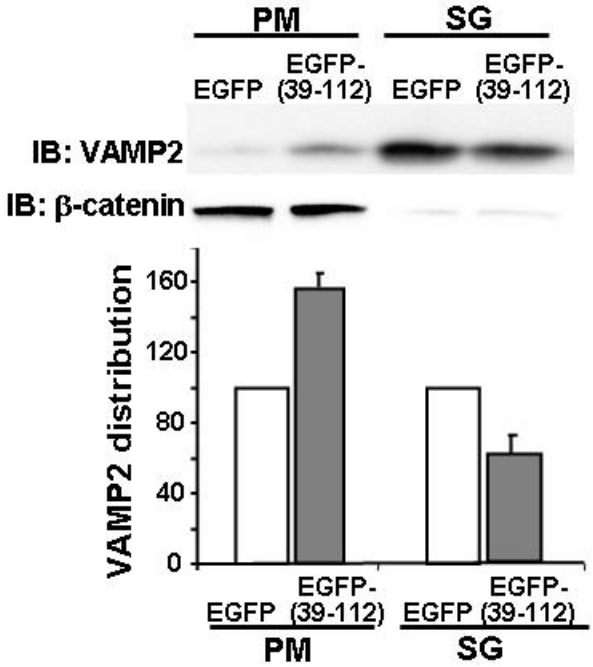

Figure 4-7 Like Latrunculin Treatment, Expression of EGFP-(39-112) Mobilizes Granules into the PM Compartment from the Storage Granule Pool Under Basal Conditions. MIN6 cells were transfected with EGFP or EGFP-(39-112) DNA and 48 h later were subfractionated and 20 µg protein from of each plasma membrane (PM) and storage granule (SG) fractions resolved on 12% SDS-PAGE for immunoblotting. Optical density scanning quantitation (each set of fractions normalized to EGFP control=100%) of VAMP2; data shown as average ± S.E. of 4 independent sets of fractions. β-catenin immunodetection was used to verify PM fraction integrity and equal protein loading in each set of PM fractions; Ponceau staining used to verify loading in SG and PM fractions in each experiment.

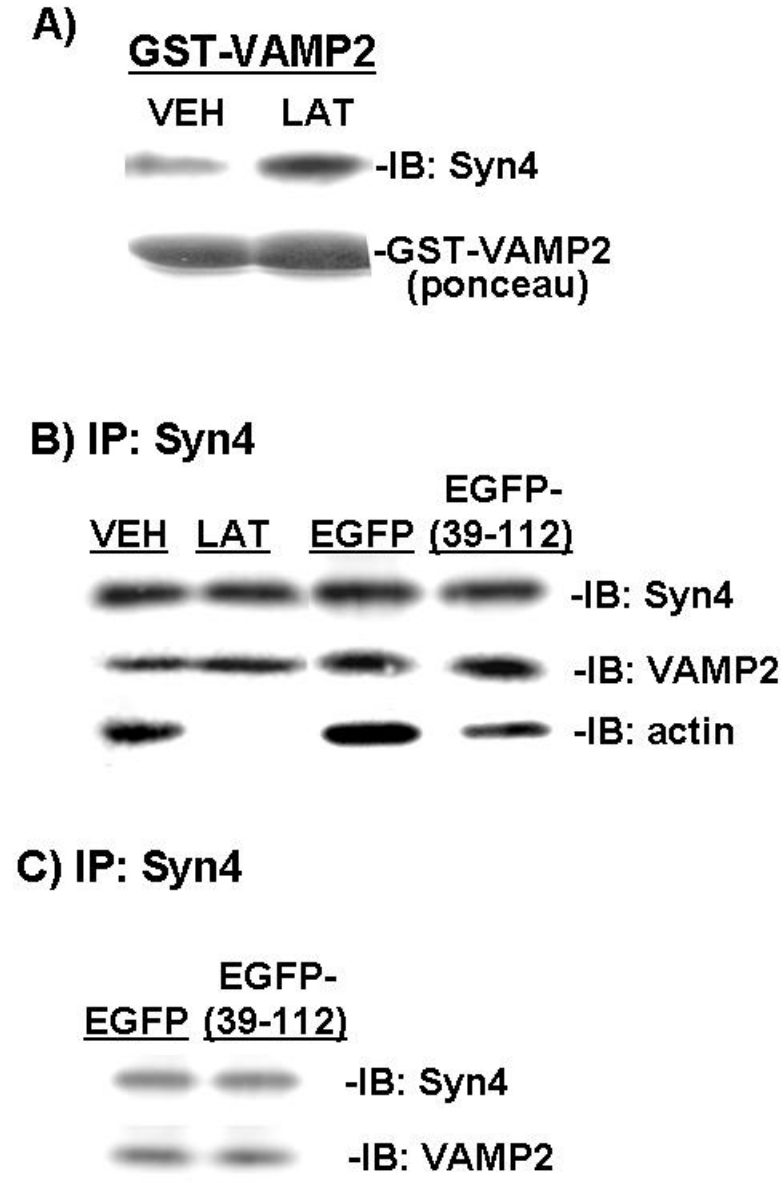

Figure 4-8 EGFP-Syntaxin4 (39-112) Expression Increases Syntaxin 4 Accessibility but not VAMP2 Docking/Fusion at Syntaxin 4 Sites. A) MIN6 cells were treated with vehicle (VEH) or Latrunculin (LAT) for 2 hours in glucose-free MKRBB for preparation of cleared detergent lysates for use in GST-VAMP2 (soluble form) interaction assays. Lysate protein (2-3 mg) was combined with 20 µl GST-VAMP2 linked to beads, and precipitated proteins resolved on 10% SDS-PAGE for Syntaxin 4 immunoblotting. Data representative of 4 independent sets

of cell lysates. B) MIN6 cells were left untransfected or were transfected with pEGFP or pEGFP-(39-112) DNA. Forty-eight hours later cells were preincubated in glucose-free MKRBB for 2 hours and harvested for preparation of cleared detergent lysates. Lysate protein (2 mg per reaction) was incubated with anti-Syntaxin 4, co-immunoprecipitated proteins resolved on 12% SDS-PAGE for immunoblotting with anti-Syntaxin 4, anti-VAMP2 and anti-actin antibodies. C) MIN6 cells were transfected with EGFP or EGFP-(39-112) DNA and 48 hours later were subfractionated and ~200 µg from the PM fraction was incubated with anti-Syntaxin 4, and co-immunoprecipitated proteins resolved on 12% SDS-PAGE for immunoblotting with anti-Syntaxin 4 and anti-VAMP2. Data representative of 3-6 independent experiments.

Upon glucose-stimulated actin reorganization (Figure 4-9, right panel), granules mobilize and may preferentially dock at 'open' Syntaxin 4 sites for subsequent fusion and insulin release. The novel F-actin binding motif of Syntaxin 4 functioned as a competitive inhibitor of the direct association between F-actin-Syntaxin 4, mimicking actions of Latrunculin but without inducing global changes in cellular F-actin content. This suggests that it may be through this interaction with Syntaxin 4 that F-actin exerts some of its "barrier" function in exocytosis. Whether this association also plays a role in the 'positive' role for F-actin in granule mobilization remains untested. To date there is evidence to suggest that the positive role is mediated by vesicle-microfilament interactions (214-217).

However, VAMP2 association with Syntaxin was not increased upon release of F-actin binding from Syntaxin 4, which could be due to a requirement for additional stimulus-dependent/induced step(s) preceding the docking and fusion steps in exocytosis. It is known that VAMP2-Syntaxin binding occurs more efficiently in cells than *in vitro*, and this has been proposed to be due to a requirement for VAMP2 activation, Syntaxin accessibility, or both (5). Thus, the reason that docking/fusion was not enhanced under conditions where Syntaxin 4 accessibility and granule mobilization to the PM were both increased was because of a missing cellular signal triggered by glucose required for VAMP2 activation. The small Rho-family GTPase Cdc42 has been suggested as a possible candidate (5), based upon data showing: 1) Cdc42 binds directly to the N-terminal 28 residues of the VAMP2 protein on the insulin granule (210), 2) Cdc42 activation correlates with mobilization of VAMP2-bound granules to the PM, specifically in response to stimulation with glucose and not KCl (182,210), 3) de-regulation of Cdc42 activation via depletion of its GDI results in inappropriate fusion and release of insulin in the absence of the glucose stimulus (218), and 4) Cdc42 is required exclusively for the second phase/mobilization phase of insulin secretion from islets (182). This would be a glucose-specific signal independent of the calcium signal that is thought to couple the calcium-sensitive Complexin protein in mediating Syntaxin 1A-dependent exocytosis in neurotransmitter release (219). However, the specifics as to how glucose Cdc42 might activate

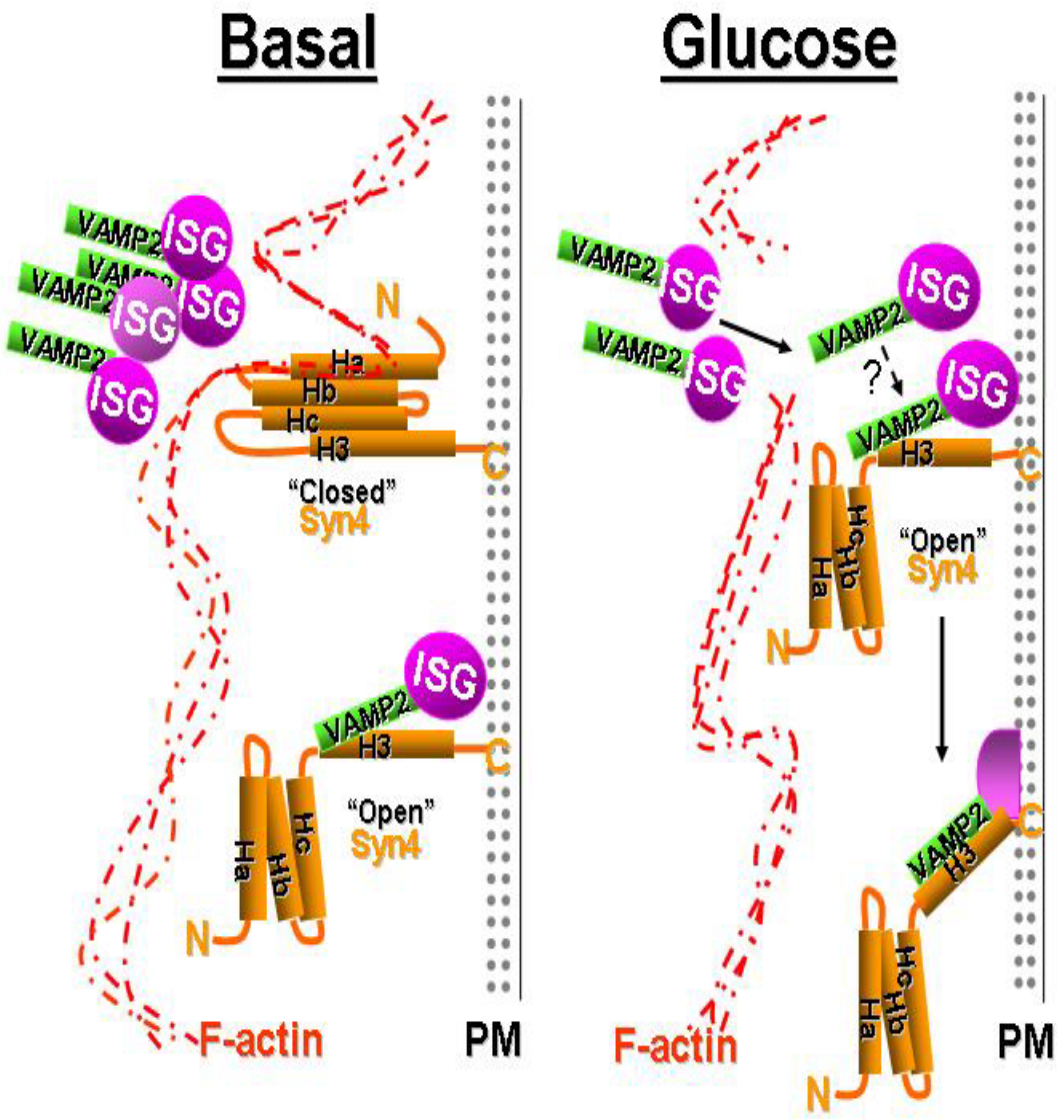

Figure 4-9 Model depicting potential mechanism of regulation of insulin exocytosis by F-actin-Syntaxin 4 complexes under basal and glucose stimulated conditions. Left panel: under basal conditions, F-actin binds to residues 39-112 of Syntaxin 4 (Ha-Hb domains), decreasing Syntaxin 4 accessibility to VAMP2 (consistent with Syntaxin 4 being in 'closed' conformation), and also restricting the flow of storage pool granules into the readily releasable pool at the plasma membrane. However some Syntaxin 4 sites are occupied by granules, consistent with the requirement for Syntaxin 4 in first-phase insulin release (26). Right panel: glucose stimulation results in the localized reorganization of actin which allows the storage pool of insulin granules to traffic to the plasma membrane, and increases accessibility of VAMP2 to Syntaxin 4 sites ('open' conformation) to facilitate granule fusion and insulin release. An additional step triggered by glucose to 'activate' VAMP2 docking is suggested (see question mark).

VAMP2 to promote granule targeting to particular Syntaxin-based active sites to facilitate second-phase secretion is unclear because the characterization of such active sites remains incomplete.

Our finding that Syntaxin 4 in particular associated directly with F-actin represents a step towards distinguishing the functions of Syntaxin 4 from Syntaxin 1A, and in characterizing the active site used for second-phase secretion. Syntaxin 4 binding to F-actin was mediated via its N-terminal Ha-Hb region and not through its H3/SNARE domain, consistent with alignments showing lesser conservation in the N-terminus of these Syntaxin isoform (35% identical in Ha, 38% in Hb versus 56% in H3 domain). Moreover, VAMP2 contains the conserved SNARE domain and yet failed to bind. Only very recently has another SNARE protein been reported to directly interact with actin, the R-SNARE protein Ykt6p, although the binding motif remains to be identified (220). A second distinguishing characteristic was the slow and incomplete re-association of F-actin with Syntaxin 4 after the initial glucose-induced disruption of binding in the co-immunoprecipitation studies, relative to the kinetics of F-actin and Syntaxin 1A association. These kinetic differences are consistent with the notion that Syntaxin 4 docking sites are accessible and operative during second-phase secretion, although this awaits further examination using primary beta cells.

Differential localization to caveolae may also mark distinct syntaxin-based active sites. Data from multiple studies in divergent cell types show that Syntaxin 1A is clustered into ‘active sites’ by caveolae (221-223). A recent study used STED microscopy to show that the SNARE motifs of Syntaxin 1 and 4 mediate specific Syntaxin clustering by homoligomerization, thereby spatially separating sites for different biological activities (224). Moreover, caveolar clustering can be induced by localized F-actin depolymerization (225). Furthermore, L-type calcium channels have been localized in or nearby caveolae (226), and over-expression studies performed in cultured beta cells showed that increased Syntaxin 1A protein inhibited L-type calcium channel activity, whereas over-expression of Syntaxin 4 was without effect (227).

The Syntaxin 4 fragment comprising the Ha-Hb domain markedly increased granule flow to the PM, mimicking the effects induced by Latrunculin in unstimulated cells, as well as mimicking the effect of acute glucose stimulation (210). Like glucose stimulation, the 39-112 inhibitory fragment did not cause global changes in F-actin content, while Latrunculin is a global depolymerizing agent. These data suggest then that Syntaxin 4-F-actin complexes may be a target of glucose-induced localized F-actin reorganization, and may be the means by which glucose coordinates the timing of increased Syntaxin 4 accessibility with increased granule accumulation at the plasma membrane. Alternatively, it is possible that this 39-112 fragment interfered with Syntaxin 4 binding to other factors involved in actin remodeling. Of the SNARE and SNARE accessory proteins, only n-Sec1/Munc18 and Munc13 proteins are known to interact with the N-terminal helices of Syntaxin proteins (113,151), yet we failed to see alteration in endogenous Syntaxin 4-Munc18c association in cells expressing the 39-112 fragment, and the Syntaxin 4 isoform has yet to be shown to interact with Munc13. However Syntaxin 4 has been shown to directly bind the actin binding protein α-fodrin (228), and in 3T3L1 adipocytes the Syntaxin 4-fodrin complex is functionally important in insulin-stimulated GLUT4 translocation (173). In addition, the F-actin severing proteins such as Gelsolin and Scinderin have been shown to be important in stimulus-secretion coupling in cultured beta cells (175,229), and pilot data from our laboratory suggest that Syntaxin 4 may associate with both Scinderin and Gelsolin under unstimulated conditions (Kalwat and Thurmond, unpublished).

In summary, these studies support a new model whereby the negative ‘barrier’ function of cortical F- actin is mediated in part by a discrete and direct interaction with Syntaxin 4 at the plasma membrane, and further reveal the existence of a new step in stimulus-induced granule exocytosis that precedes docking. In islet beta cells this new step requires glucose as the stimulus. Although the Syntaxin 4-F-actin interaction will likely impact exocytosis events in many cells, given the ubiquitous expression pattern of these proteins, the kinetics of biphasic insulin release are quite distinct from events such as neurotransmitter

secretion or GLUT4 translocation. Second-phase insulin release can occur over a long time period (hours), requiring the readily releasable pool at the plasma membrane to be refilled from the more intracellular storage pool in a carefully metered manner. F-actin is well-suited to this task, since release and refill events must occur across the expanses of the cell, yet be coordinated to occur simultaneously to achieve the precisely-timed biphasic release of insulin. Future studies will be required to determine whether the importance and specific utilization of the Syntaxin 4-F-actin complex in these other cell types.

CHAPTER 5: CONCLUDING REMARKS

Type 2 Diabetes results from defects in multiple organs, wherein the exocytosis mechanism of pancreatic insulin secretion and subsequent insulin-stimulated glucose clearance by peripheral tissues are compromised. Both pancreatic beta cell insulin secretion and skeletal muscle/adipose tissue glucose transport have been shown to utilize Syntaxin 4-Munc18c complexes, and with commonalities in molecular mechanism. In this thesis, I have used complementary *in vitro*, cell-based approaches, and animal tissue extracts to detail protein modifications and protein-protein interactions that affect SNARE core complex assembly and vesicle exocytosis mechanisms. Using biochemical, molecular and cellular biology techniques, I have been able to determine that Syntaxin 4-Munc18c complexes are regulated through tyrosine phosphorylation and interaction with factors such as Doc2β, the Insulin Receptor, and F-actin. More specifically, the tyrosine phosphorylation of Munc18c at residues Y219 and Y521, regulate its interaction with Syntaxin 4. In the beta cell, stimulus induced Munc18c Y219 phosphorylation results in a 2-fold decrease in Syntaxin 4-Munc18c association and a parallel 2-fold increase in Munc18c-Doc2β formation at the plasma membrane resulting in an increase in insulin secretion. We have termed this exchange “the switch mechanism.” Similarly, Munc18c Y219 phosphorylation is also seen in adipocytes, along with phosphorylation at a second site, Y521. In response to insulin, the Insulin Receptor interacted with Munc18c with the same time course as observed for the stimulus-induced phosphorylation of Munc18c. Further investigation identified the Insulin Receptor as the first example of a Munc18c tyrosine kinase, phosphorylating Munc18c at Y521. Interestingly, Y521 resides in a disordered region, a type of region thought to be a “hot spot” for protein phosphorylation and protein-protein interaction sites (230-232). Finally, it was found that stimulus-induced changes occurred also with Syntaxin 4, in the beta cells. Syntaxin 4-mediated insulin release requires F-actin remodeling to mobilize insulin granules to the plasma membrane. Syntaxin 4 was seen to directly associate with F-actin in MIN6 beta cells, and disruption of this complex correlates with an increase in glucose-stimulated insulin secretion. Altogether, this thesis demonstrates that modulating Syntaxin 4-Munc18c

complexes through post-translational modifications and through binding partners can regulate both insulin secretion and glucose uptake.

My studies have also helped to clarify the Munc18c-Syntaxin 4 interaction in beta cells and mouse skeletal muscle, in terms of whether Munc18c interacts with Syntaxin 4 alone or with Syntaxin 4 when it is in the SNARE complex. There are three models in the literature to date: (1) Where Munc18c holds Syntaxin 4 in a "closed" conformation exclusive of the SNARE complex (110-112); (2) Where Munc18c can interact with the Syntaxin 4-SNARE complex through an N-terminal peptide of Syntaxin 4 (114,129,185-187); (3) And most recently, where Munc18 proteins can bind to the SNARE complex via the four alpha-helical bundle (116). My data suggest that model one holds true in the beta cell, adipose and muscle. This model is confirmed by my data in which I delineated the minimal binding domain of Syntaxin 4 that interacts with Munc18c to be its Hc-Linker Region (residues 118-194). Model 3 is disputed based upon *in vitro* binding studies which failed to show that deletion of the SNARE interacting domain (H3) of Syntaxin 4 impairs its association with Munc18c. Model 2 is undermined by failure of the Syntaxin 4 N-terminal peptide to function as an effective competitive inhibitor of endogenous Syntaxin 4-Munc18c complexes as well as its inability to suffice as a Munc18c binding peptide (115,139). Molecular modeling studies support the the hypothesis that the Hc-Linker region as the critical contact region on Syntaxin 4, the region which also confers interaction with Munc18c, and has further unveiled new residues in which to examine for roles in Munc18c-Syntaxin 4 interaction. Some of these residues exist exclusively in the Syntaxin 4 isoform, and may be critical specifiers of the Syntaxin 4-Munc18c interaction.

A previous study from the laboratory has shown that Munc18c interacts with Doc2β through its second C2 domain (C2B), exclusive from formation of Syntaxin 4-Munc18c complexes at the plasma membrane in beta cells. Furthermore, I have shown that the phosphorylated form of Munc18c interacts with Doc2β at the plasma membrane. Interestingly, the Doc2β binding site on Munc18c (residues 173-255) includes the regulatory Y219 site, suggesting that

Doc2β may have to dissociate before Munc18c can be dephosphorylated by a phosphatase. Doc2β exerts positive effects on insulin granule and GLUT4 vesicle exocytosis, and while the precise mechanisms are still not understood, one possibility is that by binding to phosphorylated Munc18c, Doc2β relieves the inhibition that Munc18c exerts on Syntaxin 4 (145,146). Alternatively, a very recent report shows that Doc2β interacts directly with the SNARE complex (149). Doc2β may serve as a scaffold to capture transiently dissociating Munc18 proteins, since it can dock Munc18-1 through its first C2 domain (C2A) and Munc18c through its second C2 domain (C2B), to facilitate SNARE-mediated exocytosis events (146,148)

Insulin-stimulated Munc18c tyrosine phosphorylation and disruption of Munc18c-Syntaxin 4 complexes was observed to occur early in the time course of insulin signaling in adipocytes or skeletal muscle (within 5 minutes of insulin stimulation), yet occurred in a manner independent of PI3K, suggesting that IR signaling and preparation for SNARE-mediated GLUT4 vesicle docking occurs simultaneously in the adipose and skeletal muscle. After 15 minutes of insulin stimulation, Munc18c tyrosine phosphorylation had returned to basal, implying the activation of a Munc18c phosphatase downstream in the insulin signaling cascade. In my studies, the Insulin Receptor was identified as the first known Munc18c tyrosine kinase effectively utilizing Munc18c as a direct substrate *in vitro* kinase assays. Interestingly, both tyrosines Y219 and Y521 are in the same 3D structural vicinity, suggesting that this region of Munc18c may be key in regulating Munc18c-Syntaxin 4 and Munc18c-Doc2β interactions. Furthermore, depletion of Munc18c decreased GLUT4 translocation in adipocytes, similar to the decrease in insulin granule localization in MIN6 beta cells (56), suggesting that Munc18c plays a conserved positive role in exocytosis. Studies are now underway to determine the functional effect of Y219 and Y521 phosphorylation of Munc18c for GLUT4 translocation to the plasma membrane.

Under non-glucose stimulated conditions, Syntaxin 4 (residues 39-112, Ha-Hb Domains), was found to directly bind to F-actin but not G-actin, and block granule localization to the plasma membrane and SNARE core complex

assembly. The role of Munc18c in this process is unknown. However, pilot data from our lab has revealed that Munc18c association with Syntaxin 4 was diminished in cells devoid of F-actin (depolymerized to G-actin by Latrunculin treatment) suggesting that this interaction is somehow linked to intact filaments. Moreover, depletion of Munc18c resulted in reduced Syntaxin 4 association with F-actin (unpublished data, Oh and Thurmond). Future experiments will test how Munc18c associates with F-actin-Syntaxin 4 and why its participation is important for Syntaxin 4 function.

Munc18c and Syntaxin 4 are clearly common links in the known mechanisms of insulin granule exocytosis and GLUT4 vesicle translocation, and yet the molecular details of their actions in these processes remain incomplete. With regards to Munc18c, significant progress has been made in its characterization as a positive effector of both processes, as well as the recent identifications of novel binding factors that implicate it in both Syntaxin 4-dependent (vesicle docking/fusion at the plasma membrane) and Syntaxin 4-independent (granule mobilization/localization) mechanisms. The possibility that Munc18c functions in a Syntaxin 4-independent role in facilitating insulin granule delivery is particularly important, given that granule recruitment to the readily releasable pool of a β-cell is a rate-limiting component of insulin release. Pharmacological targeting of Munc18c function, directly or indirectly, via a binding partner implicated in that mechanism, could presumably exert profound effects upon the capacity of the β-cell to sustain insulin release beyond the first few minutes. The ability to sustain insulin release in a regulated biphasic manner, as opposed to the constitutive release triggered by current popular oral medications which cause hypoglycemia and hasten beta cell failure, would be of tremendous advantage as it would allow for restoration of glucose homeostasis with lower resting insulin levels and hence less risk of hypoglycemic episodes.

In addition to gaining more insight into how Munc18c-Syntaxin 4 complexes are regulated, it will be particularly important to determine how and why Syntaxin 4 and Munc18c protein levels decrease under conditions of obesity and Type 2 diabetes in humans and rodent models. Interestingly, knockout and

transgenic mouse model studies suggest that Munc18c protein levels are controlled by Syntaxin 4. Thus, future studies aimed towards gaining the ability to control Syntaxin 4 expression could be advantageous to improving whole body glucose homeostasis.

APPENDIX A: PERMISSION TO REPRODUCE PREVIOUSLY PUBLISHED MATERIAL

The American Physiological Society

9650 Rockville Pike, Bethesda, MD 20814-3991, USA
Publications Department Phone: (301) 634-7070
Fax: (301) 634-7243

March 21, 2010

Ms. Jenna L. Jewell
University of Indiana School of Medicine
Department of Biochemistry and and Molecular Biology
635 Barnhill Drive, MS4035
Indianapolis, IN 46202

The American Physiological Society grants you permission to use the following *American Journal of Physiology Regulatory, Integrative and Comparative Physiology* article in your PhD thesis for the University of Indiana School of Medicine:

Jenna L. Jewell, Eunjin Oh, and Debbie C. Thurmond

Exocytosis mechanisms underlying insulin release and glucose uptake: conserved roles for Munc18c and syntaxin 4

Am J Physiol Regul Integr Comp Physiol 298: R517-R531, 2010. First published January 6, 2010; doi:10.1152/ajpregu.00597.2009

The American Physiological Society publication must be credited as the source with the words "used with permission" added when referencing the *Am J Physiol Regul Integr Comp Physiol*

Journal of Biological Chemistry Instruction for Authors
(Last Updated on November 10th, 2009)

For authors reusing their own material:

Authors need **NOT** contact the journal to obtain rights to reuse their own material. They are automatically granted permission to do the following:

Reuse the article in print collections of their own writing.

Present a work orally in its entirety.

Use an article in a thesis and/or dissertation.

Reproduce an article for use in the author's courses. (If the author is employed by an academic institution, that institution also may reproduce the article for teaching purposes.)

Reuse a figure, photo and/or table in future commercial and noncommercial works.

Post a copy of the paper in PDF that you submitted via BenchPress.

Only authors who published their papers under the "Author's Choice" option may post the final edited PDFs created by the publisher to their own/departmental/university Web sites.

All authors may link to the journal site containing the final edited PDFs created by the publisher.

APPENDIX B: ADDITIONAL EXPERIMENTS

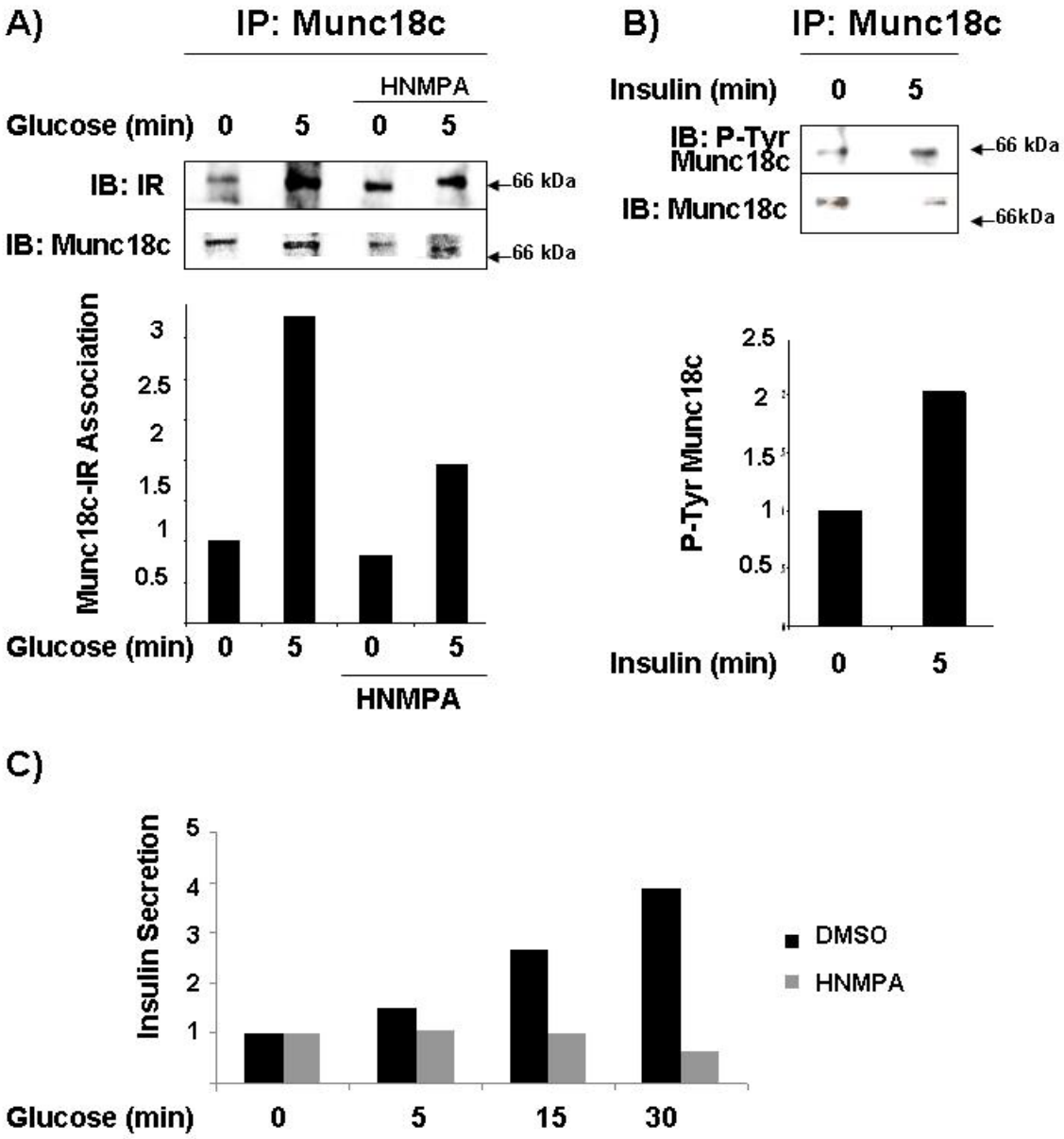

Insulin Signaling and Munc18c Tyrosine Phosphorylation in the Beta Cell. A) MIN6 cells were pre-incubated in MKRBB with or without 100 μM HNMPA-$(AM)_3$ for 2 hour prior to glucose stimulation (20mM) for 5 min. Munc18c was immunoprecipitated and co-immunoprecipitated proteins resolved by 10% SDS-PAGE and immunoblotted with anti-Munc18c and anti-IR. B) MIN6 beta cells were pre-incubated in MKRBB for two hours and stimulated with insulin (100nM) for 5 minutes. Munc18c was immunoprecipitated and co-immunoprecipitated proteins resolved by 10% SDS-PAGE and immunoblotted with anti-Munc18c and anti-4G10 (P-Tyr). C) MIN6 cells were pre-incubated in MKRBB with or without 100 μM HNMPA-$(AM)_3$ for 2 hour prior to glucose stimulation (20mM) for the indicated times. Insulin secretion was measured by RIA.

REFERENCES

1. Thurmond, D. C., Kanzaki, M., Khan, A. H., and Pessin, J. E. (2000) *Mol. Cell. Biol.* **20**, 379-388
2. Thurmond, D. C., and Pessin, J. E. (2000) *EMBO J.* **19**, 3565-3575
3. LeRoith, D., Taylor, S.I., and Olefsky, J.M. (2000) *Diabetes Mellitus* - A Fundamental and Clinical Test., Second Edition Ed., Lippincott Williams.
4. Beckles, G. L. a. T.-R., P. E. (2001)
5. Jahn, R., and Scheller, R. H. (2006) *Nat Rev Mol Cell Biol* **7**, 631-643. Epub 2006 Aug 2016
6. Foster, L. J., and Klip, A. (2000) *Am J Physiol Cell Physiol* **279**, C877-890
7. Thurmond, D. C. (2007) *Regulation of insulin action and insulin secretion by SNARE-mediated vesicle exocytosis*, Landes Bioscience, Georgetown, TX
8. Eliasson, L., Abdulkader, F., Braun, M., Galvanovskis, J., Hoppa, M. B., and Rorsman, P. (2008) *J Physiol* **586**, 3313-3324. Epub 2008 May 3329
9. Olson, A. L., Knight, J. B., and Pessin, J. E. (1997) *Mol. Cell. Biol.* **17**, 2425-2435
10. Regazzi, R., Wollheim, C. B., Lang, J., Theler, J. M., Rossetto, O., Montecucco, C., Sadoul, K., Weller, U., Palmer, M., and Thorens, B. (1995) *EMBO J.* **14**, 2723-2730
11. Volchuk, A., Mitsumoto, Y., He, L., Liu, Z., Habermann, E., Trimble, W., and Klip, A. (1994) *Biochem. J.* **304 (Pt 1)**, 139-145
12. Williams, D., and Pessin, J. E. (2008) *J. Cell Biol.* **180**, 375-387
13. Tamori, Y., Hashiramoto, M., Araki, S., Kamata, Y., Takahashi, M., Kozaki, S., and Kasuga, M. (1996) *Biochem. Biophys. Res. Commun.* **220**, 740-745
14. Wheeler, M. B., Sheu, L., Ghai, M., Bouquillon, A., Grondin, G., Weller, U., Beaudoin, A. R., Bennett, M. K., Trimble, W. S., and Gaisano, H. Y. (1996) *Endocrinology* **137**, 1340-1348
15. Steegmaier, M., Klumperman, J., Foletti, D. L., Yoo, J. S., and Scheller, R. H. (1999) *Mol. Biol. Cell* **10**, 1957-1972
16. Zeng, Q., Subramaniam, V. N., Wong, S. H., Tang, B. L., Parton, R. G., Rea, S., James, D. E., and Hong, W. (1998) *Mol. Biol. Cell* **9**, 2423-2437
17. Nagamatsu, S., Nakamichi, Y., Watanabe, T., Matsushima, S., Yamaguchi, S., Ni, J., Itagaki, E., and Ishida, H. (2001) *J. Cell Sci.* **114**, 219-227
18. Nagamatsu, S., Fujiwara, T., Nakamichi, Y., Watanabe, T., Katahira, H., Sawa, H., and Akagawa, K. (1996) *J. Biol. Chem.* **271**, 1160-1165
19. Ohara-Imaizumi, M., Fujiwara, T., Nakamichi, Y., Okamura, T., Akimoto, Y., Kawai, J., Matsushima, S., Kawakami, H., Watanabe, T., Akagawa, K., and Nagamatsu, S. (2007) *J. Cell Biol.* **177**, 695-705. Epub 2007 May 2014
20. Pasyk, E. A., Kang, Y., Huang, X., Cui, N., Sheu, L., and Gaisano, H. Y. (2004) *J. Biol. Chem.* **279**, 4234-4240
21. Volchuk, A., Wang, Q., Ewart, H. S., Liu, Z., He, L., Bennett, M. K., and Klip, A. (1996) *Mol. Biol. Cell* **7**, 1075-1082
22. Zhang, Y., Kang, Y. H., Chang, N., Lam, P. P., Liu, Y., Olkkonen, V. M., and Gaisano, H. Y. (2009) *J. Biol. Chem.* **284**, 20840-20847
23. Timmers, K. I., Clark, A. E., Omatsu-Kanbe, M., Whiteheart, S. W., Bennett, M. K., Holman, G. D., and Cushman, S. W. (1996) *Biochem. J.* **320**, 429-436

24. Watson, R. T., and Pessin, J. E. (2001) *Am J Physiol Cell Physiol* **281**, C215-223
25. Spurlin, B. A., Park, S. Y., Nevins, A. K., Kim, J. K., and Thurmond, D. C. (2004) *Diabetes* **53**, 2223-2231
26. Spurlin, B. A., and Thurmond, D. C. (2006) *Mol. Endocrinol.* **20**, 183-193. Epub 2005 Aug 2011
27. Perera, H. K., Clarke, M., Morris, N. J., Hong, W., Chamberlain, L. H., and Gould, G. W. (2003) *Mol. Biol. Cell* **14**, 2946-2958
28. Shewan, A. M., van Dam, E. M., Martin, S., Luen, T. B., Hong, W., Bryant, N. J., and James, D. E. (2003) *Mol. Biol. Cell* **14**, 973-986
29. Thurmond, D. C., Gonelle-Gispert, C., Furukawa, M., Halban, P. A., and Pessin, J. E. (2003) *Mol. Endocrinol.* **17**, 732-742
30. Parton, L. E., McMillen, P. J., Shen, Y., Docherty, E., Sharpe, E., Diraison, F., Briscoe, C. P., and Rutter, G. A. (2006) *Am J Physiol Endocrinol Metab* **291**, E982-994
31. Tang, B. L., Low, D. Y., Tan, A. E., and Hong, W. (1998) *Biochem. Biophys. Res. Commun.* **242**, 345-350
32. Ravichandran, V., Chawla, A., and Roche, P. A. (1996) *J Biol Chem* **271**, 13300-13303
33. Wang, G., Witkin, J. W., Hao, G., Bankaitis, V. A., Scherer, P. E., and Baldini, G. (1997) *J. Cell Sci.* **110 (Pt 4)**, 505-513
34. Sadoul, K., Lang, J., Montecucco, C., Weller, U., Regazzi, R., Catsicas, S., Wollheim, C. B., and Halban, P. A. (1995) *J. Cell Biol.* **128**, 1019-1028
35. Lang, J. (1999) *Eur. J. Biochem.* **259**, 3-17
36. Rhodes, C. J. (2000) Processing of the insulin molecule. in *Diabetes Mellitus: a fundamental and clinical text (*LeRoith, T., and Olefsky, Eds. ed., Lippincott Williams & Wilkins, Philadelphia, PA
37. Curry, D. L., Bennett, L. L., and Grodsky, G. M. (1968) *Endocrinology* **83**, 572-584
38. Henquin, J. C., Dufrane, D., and Nenquin, M. (2006) *Diabetes* **55**, 3470-3477
39. Henquin, J. C., Nenquin, M., Stiernet, P., and Ahren, B. (2006) *Diabetes* **55**, 441-451.
40. Grodsky, G. M. (2000) Kinetics of insulin secretion: underlying metabolic events. in *Diabetes Mellitus: a fundamental and clinical text (*LeRoith, D., Taylor, S., and Olefsky, J. eds.), Lippincott Williams & Wilkins, Philadelphia, PA
41. Renstrom, E., Eliasson, L., Bokvist, K., and Rorsman, P. (1996) *J Physiol* **494**, 41-52
42. Barg, S., Eliasson, L., Renstrom, E., and Rorsman, P. (2002) *Diabetes* **51**, S74-82.
43. Gembal, M., Gilon, P., and Henquin, J. C. (1992) *J. Clin. Invest.* **89**, 1288-1295.
44. Watson, R. T., and Pessin, J. E. (2007) *Cell. Signal.* **19**, 2209-2217. Epub 2007 Jun 2221
45. Bryant, N. J., Govers, R., and James, D. E. (2002) *Nat Rev Mol Cell Biol* **3**, 267-277
46. Huang, S., and Czech, M. P. (2007) *Cell Metab* **5**, 237-252
47. Gerber, S. H., Rah, J. C., Min, S. W., Liu, X., de Wit, H., Dulubova, I., Meyer, A. C., Rizo, J., Arancillo, M., Hammer, R. E., Verhage, M., Rosenmund, C., and Sudhof, T. C. (2008) *Science* **321**, 1507-1510. Epub 2008 Aug 1514.

48. Lam, P. P., Leung, Y. M., Sheu, L., Ellis, J., Tsushima, R. G., Osborne, L. R., and Gaisano, H. Y. (2005) *Diabetes* **54**, 2744-2754
49. Yang, C., Coker, K. J., Kim, J. K., Mora, S., Thurmond, D. C., Davis, A. C., Yang, B., Williamson, R. A., Shulman, G. I., and Pessin, J. E. (2001) *J. Clin. Invest.* **107**, 1311-1318
50. Verhage, M., Maia, A. S., Plomp, J. J., Brussaard, A. B., Heeroma, J. H., Vermeer, H., Toonen, R. F., Hammer, R. E., van den Berg, T. K., Missler, M., Geuze, H. J., Sudhof, T. C., de Vries, K. J., Geijtenbeek, A., Brian, E. C., de Graan, P. N., and Ghijsen, W. E. (2000) *Science* **287**, 864-869
51. Voets, T., Toonen, R. F., Brian, E. C., de Wit, H., Moser, T., Rettig, J., Sudhof, T. C., Neher, E., and Verhage, M. (2001) *Neuron* **31**, 581-591
52. Toonen, R. F., Wierda, K., Sons, M. S., de Wit, H., Cornelisse, L. N., Brussaard, A., Plomp, J. J., and Verhage, M. (2006) *Proc. Natl. Acad. Sci. U. S. A.* **103**, 18332-18337
53. Spurlin, B. A., Thomas, R. M., Nevins, A. K., Kim, H. J., Noh, H. J., Kim, J. A., Shulman, G. I., Thurmond, D. C. (2003) *Diabetes* **52**, 1910-1917
54. Kanda, H., Tamori, Y., Shinoda, H., Yoshikawa, M., Sakaue, M., Udagawa, J., Otani, H., Tashiro, F., Miyazaki, J., and Kasuga, M. (2005) *J. Clin. Invest.* **115**, 291-301
55. Oh, E., Spurlin, B. A., Pessin, J. E., and Thurmond, D. C. (2005) *Diabetes* **54**, 638-647
56. Oh, E., and Thurmond, D. C. (2009) *Diabetes* **58**, 1165-1174
57. Schoch, S., Deak, F., Konigstorfer, A., Mozhayeva, M., Sara, Y., Sudhof, T. C., and Kavalali, E. T. (2001) *Science* **294**, 1117-1122
58. Yang, C., Mora, S., Ryder, J. W., Coker, K. J., Hansen, P., Allen, L. A., and Pessin, J. E. (2001) *Mol. Cell. Biol.* **21**, 1573-1580
59. Ren, Q., Barber, H. K., Crawford, G. L., Karim, Z. A., Zhao, C., Choi, W., Wang, C. C., Hong, W., and Whiteheart, S. W. (2007) *Mol. Biol. Cell* **18**, 24-33
60. Wang, C. C., Ng, C. P., Lu, L., Atlashkin, V., Zhang, W., Seet, L. F., and Hong, W. (2004) *Dev Cell* **7**, 359-371
61. Washbourne, P., Thompson, P. M., Carta, M., Costa, E. T., Mathews, J. R., Lopez-Bendito, G., Molnar, Z., Becher, M. W., Valenzuela, C. F., Partridge, L. D., and Wilson, M. C. (2002) *Nat. Neurosci.* **5**, 19-26
62. Suh, Y. H., Terashima, A., Petralia, R. S., Wenthold, R. J., Isaac, J. T., Roche, K. W., and Roche, P. A. *Nat. Neurosci.* **13**, 338-343
63. Sano, H., Kane, S., Sano, E., Miinea, C. P., Asara, J. M., Lane, W. S., Garner, C. W., and Lienhard, G. E. (2003) *J. Biol. Chem.* **278**, 14599-14602
64. Miinea, C. P., Sano, H., Kane, S., Sano, E., Fukuda, M., Peranen, J., Lane, W. S., and Lienhard, G. E. (2005) *Biochem. J.* **391**, 87-93
65. Kristiansen, S., Hargreaves, M., and Richter, E. A. (1996) *Am. J. Physiol.* **270**, E197-201
66. Jagadish, M. N., Fernandez, C. S., Hewish, D. R., Macaulay, S. L., Gough, K. H., Grusovin, J., Verkuylen, A., Cosgrove, L., Alafaci, A., Frenkel, M. J., and Ward, C. W. (1996) *Biochem. J.* **317**, 945-954
67. Brant, A. M., Jess, T. J., Milligan, G., Brown, C. M., and Gould, G. W. (1993) *Biochem. Biophys. Res. Commun.* **192**, 1297-1302

68. Sadoul, K., Berger, A., Niemann, H., Weller, U., Roche, P. A., Klip, A., Trimble, W. S., Regazzi, R., Catsicas, S., and Halban, P. A. (1997) *J. Biol. Chem.* **272**, 33023-33027
69. Araki, S., Tamori, Y., Kawanishi, M., Shinoda, H., Masugi, J., Mori, H., Niki, T., Okazawa, H., Kubota, T., and Kasuga, M. (1997) *Biochem Biophys Res Commun* **234**, 257-262
70. Kawanishi, M., Tamori, Y., Okazawa, H., Araki, S., Shinoda, H., and Kasuga, M. (2000) *J. Biol. Chem.* **275**, 8240-8247
71. Rea, S., Martin, L. B., McIntosh, S., Macaulay, S. L., Ramsdale, T., Baldini, G., and James, D. E. (1998) *J. Biol. Chem.* **273**, 18784-18792
72. Steegmaier, M., Yang, B., Yoo, J. S., Huang, B., Shen, M., Yu, S., Luo, Y., and Scheller, R. H. (1998) *J. Biol. Chem.* **273**, 34171-34179
73. Hohenstein, A. C., and Roche, P. A. (2001) *Biochem. Biophys. Res. Commun.* **285**, 167-171
74. Chen, Y. A., and Scheller, R. H. (2001) *Nat Rev Mol Cell Biol* **2**, 98-106.
75. Rossetto, O., Gorza, L., Schiavo, G., Schiavo, N., Scheller, R. H., and Montecucco, C. (1996) *J. Cell Biol.* **132**, 167-179
76. Martin, L. B., Shewan, A., Millar, C. A., Gould, G. W., and James, D. E. (1998) *J. Biol. Chem.* **273**, 1444-1452
77. Rose, A. J., Jeppesen, J., Kiens, B., and Richter, E. A.
78. Li, D., Randhawa, V. K., Patel, N., Hayashi, M., and Klip, A. (2001) *J. Biol. Chem.* **276**, 22883-22891
79. Rizo, J., and Sudhof, T. C. (2002) *Nat Rev Neurosci* **3**, 641-653
80. Hata, Y., Slaughter, C. A., and Sudhof, T. C. (1993) *Nature* **366**, 347-351
81. Thurmond, D. C., Ceresa, B. P., Okada, S., Elmendorf, J. S., Coker, K., and Pessin, J. E. (1998) *J. Biol. Chem.* **273**, 33876-33883
82. Aran, V., Brandie, F. M., Boyd, A. R., Kantidakis, T., Rideout, E. J., Kelly, S. M., Gould, G. W., and Bryant, N. J. (2009) *Biochem. J.* **419**, 655-660
83. Fujita, H., Tuma, P. L., Finnegan, C. M., Locco, L., and Hubbard, A. L. (1998) *Biochem. J.* **329**, 527-538
84. Tellam, J. T., McIntosh, S., and James, D. E. (1995) *J. Biol. Chem.* **270**, 5857-5863
85. Bergman, B. C., Cornier, M. A., Horton, T. J., Bessesen, D. H., and Eckel, R. H. (2008) *Nutr Metab (Lond)* **5**, 21
86. Ostenson, C. G., Gaisano, H., Sheu, L., Tibell, A., and Bartfai, T. (2006) *Diabetes* **55**, 435-440
87. Gaisano, H. Y., Ostenson, C. G., Sheu, L., Wheeler, M. B., and Efendic, S. (2002) *Endocrinology* **143**, 4218-4226
88. Yechoor, V. K., Patti, M. E., Ueki, K., Laustsen, P. G., Saccone, R., Rauniyar, R., and Kahn, C. R. (2004) *Proc. Natl. Acad. Sci. U. S. A.* **101**, 16525-16530. Epub 12004 Nov 16516
89. Nagamatsu, S., Nakamichi, Y., Yamamura, C., Matsushima, S., Watanabe, T., Ozawa, S., Furukawa, H., and Ishida, H. (1999) *Diabetes* **48**, 2367-2373

90. Keller, M. P., Choi, Y., Wang, P., Davis, D. B., Rabaglia, M. E., Oler, A. T., Stapleton, D. S., Argmann, C., Schueler, K. L., Edwards, S., Steinberg, H. A., Chaibub Neto, E., Kleinhanz, R., Turner, S., Hellerstein, M. K., Schadt, E. E., Yandell, B. S., Kendziorski, C., and Attie, A. D. (2008) *Genome Res.* **18**, 706-716
91. Riento, K., Jantti, J., Jansson, S., Hielm, S., Lehtonen, E., Ehnholm, C., Keranen, S., and Olkkonen, V. M. (1996) *Eur. J. Biochem.* **239**, 638-646
92. Riento, K., Kauppi, M., Keranen, S., and Olkkonen, V. M. (2000) *J. Biol. Chem.* **275**, 13476-13483
93. Tamori, Y., Kawanishi, M., Niki, T., Shinoda, H., Araki, S., Okazawa, H., and Kasuga, M. (1998) *J. Biol. Chem.* **273**, 19740-19746
94. Tellam, J. T., Macaulay, S. L., McIntosh, S., Hewish, D. R., Ward, C. W., and James, D. E. (1997) *J. Biol. Chem.* **272**, 6179-6186
95. Oh, E., and Thurmond, D. C. (2006) *J. Biol. Chem.* **281**, 17624-17634. Epub 12006 Apr 17625
96. Dascher, C., and Balch, W. E. (1996) *J. Biol. Chem.* **271**, 15866-15869
97. Yamaguchi, T., Dulubova, I., Min, S. W., Chen, X., Rizo, J., and Sudhof, T. C. (2002) *Dev Cell* **2**, 295-305
98. Tellam, J. T., James, D. E., Stevens, T. H., and Piper, R. C. (1997) *J. Biol. Chem.* **272**, 6187-6193
99. Dulubova, I., Yamaguchi, T., Gao, Y., Min, S. W., Huryeva, I., Sudhof, T. C., and Rizo, J. (2002) *EMBO J.* **21**, 3620-3631
100. Brochetta, C., Vita, F., Tiwari, N., Scandiuzzi, L., Soranzo, M. R., Guerin-Marchand, C., Zabucchi, G., and Blank, U. (2008) *Biochim. Biophys. Acta* **1783**, 1781-1791
101. Corominas, R., Ribases, M., Cuenca-Leon, E., Cormand, B., and Macaya, A. (2009) *Eur. J. Neurol.* **16**, 413-415
102. He, Y., and Linder, M. E. (2009) *J. Lipid Res.* **50**, 398-404
103. Fujiwara, T., Mishima, T., Kofuji, T., Chiba, T., Tanaka, K., Yamamoto, A., and Akagawa, K. (2006) *J. Neurosci.* **26**, 5767-5776
104. Wyman, A. H., Chi, M., Riley, J., Carayannopoulos, M. O., Yang, C., Coker, K. J., Pessin, J. E., and Moley, K. H. (2003) *Mol. Endocrinol.* **17**, 2096-2102. Epub 2003 Jun 2026
105. Tomas, A., Meda, P., Regazzi, R., Pessin, J. E., and Halban, P. A. (2008) *Traffic* **9**, 813-832. Epub 2008 Jan 2019
106. Khan, A. H., Thurmond, D. C., Yang, C., Ceresa, B. P., Sigmund, C. D., and Pessin, J. E. (2001) *J. Biol. Chem.* **276**, 4063-4069
107. Harrison, S. D., Broadie, K., van de Goor, J., and Rubin, G. M. (1994) *Neuron* **13**, 555-566
108. Toonen, R. F., Kochubey, O., de Wit, H., Gulyas-Kovacs, A., Konijnenburg, B., Sorensen, J. B., Klingauf, J., and Verhage, M. (2006) *EMBO J.* **25**, 3725-3737
109. Volchuk, A., Sargeant, R., Sumitani, S., Liu, Z., He, L. J., and Klip, A. (1995) *J. Biol. Chem.* **270**, 8233-8240
110. Misura, K. M., Scheller, R. H., and Weis, W. I. (2000) *Nature* **404**, 355-362
111. Dulubova, I., Sugita, S., Hill, S., Hosaka, M., Fernandez, I., Sudhof, T. C., and Rizo, J. (1999) *EMBO J.* **18**, 4372-4382

112. Bracher, A., Perrakis, A., Dresbach, T., Betz, H., and Weissenhorn, W. (2000) *Structure Fold Des* **8**, 685-694
113. Fujita, Y., Shirataki, H., Sakisaka, T., Asakura, T., Ohya, T., Kotani, H., Yokoyama, S., Nishioka, H., Matsuura, Y., Mizoguchi, A., Scheller, R. H., and Takai, Y. (1998) *Neuron* **20**, 905-915
114. Hu, S. H., Latham, C. F., Gee, C. L., James, D. E., and Martin, J. L. (2007) *Proc. Natl. Acad. Sci. U. S. A.* **104**, 8773-8778. Epub 2007 May 8716
115. D'Andrea-Merrins, M., Chang, L., Lam, A. D., Ernst, S. A., and Stuenkel, E. L. (2007) *J. Biol. Chem.* **282**, 16553-16566. Epub 12007 Apr 16555
116. Shen, J., Tareste, D. C., Paumet, F., Rothman, J. E., and Melia, T. J. (2007) *Cell* **128**, 183-195
117. Maximov, A., Tang, J., Yang, X., Pang, Z. P., and Sudhof, T. C. (2009) *Science* **323**, 516-521
118. Giraudo, C. G., Garcia-Diaz, A., Eng, W. S., Chen, Y., Hendrickson, W. A., Melia, T. J., and Rothman, J. E. (2009) *Science* **323**, 512-516
119. McMahon, H. T., Missler, M., Li, C., and Sudhof, T. C. (1995) *Cell* **83**, 111-119
120. Reim, K., Mansour, M., Varoqueaux, F., McMahon, H. T., Sudhof, T. C., Brose, N., and Rosenmund, C. (2001) *Cell* **104**, 71-81
121. Tokumaru, H., Umayahara, K., Pellegrini, L. L., Ishizuka, T., Saisu, H., Betz, H., Augustine, G. J., and Abe, T. (2001) *Cell* **104**, 421-432
122. Chen, X., Tomchick, D. R., Kovrigin, E., Arac, D., Machius, M., Sudhof, T. C., and Rizo, J. (2002) *Neuron* **33**, 397-409
123. Brose, N. (2008) *Traffic* **9**, 1403-1413
124. Weninger, K., Bowen, M. E., Choi, U. B., Chu, S., and Brunger, A. T. (2008) *Structure* **16**, 308-320
125. Deak, F., Xu, Y., Chang, W. P., Dulubova, I., Khvotchev, M., Liu, X., Sudhof, T. C., and Rizo, J. (2009) *J. Cell Biol.* **184**, 751-764
126. Abderrahmani, A., Niederhauser, G., Plaisance, V., Roehrich, M. E., Lenain, V., Coppola, T., Regazzi, R., and Waeber, G. (2004) *J. Cell Sci.* **117**, 2239-2247
127. Pevsner, J., Hsu, S. C., and Scheller, R. H. (1994) *Proc. Natl. Acad. Sci. U. S. A.* **91**, 1445-1449
128. Yang, B., Steegmaier, M., Gonzalez, L. C., Jr., and Scheller, R. H. (2000) *J. Cell Biol.* **148**, 247-252
129. Latham, C. F., Lopez, J. A., Hu, S. H., Gee, C. L., Westbury, E., Blair, D. H., Armishaw, C. J., Alewood, P. F., Bryant, N. J., James, D. E., and Martin, J. L. (2006) *Traffic* **7**, 1408-1419
130. Zilly, F. E., Sorensen, J. B., Jahn, R., and Lang, T. (2006) *PLoS biology* **4**, e330
131. Barclay, J. W., Craig, T. J., Fisher, R. J., Ciufo, L. F., Evans, G. J., Morgan, A., and Burgoyne, R. D. (2003) *J. Biol. Chem.* **278**, 10538-10545
132. Bhaskar, K., Shareef, M. M., Sharma, V. M., Shetty, A. P., Ramamohan, Y., Pant, H. C., Raju, T. R., and Shetty, K. T. (2004) *Neurochem. Int.* **44**, 35-44
133. Fletcher, A. I., Shuang, R., Giovannucci, D. R., Zhang, L., Bittner, M. A., and Stuenkel, E. L. (1999) *J. Biol. Chem.* **274**, 4027-4035
134. Fujita, Y., Sasaki, T., Fukui, K., Kotani, H., Kimura, T., Hata, Y., Sudhof, T. C., Scheller, R. H., and Takai, Y. (1996) *J. Biol. Chem.* **271**, 7265-7268

135. Shuang, R., Zhang, L., Fletcher, A., Groblewski, G. E., Pevsner, J., and Stuenkel, E. L. (1998) *J. Biol. Chem.* **273**, 4957-4966
136. Cosen-Binker, L. I., Lam, P. P., Binker, M. G., Reeve, J., Pandol, S., and Gaisano, H. Y. (2007) *J. Biol. Chem.* **282**, 13047-13058
137. Tian, J. H., Das, S., and Sheng, Z. H. (2003) *J. Biol. Chem.* **278**, 26265-26274. Epub 22003 May 26262
138. Nolasco, L. H., Gushiken, F. C., Turner, N. A., Khatlani, T. S., Pradhan, S., Dong, J. F., Moake, J. L., and Vijayan, K. V. (2009) *J Thromb Haemost* **7**, 1009-1018
139. Jewell, J. L., Oh, E., Bennett, S. M., Meroueh, S. O., and Thurmond, D. C. (2008) *J. Biol. Chem.* **283**, 21734-21746. Epub 22008 Jun 21739
140. Schmelzle, K., Kane, S., Gridley, S., Lienhard, G. E., and White, F. M. (2006) *Diabetes* **55**, 2171-2179
141. Umahara, M., Okada, S., Yamada, E., Saito, T., Ohshima, K., Hashimoto, K., Yamada, M., Shimizu, H., Pessin, J. E., and Mori, M. (2008) *Endocrinology* **149**, 40-49. Epub 2007 Oct 2004
142. Palmer, Z. J., Duncan, R., Johnson, J., Lian, L. Y., Mello, L. V., Booth, D., Barclay, J. W., Graham, M. E., Burgoyne, R. D., Prior, I., and Morgan, A. (2008) *Biochem. J.*
143. Chen, G., Liu, P., Thurmond, D. C., and Elmendorf, J. S. (2003) *FEBS Lett.* **534**, 54-60
144. Nelson, B. A., Robinson, K. A., and Buse, M. G. (2002) *J. Biol. Chem.* **277**, 3809-3812
145. Fukuda, N., Emoto, M., Nakamori, Y., Taguchi, A., Miyamoto, S., Uraki, S., Oka, Y., and Tanizawa, Y. (2009) *Diabetes* **58**, 377-384. Epub 2008 Nov 2025.
146. Ke, B., Oh, E., and Thurmond, D. C. (2007) *J. Biol. Chem.* **282**, 21786-21797. Epub 22007 Jun 21784
147. Miyazaki, M., Emoto, M., Fukuda, N., Hatanaka, M., Taguchi, A., Miyamoto, S., and Tanizawa, Y. (2009) *Biochem. Biophys. Res. Commun.* **384**, 461-465. Epub 2009 May 2003
148. Verhage, M., de Vries, K. J., Roshol, H., Burbach, J. P., Gispen, W. H., and Sudhof, T. C. (1997) *Neuron* **18**, 453-461
149. Groffen, A. J., Martens, S., Diez Arazola, R., Cornelisse, L. N., Lozovaya, N., de Jong, A. P., Goriounova, N. A., Habets, R. L., Takai, Y., Borst, J. G., Brose, N., McMahon, H. T., and Verhage, M. *Science* **327**, 1614-1618
150. Sheu, L., Pasyk, E. A., Ji, J., Huang, X., Gao, X., Varoqueaux, F., Brose, N., and Gaisano, H. Y. (2003) *J. Biol. Chem.* **278**, 27556-27563. Epub 22003 May 27513
151. Betz, A., Okamoto, M., Benseler, F., and Brose, N. (1997) *J. Biol. Chem.* **272**, 2520-2526
152. Kwan, E. P., Xie, L., Sheu, L., Nolan, C. J., Prentki, M., Betz, A., Brose, N., and Gaisano, H. Y. (2006) *Diabetes* **55**, 1421-1429
153. Xu, B., English, J. M., Wilsbacher, J. L., Stippec, S., Goldsmith, E. J., and Cobb, M. H. (2000) *J. Biol. Chem.* **275**, 16795-16801
154. Wilson, F. H., Disse-Nicodeme, S., Choate, K. A., Ishikawa, K., Nelson-Williams, C., Desitter, I., Gunel, M., Milford, D. V., Lipkin, G. W., Achard, J. M., Feely, M. P., Dussol, B., Berland, Y., Unwin, R. J., Mayan, H., Simon, D. B., Farfel, Z., Jeunemaitre, X., and Lifton, R. P. (2001) *Science* **293**, 1107-1112

155. Jiang, Z. Y., Zhou, Q. L., Holik, J., Patel, S., Leszyk, J., Coleman, K., Chouinard, M., and Czech, M. P. (2005) *J. Biol. Chem.* **280**, 21622-21628. Epub 22005 Mar 21630
156. Lee, B. H., Min, X., Heise, C. J., Xu, B. E., Chen, S., Shu, H., Luby-Phelps, K., Goldsmith, E. J., and Cobb, M. H. (2004) *Mol. Cell* **15**, 741-751.
157. Oh, E., Heise, C. J., English, J. M., Cobb, M. H., and Thurmond, D. C. (2007) *J. Biol. Chem.* **282**, 32613-32622
158. Hodgkinson, C. P., Mander, A., and Sale, G. J. (2005) *Biochem. J.* **388**, 785-793
159. Brule, S., Rabahi, F., Faure, R., Beckers, J. F., Silversides, D. W., and Lussier, J. G. (2000) *Biol. Reprod.* **62**, 642-654
160. Smithers, N. P., Hodgkinson, C. P., Cuttle, M., and Sale, G. J. (2008) *J. Recept. Signal Transduct. Res.* **28**, 581-589
161. Graham, M. E., Handley, M. T., Barclay, J. W., Ciufo, L. F., Barrow, S. L., Morgan, A., and Burgoyne, R. D. (2008) *Biochem. J.* **409**, 407-416
162. Yaekura, K., Julyan, R., Wicksteed, B. L., Hays, L. B., Alarcon, C., Sommers, S., Poitout, V., Baskin, D. G., Wang, Y., Philipson, L. H., and Rhodes, C. J. (2003) *J. Biol. Chem.* **278**, 9715-9721. Epub 2003 Jan 9711
163. Min, J., Okada, S., Kanzaki, M., Elmendorf, J. S., Coker, K. J., Ceresa, B. P., Syu, L. J., Noda, Y., Saltiel, A. R., and Pessin, J. E. (1999) *Mol. Cell* **3**, 751-760
164. Okada, S., Ohshima, K., Uehara, Y., Shimizu, H., Hashimoto, K., Yamada, M., and Mori, M. (2007) *Biochem. Biophys. Res. Commun.* **356**, 102-106
165. Yamada, E., Okada, S., Saito, T., Ohshima, K., Sato, M., Tsuchiya, T., Uehara, Y., Shimizu, H., and Mori, M. (2005) *J. Cell Biol.* **168**, 921-928
166. Sano, H., Kane, S., Sano, E., and Lienhard, G. E. (2005) *Biochem. Biophys. Res. Commun.* **332**, 880-884
167. Saito, T., Okada, S., Yamada, E., Ohshima, K., Shimizu, H., Shimomura, K., Sato, M., Pessin, J. E., and Mori, M. (2003) *J. Biol. Chem.* **278**, 36718-36725. Epub 32003 Jul 36719
168. Groffen, A. J., Jacobsen, L., Schut, D., and Verhage, M. (2005) *J. Neurochem.* **92**, 554-568
169. Widberg, C. H., Bryant, N. J., Girotti, M., Rea, S., and James, D. E. (2003) *J. Biol. Chem.* **278**, 35093-35101
170. Cheviet, S., Bezzi, P., Ivarsson, R., Renstrom, E., Viertl, D., Kasas, S., Catsicas, S., and Regazzi, R. (2006) *J. Cell Sci.* **119**, 2912-2920. Epub 2006 Jun 2920
171. Zhang, W., Lilja, L., Mandic, S. A., Gromada, J., Smidt, K., Janson, J., Takai, Y., Bark, C., Berggren, P. O., and Meister, B. (2006) *Diabetes* **55**, 574-581
172. Sakisaka, T., Yamamoto, Y., Mochida, S., Nakamura, M., Nishikawa, K., Ishizaki, H., Okamoto-Tanaka, M., Miyoshi, J., Fujiyoshi, Y., Manabe, T., and Takai, Y. (2008) *J. Cell Biol.* **183**, 323-337
173. Liu, L., Jedrychowski, M. P., Gygi, S. P., and Pilch, P. F. (2006) *Mol. Biol. Cell* **17**, 4249-4256. Epub 2006 Jul 4226
174. Omata, W., Shibata, H., Li, L., Takata, K., and Kojima, I. (2000) *Biochem. J.* **346**, 321-328
175. Tomas, A., Yermen, B., Min, L., Pessin, J. E., and Halban, P. A. (2006) *J. Cell Sci.* **119**, 2156-2167. Epub 2006 Apr 2125
176. Tsakiridis, T., Vranic, M., and Klip, A. (1994) *J. Biol. Chem.* **269**, 29934-29942

177. Brozinick, J. T., Jr., Hawkins, E. D., Strawbridge, A. B., and Elmendorf, J. S. (2004) *J. Biol. Chem.* **279**, 40699-40706. Epub 42004 Jul 40696
178. Romeo, S., Sentinelli, F., Cavallo, M. G., Leonetti, F., Fallarino, M., Mariotti, S., and Baroni, M. G. (2008) *Int J Obes (Lond)* **32**, 413-420. Epub 2007 Oct 2002
179. Tsunoda, K., Sanke, T., Nakagawa, T., Furuta, H., and Nanjo, K. (2001) *Diabetologia* **44**, 2092-2097
180. Bracher, A., and Weissenhorn, W. (2001) *J. Mol. Biol.* **306**, 7-13
181. Peng, R., and Gallwitz, D. (2002) *J. Cell Biol.* **157**, 645-655
182. Wang, Z., Oh, E., and Thurmond, D. C. (2007) *J. Biol. Chem.* **282**, 9536-9546
183. Lofas, S., and Johnsson, B. J. (1990) *J. Chem. Soc. Chem. Commun.* **21**, 1526-1528
184. Stenberg, A., Larsson, G., Johnson, P., Heimer, G., and Ulmsten, U. (1999) *Acta Obstet. Gynecol. Scand.* **78**, 436-442
185. Rickman, C., Medine, C. N., Bergmann, A., and Duncan, R. R. (2007) *J. Biol. Chem.* **282**, 12097-12103. Epub 12007 Jan 12030
186. Connell, E., Darios, F., Broersen, K., Gatsby, N., Peak-Chew, S. Y., Rickman, C., and Davletov, B. (2007) *EMBO reports* **8**, 414-419
187. Latham, C. F., Osborne, S. L., Cryle, M. J., and Meunier, F. A. (2007) *J. Neurochem.* **100**, 1543-1554. Epub 2006 Dec 1523
188. Pevsner, J., Hsu, S. C., Braun, J. E., Calakos, N., Ting, A. E., Bennett, M. K., and Scheller, R. H. (1994) *Neuron* **13**, 353-361
189. Garcia, E. P., Gatti, E., Butler, M., Burton, J., and De Camilli, P. (1994) *Proc Natl Acad Sci USA* **91**, 2003-2007
190. Kashima, Y., Miki, T., Shibasaki, T., Ozaki, N., Miyazaki, M., Yano, H., and Seino, S. (2001) *J. Biol. Chem.* **276**, 46046-46053
191. Mulder, H., Lu, D., Finley, J. t., An, J., Cohen, J., Antinozzi, P. A., McGarry, J. D., and Newgard, C. B. (2001) *J. Biol. Chem.* **276**, 6479-6484
192. Burkhardt, P., Hattendorf, D. A., Weis, W. I., and Fasshauer, D. (2008) *EMBO J.* **27**, 923-933
193. Chen, X., Lu, J., Dulubova, I., and Rizo, J. (2008) *J. Biomol. NMR* **41**, 43-54
194. Sassa, T., Harada, S., Ogawa, H., Rand, J. B., Maruyama, I. N., and Hosono, R. (1999) *J. Neurosci.* **19**, 4772-4777
195. Richmond, J. E., Weimer, R. M., and Jorgensen, E. M. (2001) *Nature* **412**, 338-341
196. Dulubova, I., Khvotchev, M., Liu, S., Huryeva, I., Sudhof, T. C., and Rizo, J. (2007) *Proc. Natl. Acad. Sci. U. S. A.* **104**, 2697-2702
197. Toonen, R. F., and Verhage, M. (2007) *Trends Neurosci.* **30**, 564-572
198. Thurmond, D. C., and Pessin, J. E. (2001) *Mol. Membr. Biol.* **18**, 237-245
199. Cheatham, B., Volchuk, A., Kahn, C. R., Wang, L., Rhodes, C. J., and Klip, A. (1996) *Proc Natl Acad Sci USA* **93**, 15169-15173
200. Volchuk, A., Wang, Q., Ewart, H. S., Liu, Z., He, L., Bennett, M. K., and Klip, A. (1996) *Mol. Biol. Cell* **7**, 1075-1082
201. Macaulay, S. L., Grusovin, J., Stoichevska, V., Ryan, J. M., Castelli, L. A., and Ward, C. W. (2002) *FEBS Lett.* **528**, 154-160
202. Kralik, S. F., Liu, P., Leffler, B. J., and Elmendorf, J. S. (2002) *Endocrinology* **143**, 37-46

203. Xue, Y., Ren, J., Gao, X., Jin, C., Wen, L., and Yao, X. (2008) *Mol Cell Proteomics* **7**, 1598-1608
204. Saperstein, R., Vicario, P. P., Strout, H. V., Brady, E., Slater, E. E., Greenlee, W. J., Ondeyka, D. L., Patchett, A. A., and Hangauer, D. G. (1989) *Biochemistry (Mosc).* **28**, 5694-5701
205. Baltensperger, K., Lewis, R. E., Woon, C. W., Vissavajjhala, P., Ross, A. H., and Czech, M. P. (1992) *Proc. Natl. Acad. Sci. U. S. A.* **89**, 7885-7889
206. Saltiel, A. R., and Pessin, J. E. (2002) *Trends Cell Biol.* **12**, 65-71
207. Kimura, A., Mora, S., Shigematsu, S., Pessin, J. E., and Saltiel, A. R. (2002) *J. Biol. Chem.* **277**, 30153-30158
208. Low, S. H., Vasanji, A., Nanduri, J., He, M., Sharma, N., Koo, M., Drazba, J., and Weimbs, T. (2006) *Mol. Biol. Cell* **17**, 977-989. Epub 2005 Dec 2007
209. Beest, M. B., Chapin, S. J., Avrahami, D., and Mostov, K. E. (2005) *Mol. Biol. Cell* **16**, 5784-5792. Epub 2005 Oct 5785
210. Nevins, A. K., and Thurmond, D. C. (2005) *J. Biol. Chem.* **280**, 1944-1952
211. Li, G., Kowluru, A., and Metz, S. A. (1996) *Biochem. J.* **316**, 345-351
212. Mitchell, K. J., Tsuboi, T., and Rutter, G. A. (2004) *Diabetes* **53**, 393-400
213. Nevins, A. K., and Thurmond, D. C. (2003) *Am J Physiol Cell Physiol* **285**, C698-710
214. Varadi, A., Tsuboi, T., and Rutter, G. A. (2005) *Mol. Biol. Cell* **16**, 2670-2680. Epub 2005 Mar 2623
215. Ivarsson, R., Jing, X., Waselle, L., Regazzi, R., and Renstrom, E. (2005) *Traffic* **6**, 1027-1035
216. Kasai, K., Ohara-Imaizumi, M., Takahashi, N., Mizutani, S., Zhao, S., Kikuta, T., Kasai, H., Nagamatsu, S., Gomi, H., and Izumi, T. (2005) *J. Clin. Invest.* **115**, 388-396
217. Waselle, L., Coppola, T., Fukuda, M., Iezzi, M., El-Amraoui, A., Petit, C., and Regazzi, R. (2003) *Mol. Biol. Cell* **14**, 4103-4113. Epub 2003 Aug 4107.
218. Nevins, A. K., and Thurmond, D. C. (2006) *J. Biol. Chem.* **281**, 18961-18972. Epub 12006 May 18919
219. Giraudo, C. G., Eng, W. S., Melia, T. J., and Rothman, J. E. (2006) *Science* **313**, 676-680. Epub 2006 Jun 2022
220. Isgandarova, S., Jones, L., Forsberg, D., Loncar, A., Dawson, J., Tedrick, K., and Eitzen, G. (2007) *J. Biol. Chem.* **282**, 30466-30475. Epub 32007 Aug 30428
221. Yang, X., Xu, P., Xiao, Y., Xiong, X., Xu, T., Sieber, J. J., Willig, K. I., Heintzmann, R., Hell, S. W., and Lang, T. (2006) *J. Biol. Chem.* **281**, 15457-15463. Epub 12006 Apr 15454
222. Chamberlain, L. H., Burgoyne, R. D., and Gould, G. W. (2001) *Proc. Natl. Acad. Sci. U. S. A.* **98**, 5619-5624
223. Lang, T., Bruns, D., Wenzel, D., Riedel, D., Holroyd, P., Thiele, C., and Jahn, R. (2001) *EMBO J.* **20**, 2202-2213
224. Sieber, J. J., Willig, K. I., Heintzmann, R., Hell, S. W., and Lang, T. (2006) *Biophys. J.* **90**, 2843-2851. Epub 2006 Jan 2827
225. Mundy, D. I., Machleidt, T., Ying, Y. S., Anderson, R. G., and Bloom, G. S. (2002) *J. Cell Sci.* **115**, 4327-4339

226. Xia, F., Gao, X., Kwan, E., Lam, P. P., Chan, L., Sy, K., Sheu, L., Wheeler, M. B., Gaisano, H. Y., and Tsushima, R. G. (2004) *J. Biol. Chem.* **279**, 24685-24691. Epub 22004 Apr 24688
227. Kang, Y., Huang, X., Pasyk, E. A., Ji, J., Holz, G. G., Wheeler, M. B., Tsushima, R. G., and Gaisano, H. Y. (2002) *Diabetologia* **45**, 231-241
228. Nakano, M., Nogami, S., Sato, S., Terano, A., and Shirataki, H. (2001) *Biochem. Biophys. Res. Commun.* **288**, 468-475
229. Bruun, T. Z., Hoy, M., and Gromada, J. (2000) *Eur. J. Pharmacol.* **403**, 221-224.
230. Collins, M. O. (2009) *Science* **325**, 1635-1636
231. Collins, M. O., Yu, L., Campuzano, I., Grant, S. G., and Choudhary, J. S. (2008) *Mol Cell Proteomics* **7**, 1331-1348
232. Iakoucheva, L. M., Radivojac, P., Brown, C. J., O'Connor, T. R., Sikes, J. G., Obradovic, Z., and Dunker, A. K. (2004) *Nucleic Acids Res* **32**, 1037-1049

CURRICULUM VITAE

Jenna Lee Jewell

EDUCATION

Fort Lewis College, Durango CO 1999-2004
B.S. in Chemistry-Biochemistry Option
Dissertation: The Genomics of Osteoarthritis, the Vitamin D Receptor.
B.A. in Political Science
Dissertation: Social Capital: Is it Good for Health?

Indiana University, Indianapolis IN 2005-2010
Ph.D. in Biochemistry & Molecular Biology
Dissertation: Regulation of Exocytosis by Syntaxin 4-Munc18c Complexes
Chair/Advisor – Debbie C. Thurmond
Committee Members – Peter J. Roach, Zhong-Yin Zhang, Patricia J. Gallagher

GRANTS AND FELLOWSHIPS

DeVault Fellowship	2008
Educational Enhancement Grant	2008
American Heart Predoctoral Fellowship	2008-2010

HONORS AND AWARDS

Dean's List	2000, 2001, 2002
Who's Who in American Colleges & Universities – Future Leaders	2003, 2004
Undergraduate Institutional Honor of Cum Laude	2004
Pi Sigma Alpha – Political Science National Honorary Society	2004
Kappa Mu Epsilon – Mathematics Honor Society	2004
Phi Lambda Upsilon – Honorary Chemical Society	2004
Sigma Xi, Graduate Student Research Competition. *Honorable Mention.*	2008
IUSM Scientific Poster Session. *Student Poster Second Place*	2009

PROFESSIONAL MEMBERSHIPS AND ACTIVITIES

The Women's Resource Center, helping women find jobs and housing	2001
Habitat for Humanity, development of houses for those in need	2003
Big Brothers Big Sisters, mentor to a 9 year old girl	1999-2004
College level tutoring in writing, mathematics, chemistry, & biology	2001-2004
The Buddy Connection, high-school level tutoring in English & Geometry	2001-2004
ADA America's Walk for Diabetes	2006

IUSM Graduate Student Mentor Program	2007
Sigma Xi, The Scientific Research Society	2007-Present
Indiana Microscopy Society	2007-Present
Islet Biology Journal Club	2007-2010
JDRF Walk to Cure Diabetes	2009

PUBLICATIONS

1) **Jewell JL***, Luo W*, Oh E, Wang Z, and Thurmond DC. (2008) A Direct Association of Filamentous Actin with Syntaxin 4 Functionally Restricts Granule Accessibility to Regulate Insulin Exocytosis. *J Biol Chem* 283: 10716-10726. *Authors contributed equally
2) **Jewell JL**, Oh E, Bennett SM, Meroueh S, and Thurmond DC. (2008) The Tyrosine Phosphorylation of Munc18c Induces a Switch in Binding Specificity from Syntaxin 4 to Doc2β. *J Biol. Chem* 283: 21734-46
3) **Jewell JL**, Oh E, Thurmond DC. (2009) Exocytosis Mechanisms Underlying Insulin Release and Glucose Uptake: Conserved Roles for Munc18c and Syntaxin 4. *Am J Physiol Regulatory Integrative Comp Physiol, In Press*
4) **Jewell JL**, and Thurmond DC. (2010) Identification of an Insulin-Stimulated Munc18c Tyrosine Kinase in 3T3L1 Adipocytes and Mouse Skeletal Muscle Extracts. *In Preparation*

ABSTRACT PUBLICATIONS/PRESENTATIONS

1) Luo W, Oh E, **Jewell JL**, and Thurmond DC. (2007) Syntaxin 4 and Syntaxin 1A Differentially Interact with the Actin Cytoskeleton to Regulate Biphasic Insulin Secretion." The American Diabetes Association 67th Scientific Session Abstract. Chicago, IL
2) **Jewell JL**, Oh E, Bennett SM, Meroueh S, and Thurmond DC. (2008) The Tyrosine Phosphorylation of Munc18c Induces a Switch in Binding Specificity from Syntaxin 4 to Doc2β. The American Diabetes Association 68th Scientific Sessions Abstract. San Francisco, CA
3) **Jewell JL**, Tagliabracci VS, Tackett L, Elmendorf JS, and Thurmond DC. (2009) Identification of an Insulin-stimulated Munc18c Tyrosine Kinase in 3T3L1 Adipocytes Mouse Skeletal Muscle Extracts. FASEB Summer Research Conferences. Lucca, Italy

RESEARCH EXPERIENCE

Undergraduate Research, Mentor: Dr. Les Sommerville 2004-2005
Department of Chemistry, Fort Lewis College, Durango CO
Project: Enzyme purification and kinetics, molecular biology, and using genomics as a reference in identifying metabolic pathways of the organism Acidobacterium capsulatum.

Graduate Research, Mentor: Dr. Debbie Thurmond 2005-2010
Department of Biochemistry & Molecular Biology, Center for Diabetes Research, Indiana University School of Medicine, Indianapolis IN*Dissertation: Regulation of Exocytosis by Syntaxin 4-Munc18c Complexes.*

RESEARCH POSTER PRESENTATIONS

1) **Jewell JL,** Oh E, and Thurmond DC. (2007) The Switch Mechanism of Tyrosine Phosphorylated Munc18c from Syntaxin 4 to Doc2β Involves the Flexible Linker Region of Syntaxin 4. Biochemistry Retreat. Indianapolis, IN
2) **Jewell JL**, Oh E, Bennett SM, Meroueh S, and Thurmond DC. (2008) The Tyrosine Phosphorylation of Munc18c Induces a Switch in Binding Specificity from Syntaxin 4 to Doc2β. Biochemistry Retreat. Indianapolis, IN
3) **Jewell JL,** Tagliabracci VS, Tackett L, Elmendorf JS, and Thurmond DC. (2009) Identification of an Insulin- Stimulated Munc18c Tyrosine Kinase in 3T3L1 Adipocytes and Primary Skeletal Muscle. IUSM Scientific Poster Session. Indianapolis, IN

RESEARCH ORAL PRESENTATIONS

Sigma Xi, Graduate Student Research Competition 2008
The Role of O-linked Glycosylation in Insulin Secretion & Action, Islet Biology Journal Club 2008
Center for Diabetes Research, The Regulation of Exocytosis by Munc18c 2010

TEACHING EXPERIENCE

Teacher Assistant in Organic Chemistry, Fort Lewis College, Durango CO 2003
Teacher Assistant in General Chemistry, Fort Lewis College, Durango CO 2005